Report of Investigation 2023-1

GEOLOGIC MAP OF OKMOK VOLCANO

Jessica F. Larsen, Christina A. Neal, Janet R. Schaefer, and Christopher J. Nye

Published by
STATE OF ALASKA
DEPARTMENT OF NATURAL RESOURCES
DIVISION OF GEOLOGICAL & GEOPHYSICAL SURVEYS
2023

Cover photo. Airphoto of Okmok Volcano taken by pilot Burke Mees, April 28, 2021. Available from AVO's image database: www.avo.alaska.edu/images/image.php?id=169781.

GEOLOGIC MAP OF OKMOK VOLCANO

Jessica F. Larsen, Christina A. Neal, Janet R. Schaefer, and Christopher J. Nye

Report of Investigation 2023-1

State of Alaska
Department of Natural Resources
Division of Geological & Geophysical Surveys

STATE OF ALASKA
Mike Dunleavy, Governor

DEPARTMENT OF NATURAL RESOURCES
John Boyle, Commissioner

DIVISION OF GEOLOGICAL & GEOPHYSICAL SURVEYS
Kenneth Papp, Acting State Geologist and Director

Publications produced by the Division of Geological & Geophysical Surveys (DGGS) are available for free download from the DGGS website (dggs.alaska.gov). Publications on hard-copy or digital media can be examined or purchased in the Fairbanks office:

Alaska Division of Geological & Geophysical Surveys
3354 College Rd., Fairbanks, Alaska 99709-3707
Phone: (907) 451-5010 Fax (907) 451-5050
dggspubs@alaska.gov | dggs.alaska.gov

DGGS publications are also available at:
Alaska State Library,
Historical Collections & Talking Book Center
395 Whittier Street
Juneau, Alaska 99811

Alaska Resource Library and Information Services (ARLIS)
3150 C Street, Suite 100
Anchorage, Alaska 99503

Suggested citation:
Larsen, J.F., Neal, C.A., Schaefer, J.R., and Nye, C.J., 2023, Geologic map of Okmok Volcano: Alaska Division of Geological & Geophysical Surveys Report of Investigation 2023-1, 63 p., 4 sheets. https://doi.org/10.14509/31015

Contents

Figures

Appendix

Map Sheets

GEOLOGIC MAP OF OKMOK VOLCANO

Jessica F. Larsen[1,2], Christina A. Neal[3], Janet R. Schaefer[4], and Christopher J. Nye[4]

INTRODUCTION

The geologic map and description of map units presented here cover approximately 880 km^2 of northeastern Umnak Island, Aleutian Islands, Alaska. This report focuses on Okmok Volcano and its eruptive products and updates the mid-20th-century geologic map of Byers (1959). Mapped deposits reflect the state of the volcano just prior to the 2008 eruption. Published information about other portions of Umnak Island geology, including Mount Recheshnoi and Mount Vsevidof, can be found in Byers (1959). The 2008 eruption and its deposits are described in Larsen and others (2009, 2013, 2015).

Okmok Volcano is one of 54 historically active volcanoes in the Alaska–Aleutian volcanic arc that stretches across southern mainland Alaska and the Aleutian Islands (fig. 1; Wood and Kienle, 1990; Miller and others, 1998; Cameron and others, 2020). The highest point of the modern Okmok Caldera is along the caldera's northern rim, 967 m in elevation, and formally named "Mount Okmok" (U.S. Board on Geographic Names, www.usgs.gov/core-science-systems/ngp/board-on-geographic-names/domestic-names). Okmok Volcano dominates the northeastern portion of Umnak Island, which is 100 km southwest of Unalaska/Dutch Harbor and 1,400 km southwest of Anchorage (figs. 1, 2). The Port of Dutch Harbor on Unalaska Island produces the highest volume of seafood for any port in the United States (see fisheries.noaa.gov/resource/document/fisheries-united-states-2018-report). Unalaska city and the Port of Dutch Harbor have been impacted by ash fall and drifting ash clouds from Okmok Volcano's explosive eruptions as recently as 2008. Holocene and late Pleistocene volcanic rocks and deposits of Okmok Volcano rest upon glaciated Tertiary volcanic and sedimentary rocks (Byers, 1959).

The first geologic mapping expedition to Okmok Volcano was by the U.S. Geological Survey (USGS) after the 1945 eruption, largely in response to concerns about volcanic hazards to U.S. military activities in the Aleutians Islands (Byers and others, 1947, 1959; Byers and Brannock, 1949; Byers, 1955, 1959, 1961). The State of Alaska conducted further mapping and geochemical studies as part of its geothermal exploration program in the 1980s (Nye, 1983; Nye and Reid, 1986; Motyka and others, 1993). Additional modern geological work focused on Okmok Volcano and the rest of Umnak Island to address the geochemistry and origin of primary Aleutian arc magmas and subduction zone mass recycling (Marsh, 1982; Brophy and Marsh, 1986; Nye and Reid, 1986; Myers and Marsh, 1987; Miller and others, 1992; Fournelle and others, 1994; Kay and Kay, 1994).

In 1998, the Alaska Volcano Observatory (AVO) began a multi-year effort to expand geophysical monitoring in the central Aleutians Islands, including at Okmok Volcano. As part of this effort, AVO geologists from the University of Alaska Fairbanks Geophysical Institute (UAF/GI), the Alaska Division of Geological & Geophysical Surveys (DGGS), and USGS also began a renewed effort to document Okmok Volcano's recent eruption products. The project started with reconnaissance fieldwork to document and sample products from the 1997 eruption within Okmok Caldera. This evolved into an effort to produce an updated geologic map of Okmok Volcano and gather more information about its eruptive history and hazards. Three significant eruptions occurred at Okmok

[1]University of Alaska Fairbanks Geophysical Institute, P.O. Box 757320, Fairbanks, AK 99775
[2]University of Alaska Department of Geosciences, P.O. Box 755790, Fairbanks, AK 99775
[3]U.S. Geological Survey, Volcano Science Center, 4230 University Dr., Anchorage, AK 99508
[4]Alaska Division of Geological & Geophysical Surveys, 3354 College Rd., Fairbanks, Alaska 99709-3707

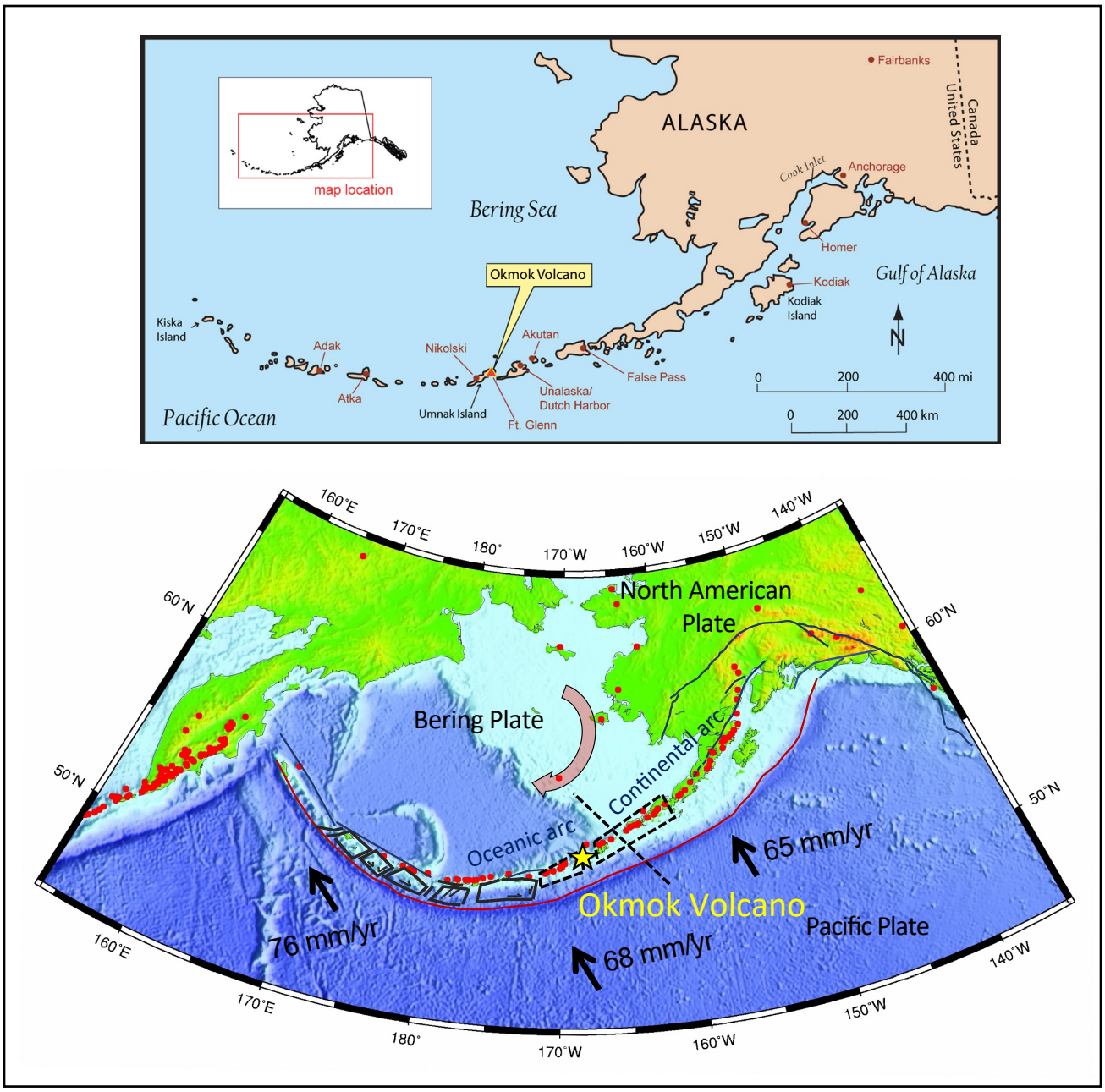

Figure 1. A. Location map of Okmok Volcano, Alaska (after Begét and others, 2005). Okmok Volcano is located on Umnak Island, approximately 100 km southwest of the towns of Unalaska and Dutch Harbor on Unalaska Island and 1,385 km from Anchorage, Alaska. **B.** Map figure showing tectonic features along the Aleutian subduction zone. Okmok Volcano is indicated by the yellow star. The convergence rates and angles between the Pacific plate, North American plate, and Bering microplate are indicated by the black vectors plotted to the south of the convergence zone (red line). Tectonic blocks extend along the oceanic portion of the arc, indicated by the solid and dashed black lines. Transparent red arrow indicates Bering plate rotation. The location of the continental-to-oceanic transition is indicated by the dark-black dashed line to the east of Okmok Volcano. Figure after Cross and Freymueller (2008), Buurman and others (2014), and Larsen (2016).

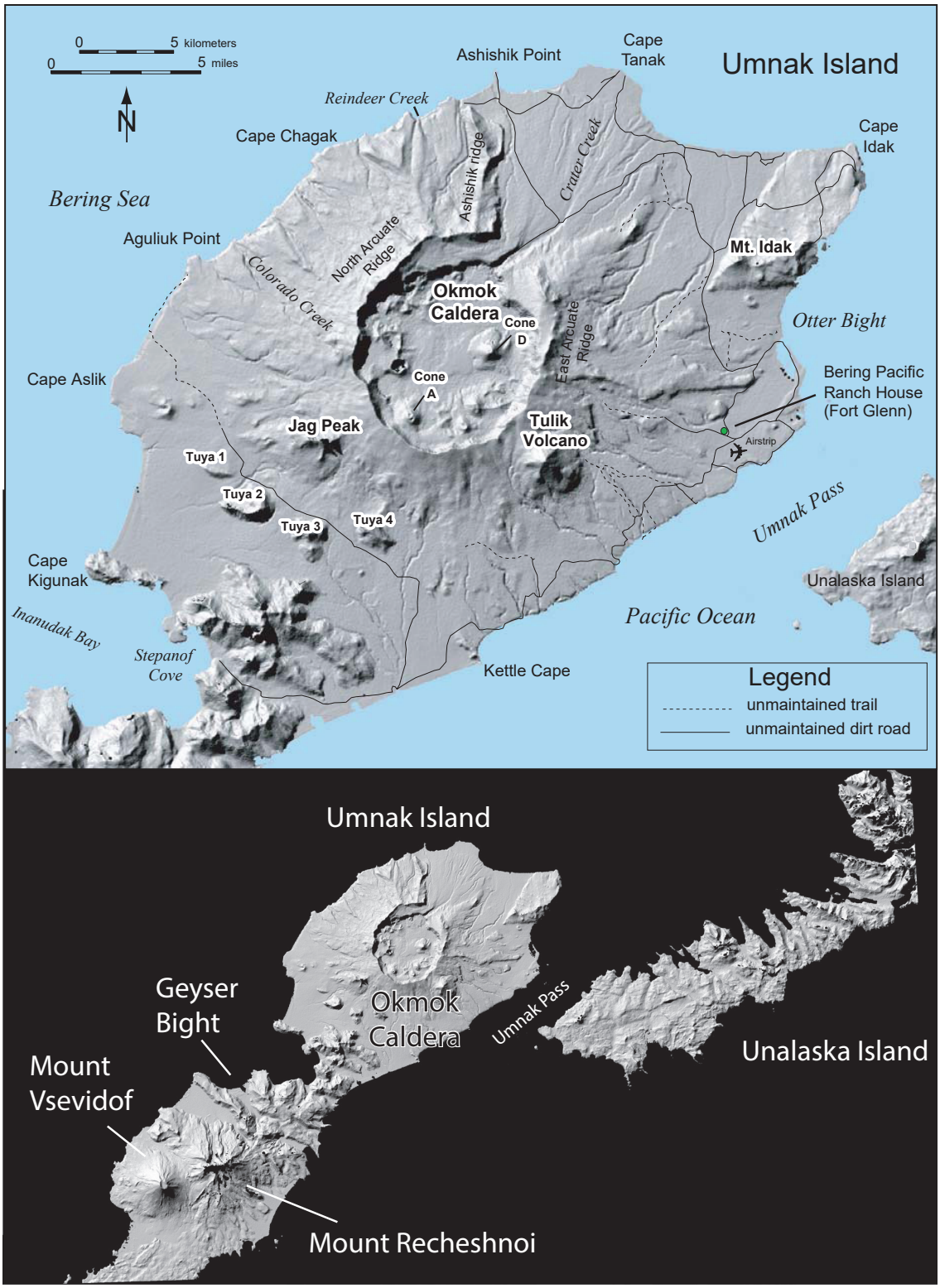

Figure 2. A. Shaded relief image showing the locations of roads and trails, and names of major geographic features used in the text (after Begét and others, 2005). The Bering Pacific Ranch at Fort Glenn is located among the remains of the U.S. Army base active during WWII. **B.** Shaded relief map showing the locations of Umnak Island, Unalaska Island, and Okmok Volcano, Mount Recheshnoi, and Mount Vsevidof (after Schaefer, 2005).

Volcano in 1958, 1997, and 2008—after fieldwork had been conducted for the original 1:63,360-scale geologic map produced by Byers (1959)—resulting in new volcanic deposits not previously described.

Okmok Volcano is one of the most frequently active volcanoes in the Aleutian volcanic arc. Seismic and geodetic monitoring indicate ongoing unrest at Okmok Volcano since at least 1997. Geodetic observations of inflation before and after the 1997 and 2008 eruptions indicate a nearly continuous input of new magma from a depth consistent with frequent eruptions of basalt and basaltic andesite magmas over the past 200 years (Larsen and others, 2013; Lu and others, 2000, 2003, 2005; Mann, 2002; Mann and others, 2002). To better understand the likelihood and character of future eruptions from Okmok Volcano, it is necessary to understand its past behavior, including eruptions since the first geologic map was published by Byers (1959).

TECTONIC SETTING

Umnak Island is set within the eastern Aleutian Islands, which is highly active both seismically and volcanically because it is situated along a convergent tectonic plate margin (Davies and House, 1979). The Aleutian subduction zone in this region consists of an oceanic island arc, where the volcanic centers are predominantly built on oceanic crust (Fliedner and Klemperer, 2000). Seismicity associated with subducting slabs of oceanic crust along convergent margins illuminates the Wadati–Benioff zone (fig. 1; Zhao and others, 1995). The locations of earthquakes underneath active arc volcanoes give an estimate of the depth of the subducting slab, and thus a measure of the process of partial melting of the mantle wedge via dehydration of the subducting sediments and/or hydrothermally altered oceanic crust (George and others, 2003).

Volcanism on Umnak Island

There are three main volcanic centers on Umnak Island: Mount Vsevidof and Mount Recheshnoi in the southwest region of the island (Byers, 1959; Miller and others, 1998), and Okmok Volcano dominating the northeastern portion of the island as a gently sloping, shield-shaped volcano truncated by two caldera-forming eruptions. Mount Vsevidof and Mount Recheshnoi were active throughout the Pleistocene, and likely the Holocene. The relatively undissected, symmetrical stratocone of Mount Vsevidof has possibly been active during historical times (Black, 1975), but little is known about its eruption history. Youthful-looking cinder cones low on its flanks may be Holocene (Black, 1975; Miller and others, 1998). Mount Recheshnoi, deeply eroded by glaciers, was active mainly during the Pleistocene (Byers, 1959). K-Ar ages obtained by Turner and Nye (1989) indicate the majority of Mount Recheshnoi lava flows range in age from ~75,000 to ~534,000 years. Its most recent eruption produced an extensive lava flow on its southeast flanks, dated by radiocarbon methods to ~3,000 yBP (Black, 1975).

History of Glaciation

The history of glaciation in the Aleutian Islands is not well known, although estimates of the extent of the ice sheet can be found in several publications (Black, 1974a, b, 1975, 1976; Mann and Hamilton, 1995; Kaufman and others, 2011; Coombs and Jicha, 2020; Dalton and others, 2020). The maximum extent of the ice cap in the Pleistocene likely covered Umnak Island (Kaufman and others, 2011). Marine isotope stage (MIS) 4 (early Wisconsin) ice sheet covered most of Umnak Island ~55,000 yBP (Gowan and others, 2021), including the caldera, leaving a small sliver of the north-northwestern coastline possibly ice-free, according to Version 2 of the Alaska Paleo-Glacier Atlas (Kaufman and others, 2011). During the MIS 2 (late-Wisconsin) interval between ~24,000 and 12,000 yBP, the ice sheet may have covered the southern part of Umnak Island, south of the caldera rim (Kaufman and others, 2011). Deglaciation in the eastern Aleutian Islands region may have commenced ~18,500 to 18,000 yBP (Coombs and Jicha, 2020; Dalton and others, 2020) or, as discussed by Black (1974a, b, 1976), possibly later, between ~12,000 and 10,000 yBP, with higher elevations retaining glaciers longer than the coastlines.

In general, the Aleutian Islands appear to have undergone two neoglacial periods with advancing alpine glaciers: between ~7,500 and 5,500 yBP and between 3,500 and 2,000 yBP, with a hypsithermal period between ~5,500 and 3,500 yBP causing glacial retreat (Black, 1981). It is possible that some glaciers advanced as far as the Bering Sea from the Okmok Caldera edifice during the neoglacial periods (Black, 1981); however, little work has been done to investigate possible moraines found around the northeastern portion of Umnak Island (J.E. Begét, personal commun., 2004). Additional work is needed to provide a more detailed record of glacial history for northeastern Umnak Island and the eastern and central Aleutian Islands in general. At present, a stagnant, ash-covered glacier lies within Okmok Caldera on the shaded southern sector of the caldera floor at the base of the inner caldera wall.

Geologic Setting of Northeastern Umnak Island

Northeastern Umnak Island hosts several volcanic landscapes that predate Okmok Volcano and form prominent geographic features, including Ashishik ridge and Ashishik Point to the north, Cape Tanak to the northeast, and Cape Idak to the east of Cape Tanak (fig. 2). The Ashishik ridge and Cape Idak areas have some of the oldest dated volcanic rocks in the northeastern part of Umnak Island and represent volcanic systems that were active before the growth of the modern Okmok Caldera edifice. Cape Tanak is a fan-shaped delta that juts into the Bering Sea to the north of the caldera, representing sedimentation from Crater Creek, which drains the caldera. Cape Tanak experiences active prograde sedimentation particularly due to lahar emplacement down Crater Creek during eruptions within the caldera, and sediment washed down from the caldera rim areas into Crater Creek.

Tulik Volcano is a 1,058-m-high subglacial to subaerial volcanic cone located just southeast of Okmok Caldera. Because of its prominence and conical shape, Tulik Volcano has been the source of questionable eruption reports during historical times (e.g., 1945; Robinson, 1947; fig. 2). Evidence for ice-contact volcanism exists in an apron or bench around the base of Tulik Volcano, indicating that it was active when Pleistocene glaciers existed on the flanks of a pre-Okmok volcanic edifice. Several additional volcanic peaks, also interpreted as tuyas (subglacially erupted volcanic vents) to the west and southwest of the caldera show evidence for similar subglacial or ice-contact volcanism. Jag Peak is the most prominent of those tuyas and is the only one formally named on the prior geologic map (Byers, 1959). Jag Peak and the other tuyas on the northeastern portion of Umnak Island are likely also related to an older volcanic system that predates modern Okmok Volcano.

There are several unnamed Holocene cinder cones in the Cape Aslik and Mount Idak areas and at higher elevations on the eastern flanks of the caldera (fig. 2; sheet 1). Although these cones and associated lava flows are undated, they are likely Holocene, based on morphology and lack of evidence for glaciation.

Okmok Caldera Physiography

The modern Okmok Caldera edifice forms a predominantly basaltic andesite shield volcano that produced two known caldera-forming eruptions in the late Pleistocene and Holocene. Okmok Caldera is a nearly circular, 300- to 500-m-deep, 10- to 12-km-diameter collapse crater that truncates a Pleistocene volcanic edifice (Larsen and others, 2007). The Okmok I and II caldera-forming eruptions created these two nested calderas (fig. 2) approximately 12,000 and 2,050 yBP, respectively (Miller and Smith, 1976, 1987; Begét and others, 2005). The flanks of the volcano surrounding the caldera are generally gently sloping to flat surfaced and plateau-like, reflecting surfaces created by the thick pyroclastic density current deposits from the second recognized caldera-forming eruption, Okmok II (~2,050 yBP; Burgisser, 2005; Larsen and others, 2007; this study). Okmok II deposits are

deeply cut by stream channels at all azimuths around the caldera, offering excellent outcrop exposure of both the late Pleistocene Okmok I and Holocene Okmok II caldera-forming eruption stratigraphy. The ground around the volcano is typically covered with thick, deep grass tussocks at lower elevations, and by ash and reworked pyroclastic debris at higher elevations. Approximately 1,000 km^2 of Okmok Volcano deposits are exposed on the island. An unknown volume of deposits extends offshore.

The walls of Okmok Caldera expose lava flows, dikes, and volcaniclastic deposits from the precaldera Okmok volcanic center. Also exposed high on the caldera rim are pyroclastic deposits from the Okmok I and II caldera-forming eruptions. Most of the caldera floor is covered with effusive and explosive eruption products from more than a dozen separate vents. Reworked volcanic materials form broad, active alluvial fans between topographic highs, and the steep caldera walls support active talus and accumulations of colluvium. The caldera walls are sheer and mostly inaccessible without technical climbing gear. Most visitors on foot access the inner caldera through a sharply defined notch in the north crater wall informally named "the Gates" (also called "the Caldera Breach" in Wolfe, 2001). Water exits the caldera via Crater Creek through the Gates, draining the caldera and flowing to the northeast into the Bering Sea at Cape Tanak (figs. 2, 3). Overall, the caldera floor slopes from about 500 m elevation at the base of Cone A in the southwest, to the northeast toward the Gates, where Crater Creek exits the caldera at about 360 m elevation (Schaefer and others, 2011). The highest point in the caldera is the summit of Cone A (890 m; fig. 2), which last

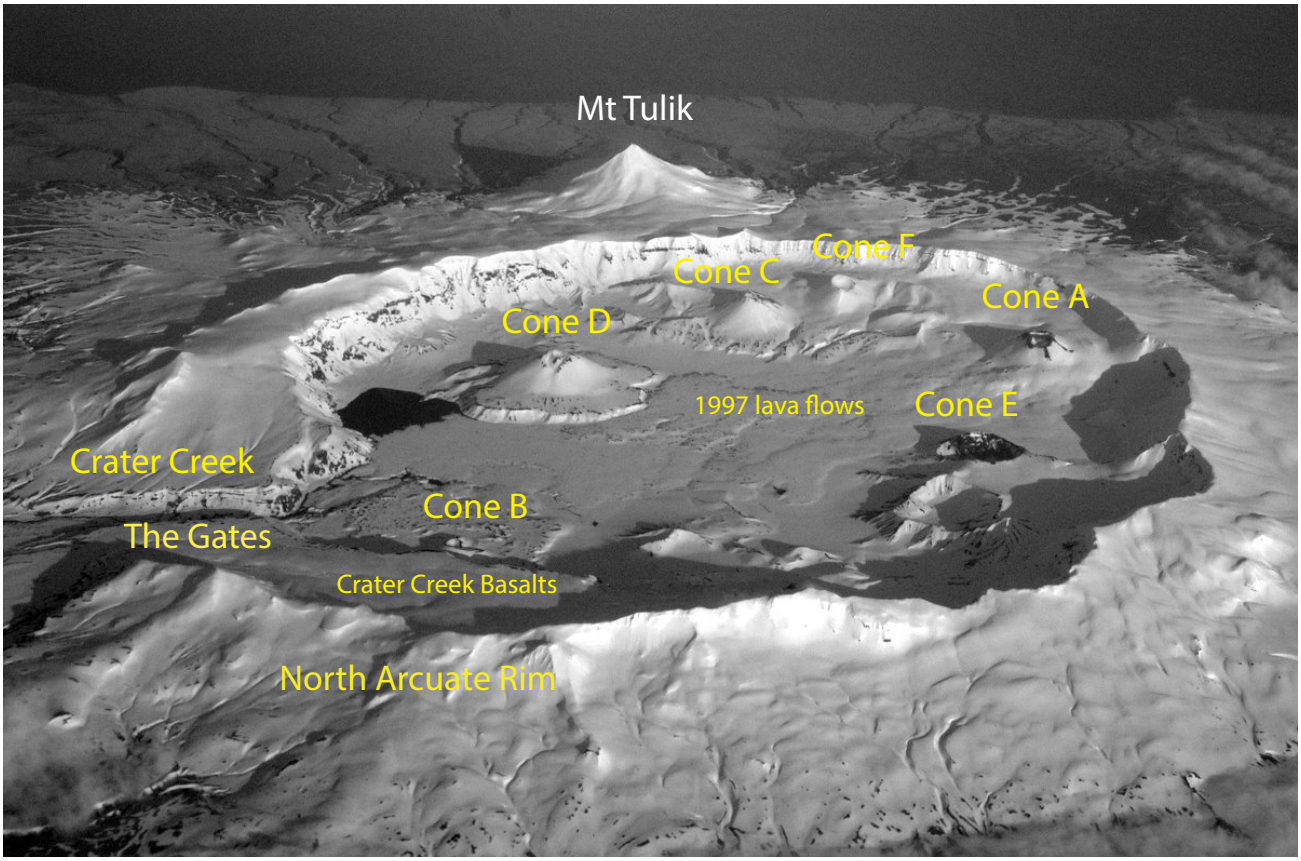

Figure 3. Okmok Caldera, looking south from an Alaska Airlines jet in early June 2007. This figure shows the locations of the most prominent cones within the caldera, cones A–F. Also shown are the locations of the Crater Creek Basalts, where they form a plateau inside North Arcuate Ridge, and the 1997 lava flows that spread across the caldera floor from their cone A source to the bench surrounding cone D approximately 5 km away. Photograph by Cyrus Read (USGS, AVO); AVO image database #13283.

erupted in 1997 (McGimsey and Wallace, 1999; Patrick and others, 2003).

Post-Okmok II eruptions have produced two primary types of volcanic landforms inside the caldera: 1) steep-sided cinder and spatter cones and their associated primarily ʻaʻā lava flow fields and 2) tuff cones with rilled, steep-sided ridges of semi-consolidated to loose pyroclastic debris from hydrovolcanic eruptions (fig. 3). The youngest example of a tuff cone is the informally named Ahmanilix, which lies in the eastern sector of the caldera and was created during the 2008 eruption (fig. 4; Larsen and others, 2015). Exposed postcaldera vents occur in two arcuate arrangements that parallel the caldera margins and are slightly elongated in a SSW–NNE direction, subparallel to the direction of convergence of the North American and Pacific plates (Mann and others, 2002; Larsen and others, 2013).

METHODS

A team of five geologists from AVO (UAF/GI and USGS partner agencies) began geologic work at Okmok Volcano in July 1998. Fieldwork was completely on foot, except for transportation to the Crater Creek region by passenger truck. For the next 2 years, repeat visits to the island in summer involved fieldwork largely on foot or via all-terrain vehicle (ATV). Beginning in June 2001, helicopter-supported geologic fieldwork was conducted during installation of a seismic network. The helicopter support facilitated access to important outcrop sites and helped accelerate the pace of mapping, stratigraphic work, and sample collection for geochemistry and geochronology. The last field season prior to the 2008 eruption was in September 2004, during which most of the focus was on completing the map and hazards report (Begét and others, 2005), describing the stratigraphy and ages of late Pleis-

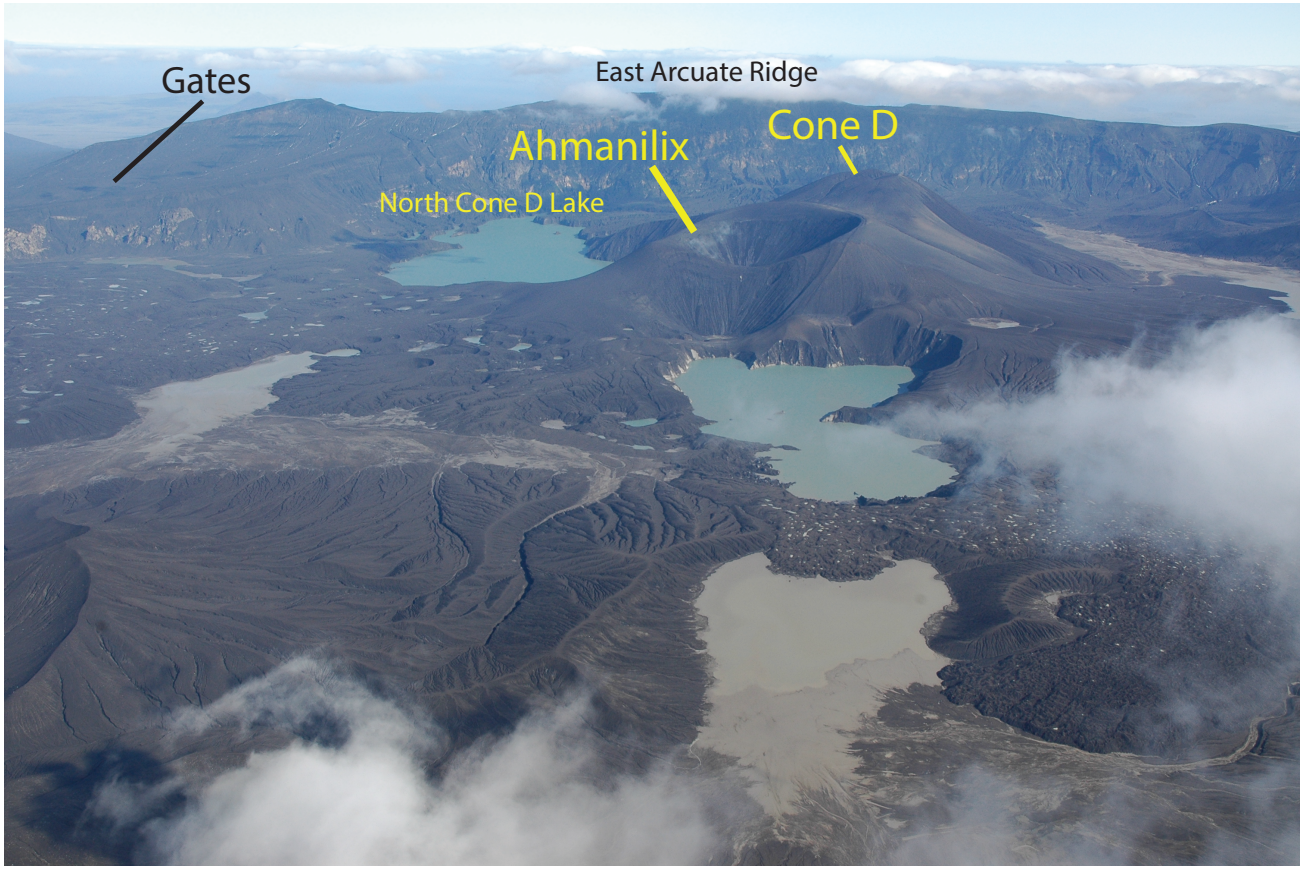

Figure 4. Oblique aerial photograph looking east, showing the Ahmanilix cone created during the 2008 eruption. Photograph taken on September 15, 2008, by Christina Neal (USGS, AVO); AVO image database #15478.

tocene to recent eruptions from Okmok Volcano, and sampling for geochronology and geochemistry. Our objective was characterization of the Holocene eruptive history of Okmok Volcano, so we focused on mapping and describing deposits that we recognized to be postglacial (~12,000 yBP). Other work focused on separating, sampling, and describing the two caldera-forming eruptions to better understand the potential for Okmok Volcano to produce highly explosive (VEI 4–6) eruptions (Larsen and others, 2007; Finney and others, 2008).

On July 12, 2008, with little warning, Okmok Volcano began a 5-week-long eruption characterized by sustained explosive phreatomagmatic activity. Geologists from AVO visited the island during the eruption from July 31 to August 3 and gathered estimates of plume heights, ash samples from the eastern flanks of the volcano, observations from residents and fishing vessels, and photographs of the state of the caldera floor in the eastern sector near the active vent, to the extent safely possible. After cessation of the eruption, a second AVO field team visited the island for a week in September 2008. This trip focused on measurements of ash deposit thickness in many places around the flanks and within the caldera, sample collection, reconnaissance stratigraphy, measurements of modified and new lake elevations, observations of lahar deposits and lahar deltas, and repair of geophysical monitoring equipment. Those observations, along with geophysical and remote sensing data from the eruptive period, were described in Larsen and others (2009, 2015).

Geologists from AVO and Northern Arizona University (NAU) returned to Okmok Volcano from July to August 2010 to perform a more thorough investigation of the 2008 eruptive products. The work focused on detailed mapping of 2008 deposits, including ballistics, ash fall, and surge deposits on Umnak Island. Detailed stratigraphy and physical volcanology work were performed by Michael Ort and Joel Unema of NAU (Unema and others, 2016). The team also resurveyed intracaldera lake elevations, documented erosion of the 2008 Ahmanilix tuff cone, and documented vents, pyroclastic deposits, and collapse features within the caldera. Additional juvenile samples were collected for petrology and geochemistry work published by Larsen and others (2013). While this map focuses on pre-2008 units and landforms, figures 22–31 include the 2008 geochemistry data for comparison with the other postcaldera units. A detailed description of the 2008 eruption chronology, landforms, and deposits is found in Larsen and others (2015) and in a physical volcanology study by Unema and others (2016).

Geographic Information System Procedures and Basemap

The geologic map was constructed in ArcGIS following the Alaska Geologic Mapping Schema (AK GeMS), an extension of the Geologic Mapping Schema (GeMS) of the USGS National Cooperative Geologic Mapping Program (Hendricks and others, 2021). Standard GIS techniques were used in compiling maps, incorporating field geologists' notes and sketches, and merging those with digitized, previously mapped units of Byers (1959). Basemap contours and shaded relief imagery were derived by combining pre-2008-eruption digital elevation model (DEM) data from both NASA's shuttle radar topography mission (SRTM) and the aircraft-mounted synthetic aperture radar (AirSAR) mission, as described in Schaefer (2005). Additional Okmok Volcano GIS basemap and metadata files can be found in Begét and others (2005). Geologic map data are presented in the World Geodetic System Datum of 1984 Universal Transverse Mercator Zone 2N projection (WGS84 UTM zone 2N).

Geochronology

$^{40}Ar/^{39}Ar$ Analytical Techniques, University of Alaska Fairbanks

Rocks were submitted for $^{40}Ar/^{39}Ar$ age dating to the geochronology laboratories at both the University of Alaska Fairbanks (UAF) and the USGS in Menlo Park.

For $^{40}Ar/^{39}Ar$ analysis at UAF, 12 samples were dated, with the data yielding the isochron

ages provided in the digital data; all ages are quoted to the ±1-sigma level and calculated using the decay constants of Steiger and Jäger (1977). The samples were crushed and washed, and whole-rock (groundmass) chips were selected for dating. The monitor mineral Taylor Creek Rhyolite (TCR)-2 sanidine with an age of 27.87 ± 0.04 Ma (Lanphere and Dalrymple, 2000) was used to monitor neutron flux (and calculate the irradiation parameter, J). Ages were recalculated with a TCR-2 sanidine age of 28.344 ± 0.011 Ma (Fleck and others, 2019) for direct comparison with USGS data. Samples and monitor minerals were wrapped in aluminum foil and loaded into aluminum cans of 2.5 cm diameter and 6 cm height, which were irradiated in position 5c of the uranium-enriched research reactor of McMaster University in Hamilton, Ontario, Canada, at 20 megawatt-hours.

Upon return from the reactor, samples and monitor minerals were loaded into 2-mm-diameter pits in a copper tray that was then loaded into an ultrahigh vacuum extraction line. Monitor minerals of TCR-2 were fused, and samples heated, using a 6-watt Ar-ion laser following the technique described in York and others (1981), Layer and others (1987), and Layer (2000). Purification of Ar was achieved using a liquid nitrogen cold trap and a SAES Zr-Al getter at 400°C. Samples were analyzed in a VG-3600 mass spectrometer at the Geophysical Institute of UAF. Isotopes of measured Ar were corrected for system blanks and mass discrimination, as well as Ca, K, and Cl interference reactions, following procedures outlined in McDougall and Harrison (1999). System blanks generally were 2 × 10–16 mol ^{40}Ar and 2 × 10–18 mol ^{36}Ar, which are 10 to 50 times smaller than fraction volumes. Mass discrimination was monitored by running both calibrated air shots and a zero-age glass sample. These measurements were made on a weekly to monthly basis to check for changes in mass discrimination.

For each sample, one or two step-heating runs of four to seven steps of increasing laser power were done, with the last step being fusion of the sample. For samples with a single run (04NYOK001 and 04NYOK011), isochron ages were calculated using all steps. For samples with duplicate runs, the step data were combined; from this stacked data, isochron ages were calculated and used in the final interpretation.

^{40}Ar/^{39}Ar Analytical Techniques, USGS Menlo Park

Analysis of ^{40}Ar/^{39}Ar geochronology was performed on 17 groundmass samples separated by crushing, sieving, and magnetic techniques, with 14 samples yielding interpretable results. Samples were handpicked under a binocular microscope. For irradiation, 80–130-mg separates were packaged in Al foil and placed in a cylindrical quartz vial, together with fluence monitors of known age and K-glass and F to measure interfering isotopes of K and Ca. Quartz vials were wrapped in 0.5-mm-thick Cd foil to shield samples from thermal neutrons during a 1-hour irradiation in the central thimble of the USGS TRIGA reactor in Denver, Colorado (Dalrymple and others, 1981). The reactor vessel was rotated continuously during irradiation to avoid lateral neutron flux gradients and oscillated vertically to minimize vertical gradients. Reactor constants determined for the TRIGA irradiations were indistinguishable from recent irradiations, and a weighted mean of constants obtained over the past five years yields ^{40}Ar/^{39}Ar K = 0.0010 ± 0.0004, ^{39}Ar/^{37}Ar Ca = 0.00071 ± 0.00005, and ^{36}Ar/^{37}Ar Ca = 0.000281 ± 0.000006. Bodie Hills sanidine (BHs; Fleck and others, 2019) was used as a fluence monitor with an age of 9.7946 ± 0.0031 Ma. Sanidine from BHs is a secondary standard calibrated against the primary intralaboratory standard, GA1550 biotite, which has an age of 98.79 ± 0.96 Ma (McDougall and Wellman, 2011). Fluence monitors were analyzed using a continuous CO_2 laser system and MAP216 mass spectrometer described in Dalrymple (1989). Unknowns were incrementally heated in 10 to 15 steps from 450 to 1200°C with a continuous diode laser system, then analyzed on the MAP216 spectrometer. Samples were degassed to either 400 or 500°C before analysis to drive off hydrocarbons,

water, and other unwanted materials, and these were measured by a Granville-Phillips Series 835 vacuum quality monitor. Gas was purified continuously during extraction using two SAES ST-175 getters operated at 4A (300°C) and 0A (room temperature).

Mass spectrometer discrimination and system blanks are important factors in the precision and accuracy of $^{40}Ar/^{39}Ar$ age determinations of Pleistocene samples because of low radiogenic yields. Discrimination is routinely monitored by analyzing splits of atmospheric Ar from a reservoir attached to the extraction line. Instrumental mass discrimination was calculated by repeated measurement of air, assuming atmospheric $^{40}Ar/^{36}Ar = 298.56 \pm 0.31$ (Lee and others, 2006). Ages were calculated using the decay constants recommended by Steiger and Jäger (1977). Uncertainties in $^{40}Ar/^{39}Ar$ ages are reported at the one-sigma level unless otherwise noted (app. A) and include propagated uncertainties in counting statistics and J values. Typical system blanks including mass spectrometer backgrounds were 1.5×10^{-18} mol of m/z 36, 9×10^{-17} mol of m/z 37, 3×10^{-18} mol of m/z 39, and 1.5×10^{-16} mol of m/z 40, where m/z is mass/charge ratio.

Radiocarbon Age Dates

Radiocarbon dating (conventional and Accelerator Mass Spectrometer [AMS]) of organic material to constrain eruption ages was carried out using Beta Analytic and Geochron Laboratories (app. B). Datable material was found typically in soils beneath tephra fall or pyroclastic density current deposits on the lower flanks of the volcano. Dating of wood and carbonized vegetation found within surge deposits was also possible in several cases. All samples were cleaned thoroughly by hand of modern plant material prior to submittal to the lab. Soil samples were treated prior to analysis in the lab by dispersion in water, isolating organic matter using agitation and ultrasound. Modern rootlets were screened with a nylon filter, and the remaining clay and organic fraction were subject to both acid and alkali washes. The humic acid fraction was precipitated, filtered, dried, and combusted in O_2 to produce CO_2 for analysis. Ages of the two caldera-forming eruptions are well constrained by this method. A compilation of dates and laboratories is provided in the digital data.

Geochemical Analyses

Whole-rock geochemical analyses of juvenile lava, pumice, and scoria involved collecting relatively unaltered samples in the field. We hand-picked pumice and scoria from host pyroclastic units and trimmed lava samples with a hammer, cleaned them in de-ionized water in an ultrasonic bath to remove surface ash and soil where necessary, and then dried them for several days at 65°C. Samples were crushed to <1-cm-sized chips or sent whole to the GeoAnalytical Lab at Washington State University (WSU) for processing. Major and trace element analyses of samples representing mapped eruptive units can be queried from the AVO Geochemical Database (www.avo.alaska.edu/geochem/; Cameron and others, 2019). Wavelength-dispersive X-ray fluorescence (WD-XRF) spectrometry was conducted following the methods outlined in Johnson and others (1999). Inductively coupled plasma-mass spectrometry (ICP-MS) for trace elements was conducted following the procedures described in Knaack and others (1994). Trace element analyses collected via ICP-MS from the WSU GeoAnalytical Lab prior to 2007 were re-calibrated to make all analyses in the AVO database internally consistent (Nye and others, 2018).

GEOLOGIC MAP UNITS

The present map includes some reorganization of the nomenclature of Byers (1959), reflecting new age dates and interpretations of volcanic deposits. For example, many of the lavas are now classified either by $^{40}Ar/^{39}Ar$ or radiocarbon age, or constrained by whether they exhibit features indicating contact with ice or subaerial extrusion. In the description of map units, where relevant, we indicate the original unit name given by Byers (1959). Divisions of geologic time follow the major chronostratigraphic and geochronologic units presented in the International Chronostratigraphic Chart (Cohen and others, 2013).

The full extent of Okmok Volcano geologic map units is shown on map sheet 1 at a scale of 1:63,360. To better represent the complexity of intracaldera geologic units, map sheet 2 shows Okmok Caldera units at a scale of 1:24,000. All geologic map units are combined in one digital geospatial database following the AK GeMS standard of Hendricks and others (2021). Map station and sample location maps are shown on sheets 3 and 4. Hundreds of images of Okmok Volcano, including those images referenced in the figure captions, can be found on the AVO public website in a searchable image database (Cameron and others, 2022; Cameron and Snedigar, 2016).

Pleistocene Volcanic Rocks of Central Umnak Island

The oldest rocks exposed in the map area are the central Umnak volcanics in the southwest sector near Inanudak Bay. These were first mapped by Byers (1959) as hydrothermally altered volcanic rocks and intensely altered, silicified potassium feldspathic rocks. Byers' (1959) original linework and most rock descriptions in this region are preserved; however, unit names and abbreviations have changed with our updated mapping, with the following renamed from Byers' (1959) mapping unit QTv is renamed "Qvsw," QTvq is renamed "Qvq," and QTvp is now "Qvp." No age dates were obtained for these rocks during this study, nor were the deposits visited by the authors. Byers (1959) suggested an age of middle Tertiary to early Quaternary; however, Nye and others (1992) dated stratigraphically equivalent rocks in the Geyser Bight area (their unit Qcuv), just southwest of the map area, and obtained a K/Ar age of 786 ± 21 ka in the upper part of the section and K/Ar ages as old as 1,124 ± 48 ka at the base. Thus, the oldest deposits in this region are now interpreted to be early Pleistocene.

Quaternary flows in this region (vent deposits of units Qfsw and Qc) were visited during the geologic mapping fieldwork. Lava flow morphology is preserved in both the upper flows (140 m to more than 500 m elevation) and is especially apparent in the Cinder Point flow, just above sea level, indicating that these flows did not experience extensive glaciation, and are therefore likely late Pleistocene to early Holocene. Cinder Point is a ~180-m-high cinder cone on the northeast edge of Inanudak Bay and is the source vent for the two lobate Cinder Point lava flows.

Pleistocene Volcanic Rocks Older than the Modern Okmok Volcano Edifice

Ashishik ridge and Cape Idak form two prominent ridges, built from stacks of basaltic lava flows, along the north and northeast flanks of the Okmok Volcano shield. They are composed of the "mafic phenocryst basalt," as named by Byers (unit Pfm, formerly QTam of Byers, 1959), and the more plagioclase-rich lava flows of unit Pfo (formerly QTab of Byers, 1959). The Ashishik Basalt (just south of Ashishik Point) has an eruption age of ~2 Ma (Bingham and Stone, 1972). Stone and Layer (2006) attempted $^{40}Ar/^{39}Ar$ age dating on 14 flows from the Ashishik flow sequence. Problems with excess argon led the authors to conclude that the average age of 1,869 ± 116 ka from nine of the samples is likely too old. Based on the inferred stratigraphic position and reversed magnetic polarity, Stone and Layer (2006) suggested a probable age of younger than 1.77 Ma. A weighted average $^{40}Ar/^{39}Ar$ plateau age of 1,822 ± 41 ka was reported for one of 19 flows in a 150-m-thick flow package in the New Jersey Creek region that mostly underlie the Ashishik ridge lavas (NJC903 flow 11; Stone and Layer, 2006).

The second prominent ridge forms Cape Idak northeast of Okmok Caldera. The high-MgO picrite lavas forming the base of Cape Idak (Nye and Reid, 1986) are similar in age to the Ashishik sequence, and a single $^{40}Ar/^{39}Ar$ age of 1,910 ± 113 ka was obtained from a mafic-phenocryst-rich basalt from Cape Idak (unit Pfm from this study). Currently, the basaltic lavas that form Ashishik ridge and the lavas of Cape Idak are interpreted as belonging to an older volcanic center, not the modern Okmok Volcano edifice.

Pleistocene Flank Lavas

Other Pleistocene volcanic deposits exposed on the Okmok Volcano flanks include tuyas, near-vent lava plugs, and related lava and pyroclastic deposits. We have separated the tuyas and related deposits into three subunits to better represent their origins: subglacial and subaerial lavas (unit Ptf) are thinly bedded and show clear ice-contact textures; unit Pth represents the fragmental pyroclastic flow, pillow fragment breccia, and hyaloclastite deposits that form the benches around the tuyas; and unit Ptv comprises the near-vent plug lavas that form the highest relief portion of the tuyas.

Jag Peak (southwest flank) and Tulik Volcano (southeast flank) are the most prominent examples of the ice-contact flank vents and tuyas in the map area. In the southwest flank region, four other prominent peaks surrounded by lava and pillow fragment breccia benches in the vicinity of Jag Peak are also interpreted to be tuyas (tuyas 1, 2, 3, and 4; fig. 2; sheet 1). Lava samples from tuya 3 and tuya 4 yield $^{40}Ar/^{39}Ar$ ages of 1,095 ± 28 to 1,989 ± 237 ka (samples 04NYOK045 and 04JLOK013; app. A). Pyroclastic units and lava flows showing pervasive ice-contact features (e.g., hyaloclastites, pillow fragment breccias, microcolumnar jointing) form bench structures around the base of these old tuyas. Outcrops along the beach near Kettle Cape are also interpreted as remnant tuyas and have peperite-like textures, with fragments of quenched basaltic dikes within pyroclastic flow deposits (fig. 5).

High on North Arcuate Ridge is a rhyolite lava flow (unit Pr; fig. 6) likely Pleistocene, described by Byers (1959) as a "biotite-phyric, high-silica rhyolite." The rhyolite lava flow extends along a ridge to the northwest from the upper flank of the caldera. The flow consists of dense black obsidian zones interlayered with light-pink, finely vesicular bands. Talus extends outward from the rhyolite lava flow outcrop, covering contacts with adjacent map units. Small inclusions (~1 to 3 cm in size) with basaltic andesite compositions exist within the obsidian (Byers, 1959) and are observed in hand sample 04JLOK023a. A sample from a nearby basaltic lava flow of unit Ps returns an age of 153 ± 32 ka (app. A), but whether that lava flow underlies or flowed around the rhyolite lava is not known. Archaeologists have described the earliest use of this obsidian by humans at ca. 9 ka (Cook, 1995; Reuther and others, 2011).

Near the "Gates" region of Crater Creek, several exposed dikes and glassy lava flows show evidence of ice-contact or even subglacial emplacement (fig. 7; units ml and pal). A Pleistocene vitreous andesite (unit ml, formerly Qva of Byers, 1959) is comprised of glassy lavas and dikes containing zones of lava pillows and microcolumnar joints; in general, this unit appears highly shattered. Unit pal includes palagonitized, hyaloclastite-like pyroclastic deposits containing dike material that spalled off into quenched enclaves. We interpret these deposits to represent subglacial eruptions and infer their correlation with other, isolated outcrops of highly palagonitized pyroclastic flow units scattered around the flanks of Okmok Volcano (unit Pg). One sample (01NYO-23) of glassy andesite from the Gates region's hyaloclastite returned an undetermined $^{40}Ar/^{39}Ar$ age when the large error bar was considered. However, the extensive ice-contact features of those units and their existence low within the caldera walls in the Gates region indicate a likely Pleistocene age, given that the modern extent of ice in the caldera is limited to a small patch along the southwestern caldera wall.

Basaltic lava outcrops (units Ps and Pg) high around the North and East Arcuate Ridges show evidence for subaerial extrusion, ice-contact, and glaciation features, which are consistent with the Pleistocene ages obtained from $^{40}Ar/^{39}Ar$ analyses (fig. 8). The edifice-building Ps lavas are dated via $^{40}Ar/^{39}Ar$ to be between ~38 and 364 ka (app. A). On the northwest flank, east of Aguliuk Point, a glaciated remnant of a fissure vent (unit Pv) feeding a stacked series of lava flows (unit Pfnw) is exposed (fig. 9), representing another Pleistocene flank vent. This vent has pyroclastic flow material from one or both caldera-forming eruptions (~11,540

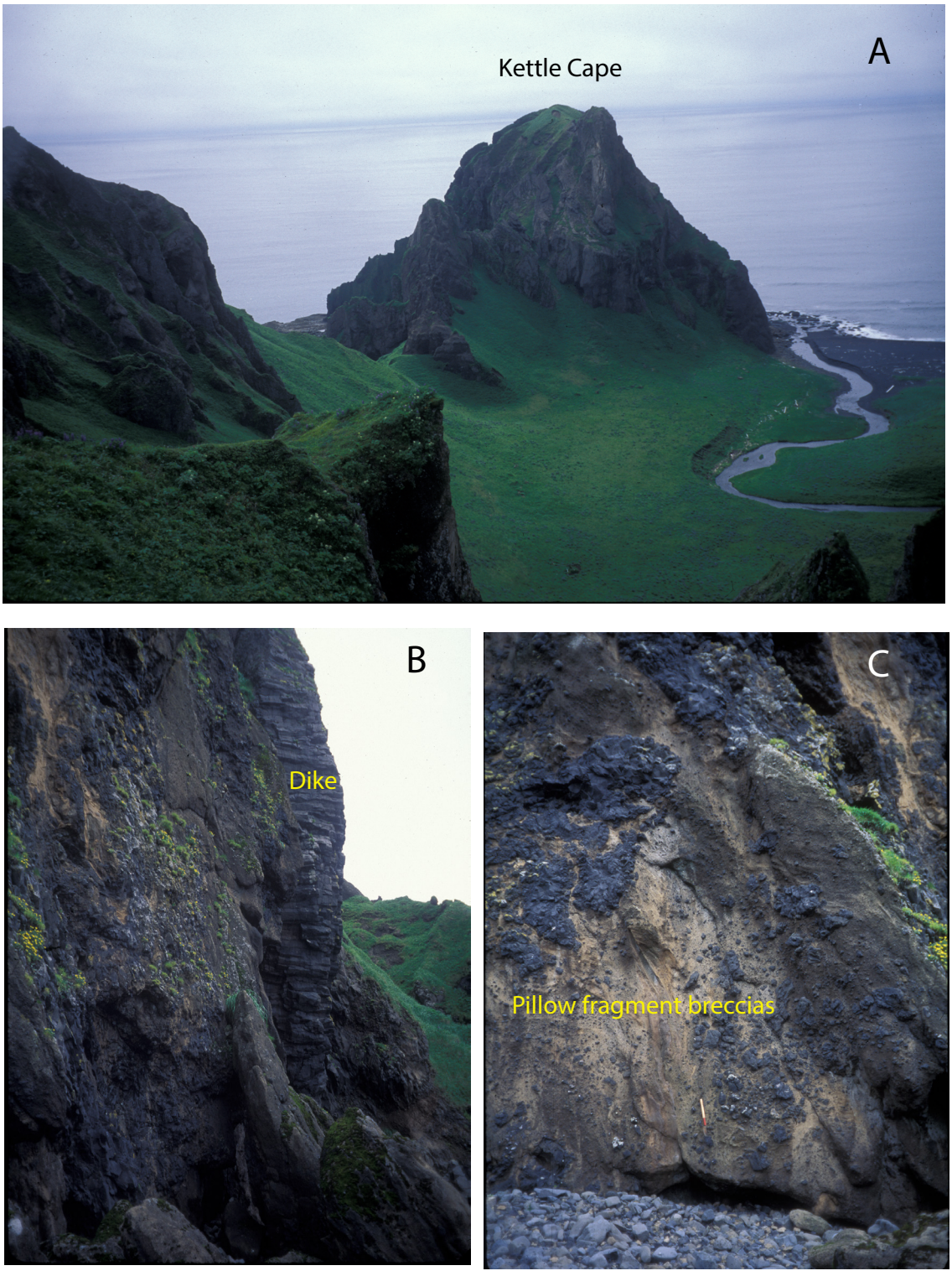

Figure 5. Photographs of Kettle Cape and peperite deposits, as examples of vent, subglacial, ice, and water-contact volcanic deposits on Umnak Island (units Pbv and Ptv). **A.** Photograph looking south over Kettle Cape; ca. 80 ka (app. A) remnant of a subglacial volcanic vent, or tuya. AVO image database #175541. **B.** Dike-intruding fragmental deposits, including hyaloclastite, palagonitized pyroclastic material, and pillow fragment breccias. The dike is approximately 1 m wide at this location; photograph taken on east side of Kettle Cape at beach level. AVO image database #175551. **C.** Mafic lavas breaking into pillow fragment breccias within palagonitized pyroclastic material; a ~0.5-m-long trowel shown for scale. AVO image database #175561. Photographs by Jessica Larsen (UAF/GI, AVO).

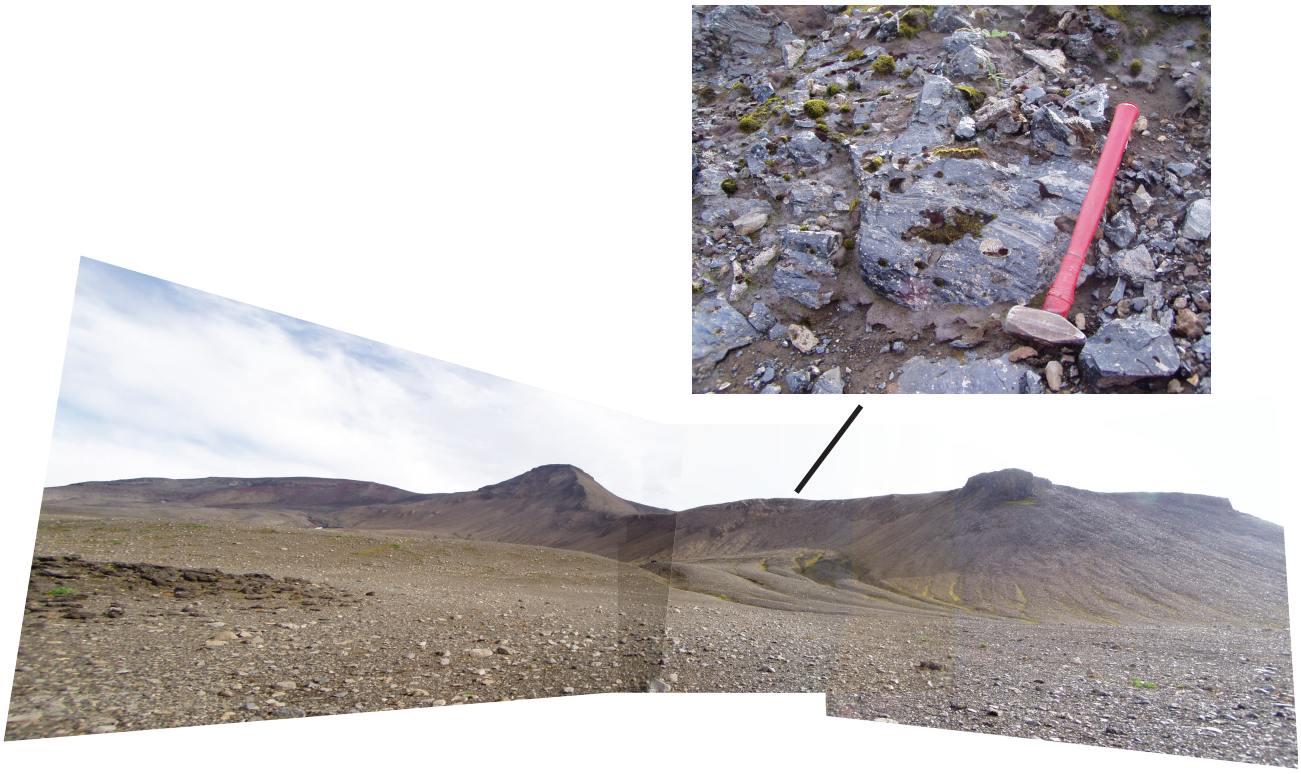

Figure 6. Photograph of rhyolite obsidian lava flow outcrop (unit Pr) located at approximately 840 m elevation on North Arcuate Ridge, taken from a lower elevation northeast of the flow (station 04JLOK023; sheet 3). Rhyolite is rare among Aleutian volcanic rocks, with obsidian being extremely rare. This outcrop has received great interest because it has been identified as the single source of obsidian used for tools by the Unangan in prehistoric time throughout the Aleutian Islands (Cook, 1995; Jeff Speakman, Smithsonian Institution, written commun., 2008; Reuther and others, 2011). Photograph by Jessica Larsen (UAF/GI, AVO); AVO image database #175571.

and 2,050 yBP) draping a low saddle along the fissure, indicating it is probably older than latest Pleistocene.

Late Pleistocene–Holocene Volcanic Rocks of Okmok Volcano

Okmok I Caldera-Forming Eruption

Late Pleistocene through Holocene volcanism on Umnak Island is dominated by Okmok Volcano's two caldera-forming eruptions, both of which produced voluminous pyroclastic density current deposits that blanketed the flanks of the volcano (fig. 10) and reached the Bering Sea and Pacific Ocean. The first eruption (Okmok I), referenced on the map as unit Pcfe1, has an estimated radiocarbon age of ~11,540 ± 40 ^{14}C yBP (13,086–13,794 cal yBP), based on an average of two soil samples collected beneath Okmok I deposits on western Unalaska Island (app. B; Begét and others, 2005; this study). Okmok I represents a catastrophic, large-volume explosive eruption that produced more than 30 km^3 of pyroclastic deposits on Umnak Island and is estimated to be at least a VEI 6 (e.g., Miller and Smith, 1987; Larsen and others, 2007). Still, outcrops of Okmok I deposits are rare, and limited to deeply incised channels on the flanks of the volcano and sea cliffs along the northern coast of Umnak Island. Okmok I deposits are often difficult to distinguish from Okmok II and the Pleistocene palagonitized pyroclastic flow deposits mapped by Byers (1959), especially at higher elevations on the volcano, and were in fact not differentiated by Byers (1959); however, one of the new features of the present map is an estimate of the outcrop distribution of Okmok I (Pcfe1). Complete sections of Okmok I are generally absent on Umnak Island, though correlation

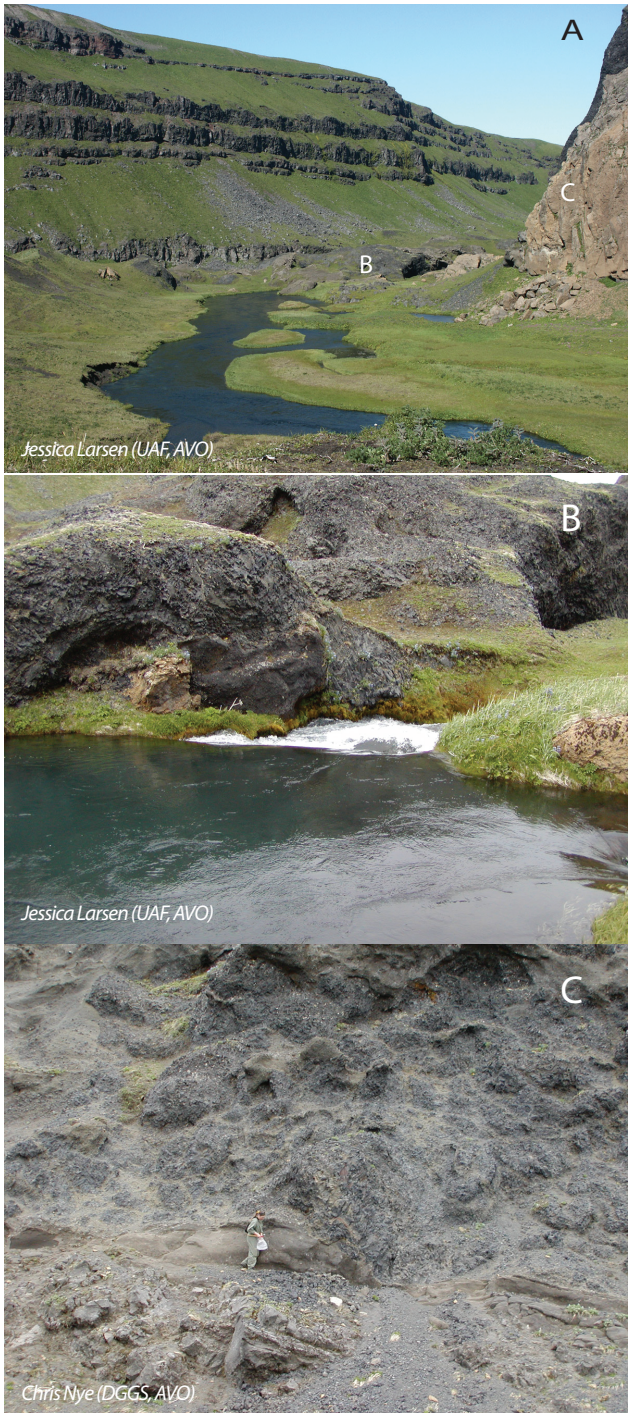

Figure 7. Photographs of ice-contact features in the Gates region of the caldera. **A.** Overview photograph of the Gates region and the thick sequence of Crater Creek Basalt lava flows. The locations of outcrops shown in (B) and (C) are annotated on this photograph. AVO image database #175581. **B.** Vitreous andesite (unit ml) outcrop on the caldera floor within the Gates. AVO image database #175591. **C.** Base of caldera wall showing ice-contact features in dikes contained within palagonitized hyaloclastite deposits (unit pal). AVO image database #175601.

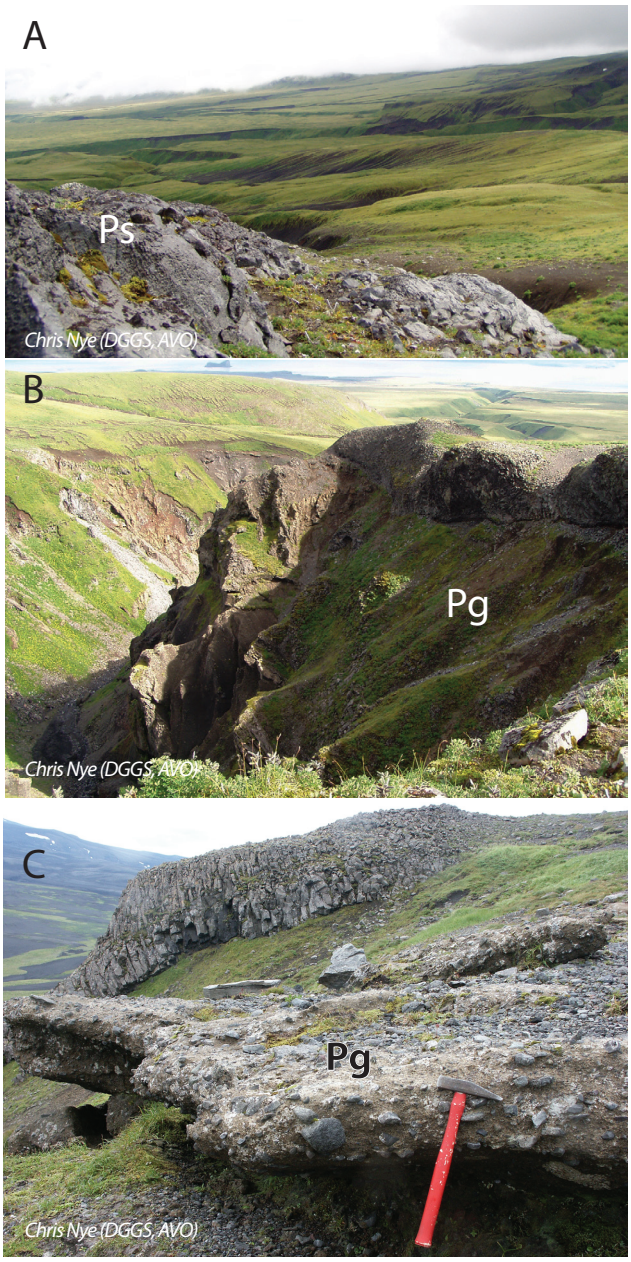

Figure 8. Photographs showing examples of units Ps and Pg outcropping on the flanks of Okmok Caldera. **A.** Example of subaerial basalt lavas from the cone-building sequence, represented by unit Ps. The outcrop in the foreground is labeled as approximately 1.5 m in height. AVO image database #175611. **B.** Unit Pg deposits that form the prominent bench surrounding the base of Tulik Volcano. Those deposits are notable, consisting of pillow fragment breccias, hyaloclastite with palagonitized fragmental material, and lavas with distinct features related to ice- and water-contact volcanism. The view is looking east at an outcrop above a stream channel approximately 20 m deep in the field of view. AVO image database #175621. **C.** Another example of unit Pg outcropping from the bench of one of the tuyas located to the southwest of Okmok Caldera; hammer in foreground shown for scale. AVO image database #175631

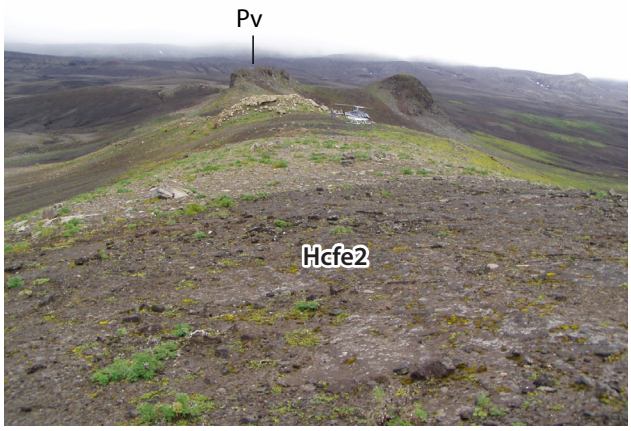

Figure 9. Photograph of the fissure vent (unit Pv) on the north flank of Okmok Volcano, looking south up toward the north rim of the caldera. At this location, the Pv unit is draped with pyroclastic flow deposits from the Okmok II caldera-forming eruption (unit Hcfe2). The helicopter to the right of the Pv outcrop is shown for scale. Photograph by Jessica Larsen (UAF/GI, AVO); AVO image database #175641.

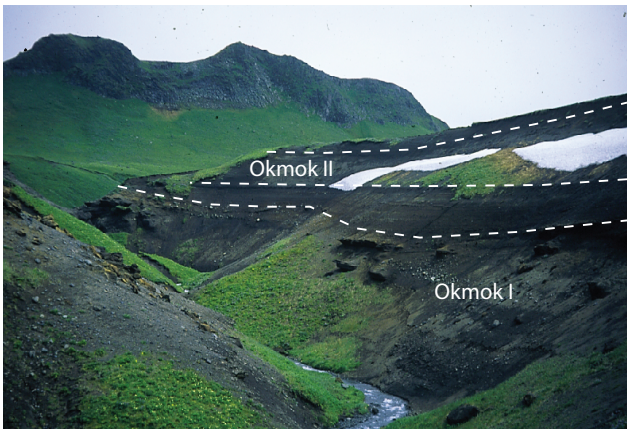

Figure 10. Outcrop in Camp Creek drainage showing Okmok I and II deposits separated by thin scoria beds. Outcrop location is station 98JLOK6 (sheet 3). Figure after Larsen and others (2007). Photograph by Jessica Larsen (UAF/GI, AVO); AVO image database #179941.

of incomplete sections enables one to infer that the base rests on glacial till or basaltic lava along the north coast. The stratigraphy and volume (>30 km^3) estimates of the Okmok I eruption sequence are described in more detail in Larsen and others (2007). However, it is worth noting that pyroclastic density currents and fallout from Okmok I apparently interacted with glacial ice on the flanks to create complex, chaotic deposits displaying soft-sediment deformation features, evidence of wet pyroclastic surges and lahars (fig. 11; see Larsen and others, 2007, for detailed information). Okmok I pyroclastic deposits also include abundant accretionary lapilli in many of the stratigraphic horizons, additional evidence for wet eruption conditions.

Okmok II Caldera-Forming Eruption

The second caldera-forming eruption, Okmok II, or Hcfe2 on the map, produced thick pyroclastic flow deposits that blanket the flanks around all azimuths and create the plateau-like tablelands topography of the volcano. Okmok II deposits were dated at 1,905 ± 25 ^{14}C yBP (app. B; this study) and 2,050 ± 50 ^{14}C yBP (Wolfe, 2001). The radiocarbon age of 1,905 ± 25 yBP (1,739–1,882 cal yBP) came from a carbon-rich layer directly below the rhyodacite pumice fall unit that marks the start of the Okmok II eruption. The radiocarbon age of 2,050 ± 50 ^{14}C yBP is from samples of charred plant fragments collected at Ashishik Point beneath the rhyodacite pumice fall horizon (Begét and Larsen, 2001). Previously, Miller and Smith (1987) reported an uncalibrated radiocarbon date of 2,400 ± 200 ^{14}C yBP, also from Ashishik Point. A weighted mean average age of 2,050 ± 30 ^{14}C yBP is cited in Wolfe (2001), with individual ages used in the average estimate presented in his table 7.2. We use the 2,050 ± 50 ^{14}C yBP (2,140–2,016 cal yBP) age for this event.

The stratigraphy and physical volcanology of Okmok II deposits are described in detail by Burgisser (2005) and Larsen and others (2007). In summary, this eruption began with a highly explosive Plinian phase from a vent along the present-day northern caldera rim (Burgisser, 2005), producing rhyodacite composition fall deposits that are thickest along northern coastal sections (fig. 12). The Okmok II type section described by Byers (1959) and Miller and Smith (1987) is located at Ashishik Point, at beach level. Another thick section occurs along Reindeer Creek, which is ~4 km west of Ashishik Point. The rhyodacite phase of the eruption also includes a small area of pyroclastic flow

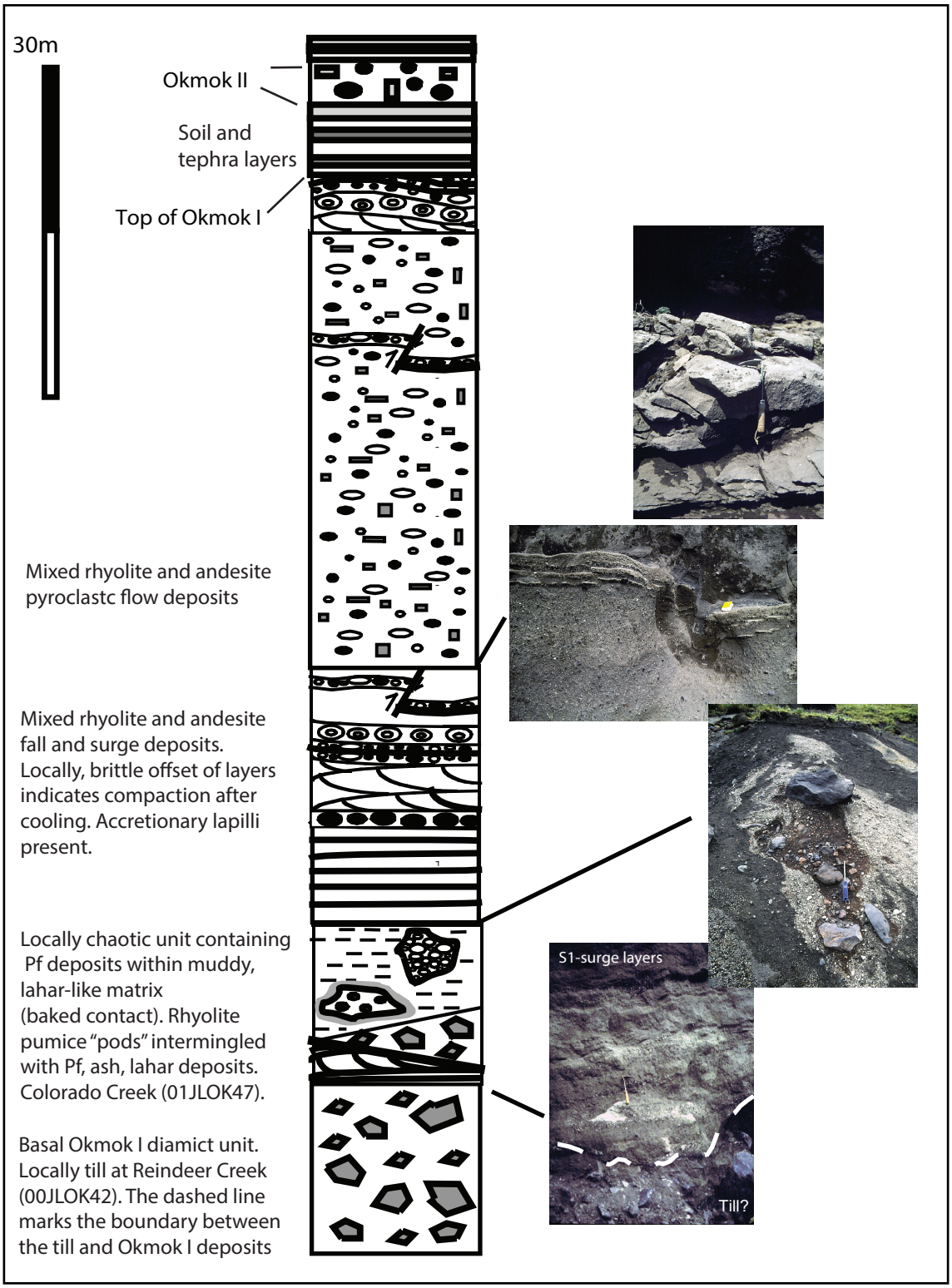

Figure 11. Stratigraphic section and photographs of Okmok I outcrops along the north flank at Reindeer Creek (station 00JLOK42) and Colorado Creek (station 01JLOK47; after Larsen and others, 2007). The photographs show examples of the unique structure and bedding within the Okmok I sequence found north of the caldera. Okmok I deposits are described in more detail in Larsen and others (2007).

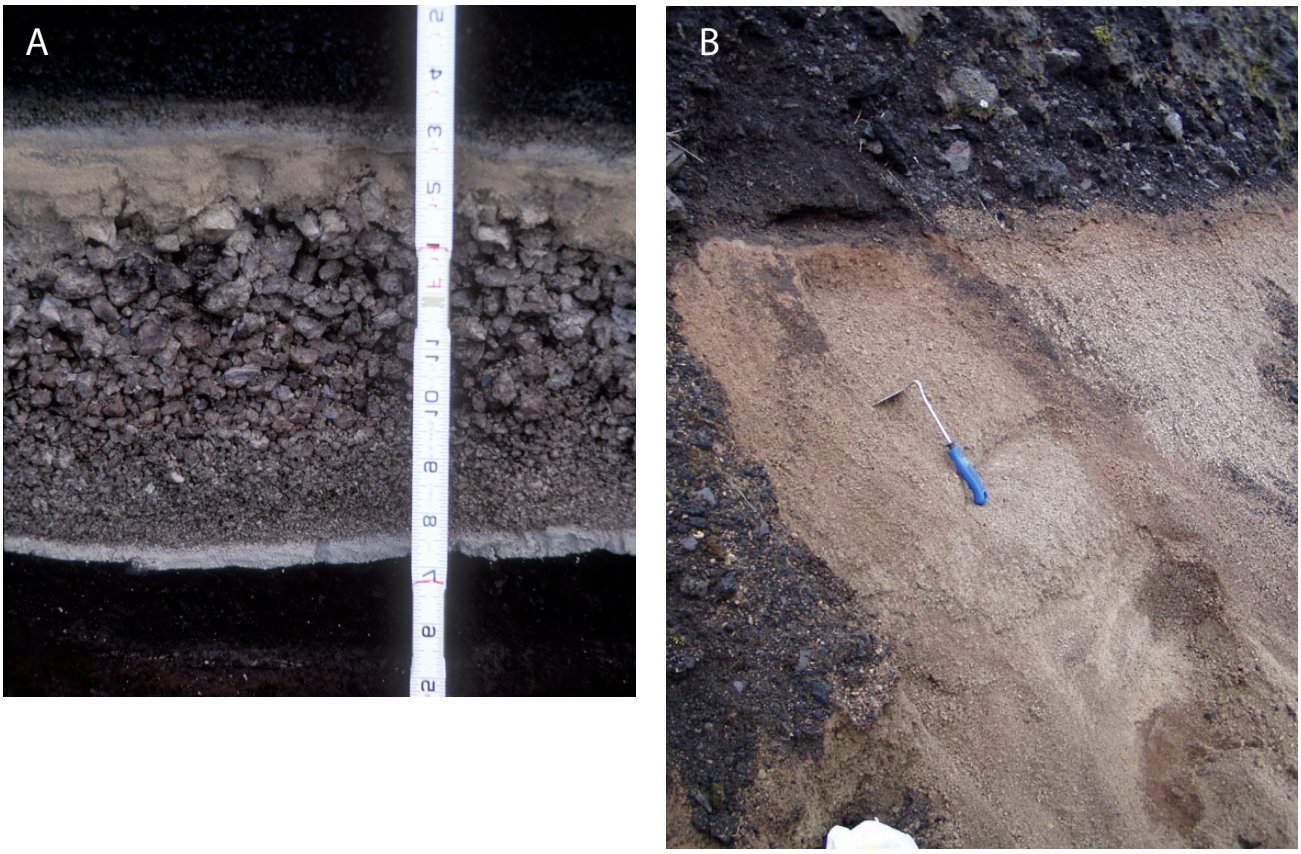

Figure 12. A. Okmok II rhyodacite Plinian fall deposit from the type location at Ashishik Point (station 98JLOK4; Byers, 1959; this study). At this location, the deposit is approximately 20 cm thick and shows layering consistent with more than one pulse in the eruption column (e.g., Burgisser, 2005). AVO image database #167241. **B.** There is only one outcrop located along the north flank (near Aguliuk Point; station 04JLOK049) that shows a pyroclastic flow deposit associated with the Okmok II Plinian rhyodacite eruption phase. The pyroclastic flow deposit here is at least 0.5 m thick, with the trowel shown for scale. AVO image database #175651. Photographs by Jessica Larsen (UAF/GI, AVO).

deposits found on the northwestern flanks near Aguliuk Point at location 04JLOK049 (fig. 12; sheet 3), most likely created by partial column collapse. The rhyodacite eruption phase was followed by an andesite phase from a vent near the eastern caldera rim region, producing fall deposits that were deposited predominantly on the northeast and east flanks of the volcano (Burgisser, 2005). The rhyodacite and andesite fall deposits are volumetrically minor components of the Okmok II eruption, estimated to be 0.25 km^3 and 0.35 km^3 dense rock equivalent (DRE), respectively (Burgisser, 2005). Most of the erupted Okmok II magma is basaltic andesite and resulted in voluminous (29 km^3 DRE) pyroclastic flow deposits (Burgisser, 2005).

The Okmok II basaltic andesite pyroclastic flow deposits display facies changes between poorly sorted ash-matrix-rich pyroclastic flows and spatter, and ribbon-bomb-rich agglutinate facies (Larsen and others, 2007). Sometimes these two facies are juxtaposed within short, ~100-m lateral distances (stations 04JLOK046 and 04JLOK047, northwest flank; sheet 3), indicating the primary eruption mechanism may have been changing within a short time period, or that lava-fountaining may have accompanied the sustained, explosive eruption column from which the pyroclastic flows originated during column collapse (fig. 13; Allen, 2004). A region along New Jersey Creek, close to the caldera rim, also shows welded tuff deposits in the Okmok II pyroclastic flow deposits. The surface of the Okmok II pyroclastic flow deposits includes

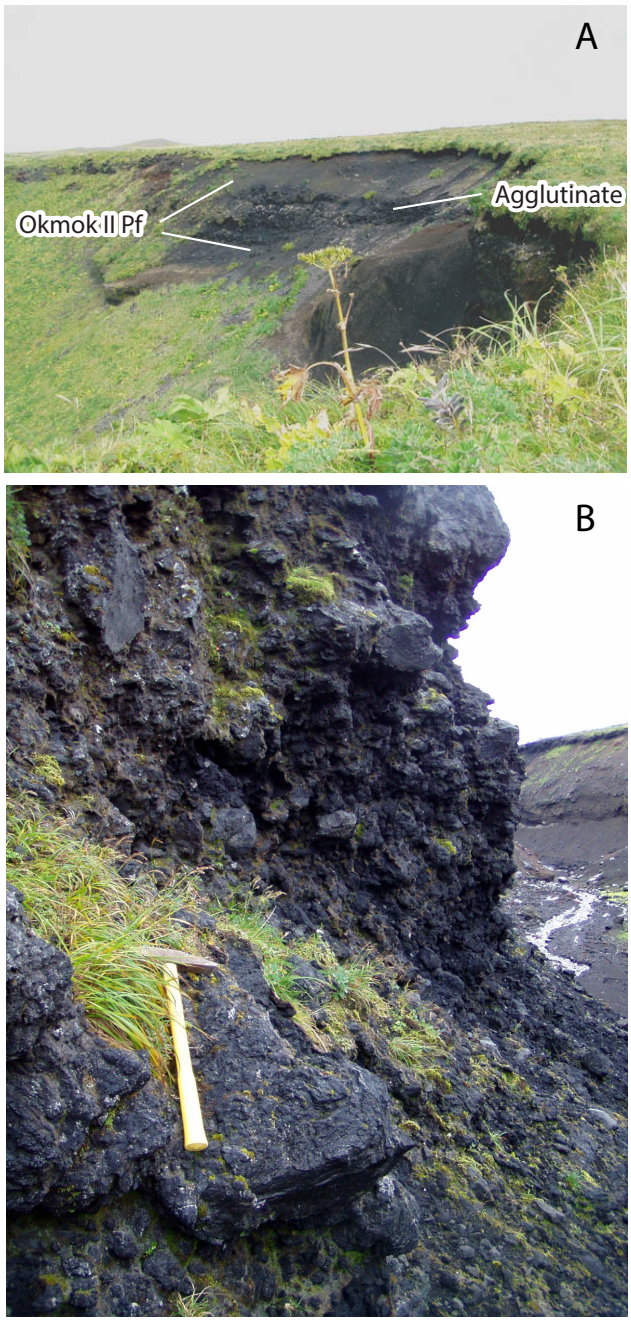

Figure 13. A. Okmok II basaltic andesite pyroclastic flow with the agglutinate facies outcropping at midstratigraphic height within the fines-rich Okmok II pyroclastic flow unit (downstream of station 04JLOK050, Colorado Creek, northwest flank). The view is looking north. AVO image database #175661. **B.** Close-up view of the agglutinate facies of the Okmok II ash-flow sheet (station 04JLOK50). Ribbon bombs reach 0.5 m across at this location. AVO image database #175671. Photographs by Jessica Larsen (UAF/GI, AVO).

topography consistent with fumarole mounds and related features along the northwestern flanks and to the south of Tulik Volcano (Sheridan, 1970).

Collapse associated with the Okmok II event produced a nearly circular, 8- to 10-km-diameter caldera, which was more than 800 m deep based on the current maximum rim-to-floor elevation change. We recognize no deposits related to the climactic Okmok II caldera-forming eruption on the caldera floor, nor any evidence for significant postcaldera uplift. The caldera-forming deposits were likely buried by lava flows and pyroclastic material from postcaldera cone eruptions. The overall slope of the caldera floor from southwest to northeast suggests that collapse may have been asymmetric, with greater subsidence in the northeast; however, this may also be due to greater postcaldera eruptive vigor in the southwest sector or other factors.

Holocene Deposits Intermediate in Age to the Two Caldera-Forming Units

Two types of deposits predominantly erupted during the period between the two caldera-forming events. The Crater Creek Basalts (unit Hccb, formerly Qcb of Byers, 1959) form a prominent bench along the inner northern rim of the modern caldera and extending partway down Crater Creek. Despite the given name of "Crater Creek Basalt," this series of up to 15 successive lava flow deposits shows a compositional evolution from basalt to andesite (Finney and others, 2008; Larsen and others, 2013; fig. 14). The Crater Creek Basalts dip north-northeast away from the center of the caldera. The rhyodacite marker bed of the Okmok II caldera-forming eruption overlays the top of the Crater Creek Basalts along the northern caldera rim. Thus, field evidence indicates that those lavas were deposited in rapid succession from a relatively high cone that existed both within and atop the older caldera rim prior to the Okmok II caldera-forming event.

Between the two caldera-forming events, several eruptions from unknown vents produced thick sequences of mafic pyroclastic fall and surge deposits along the north, east, and south flanks of

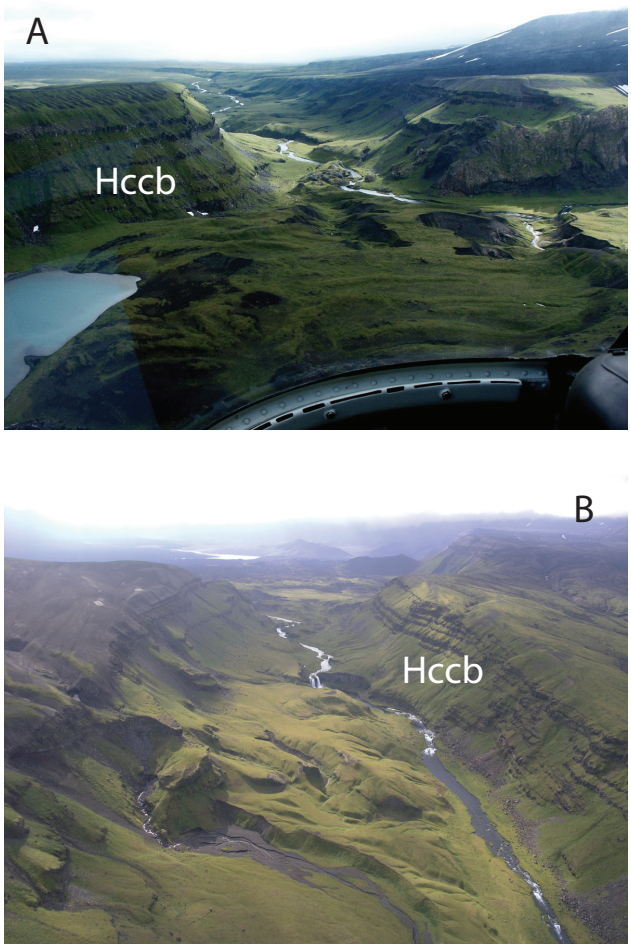

Figure 14. The stacked flows of the Crater Creek Basalt (unit Hccb). See figure 7 for an overview of Hccb lava flows in the Gates region of the caldera. **A.** Aerial view looking northeast out the Gates. Photograph by Chris Nye (DGGS, AVO); AVO image database #175681. **B.** View looking into the caldera from the north along Crater Creek, with the thick sequence of Crater Creek Basalt lava flows on the right (to the west of Crater Creek). Photograph by Jessica Larsen (UAF/GI, AVO); AVO image database #14814.

Okmok Volcano. Those deposits are not shown on the map because they are overlain by the Okmok II pyroclastic flows. The most prominent of those deposits, informally named the "Middle Scoria," was described in detail by Wong and Larsen (2010). The Middle Scoria eruption was likely an energetic, violent Strombolian to sub-Plinian phreatomagmatic eruption that deposited variably vesicular juvenile scoria and oxidized lithic fragments across the southeastern flanks of Okmok Volcano (fig. 15). The Middle Scoria eruption produced between 0.04 and 0.25 km^3 DRE tephra fall deposits primarily on Umnak Island. Deposits of the Middle Scoria unit were also found on the easternmost shore of Unalaska Island, across Umnak Pass. Although it is not represented on the map, it marks a significant explosive mafic eruption from Okmok Volcano in the mid-Holocene. Attempts to find datable material beneath Middle Scoria deposits have been unsuccessful.

Intracaldera Lake

Collapse calderas are natural catchment basins that often contain large, deep lakes. In 2008, before the July–August 2008 eruption at Okmok Volcano, a single lake that was ~1 km^2 in area and 30–60 m deep existed in the eastern sector of the caldera floor where it had been impounded by the 1958 lava flow. Wolfe (2001) and Wolfe and Begét (2002) reviewed evidence for formation and draining of a much more significant intracaldera lake following the Okmok II caldera-forming eruption at Okmok Volcano, an idea first proposed by Byers and others (1947).

Immediately after the Okmok II caldera collapse, the caldera was probably a closed basin many hundreds of meters deep, with no outlet. At some point, the caldera floor became able to impound surface water, perhaps as postcaldera hydrothermal processes altered caldera-collapse debris to clay minerals that could form a relatively impermeable zone leading to a slowly rising water column. By analogy to the historical Katmai and Pinatubo calderas, this process of "sealing" can occur within months to years (Motyka, 1977; Campita and others, 1996; Ingebritsen and others, 2020). Byers (1959) and Wolfe (2001) reviewed evidence that the lake was at least 150 m deep at its highest stand. Using a single Crater Creek discharge measurement from September 1946 (915 ft^3/s, or 23 m^3/s; Byers and Brannock, 1949) as a very rough proxy for precipitation input to the caldera basin, a 150-m-deep, 9-km-diameter lake with a volume of 9.54×10^9 m^3 would take little more than a decade to form. A single September 1946 discharge value is likely far too high an average for the entire

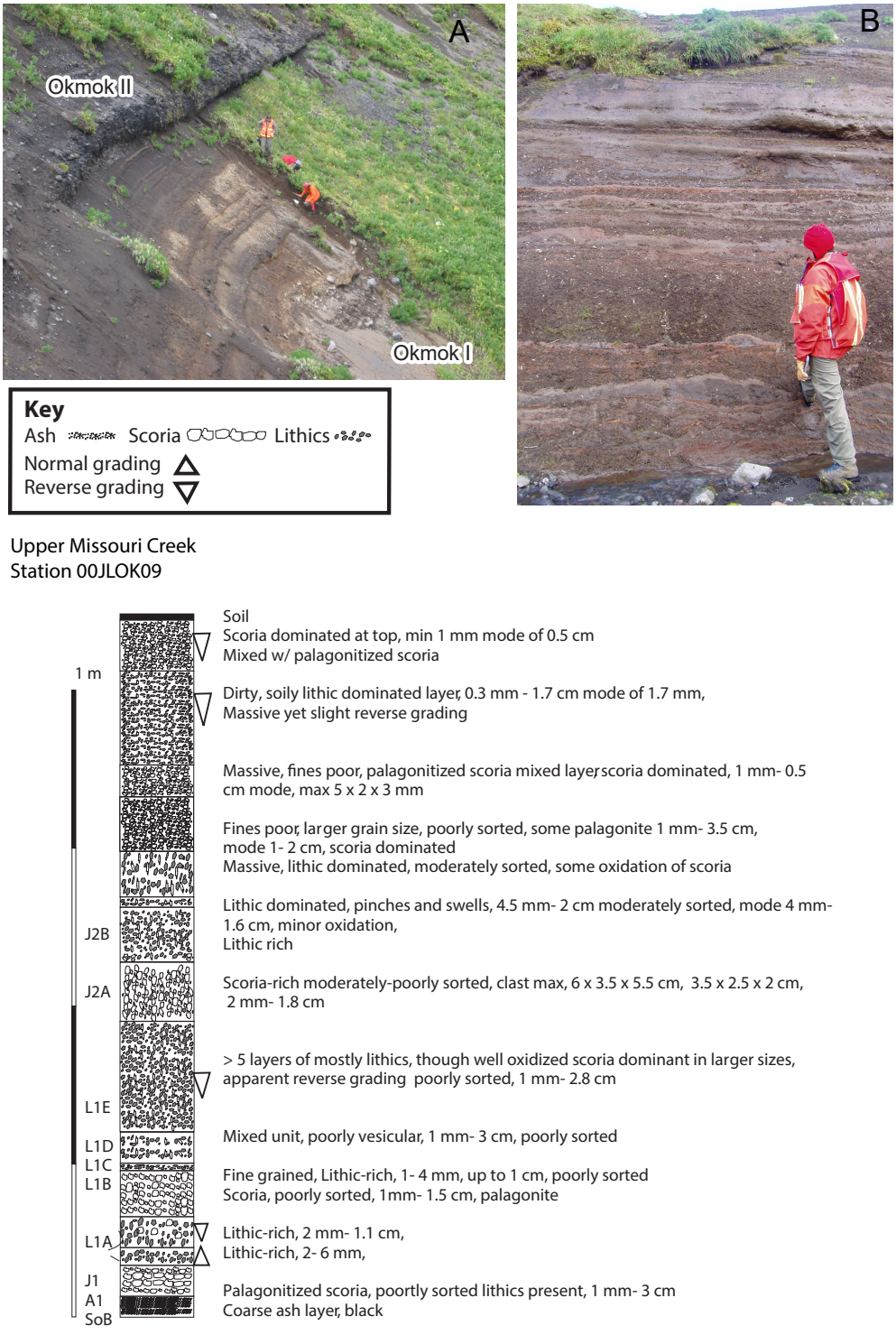

Figure 15. A. Intracaldera scoria beds of the basaltic andesite (53–55 wt. % SiO_2) Middle Scoria unit, showing relative local extent and thickness between Okmok I and Okmok II deposits (station 00JLOK29). The Middle Scoria deposits are not shown in the map but are described in detail by Wong and Larsen (2010). Photograph by Janet Schaefer; AVO image database #179961. **B.** Characteristic red oxidized nature of the Middle Scoria unit, which formed predominantly during an explosive phreatomagmatic episode that occurred over an unknown length of time. The stratigraphic section shown represents the section as pictured in (A), illustrating the cyclical nature of the repeating glassy juvenile scoria layers interspersed with poorly vesicular and lithic fragments. The contacts between individual layers are depositional. Figure after Wong and Larsen (2010). Photo: Jessica Larsen (UAF/GI, AVO); AVO image database #179971.

year, and this approach vastly simplifies a complex hydrologic system. Even with this over-estimate, it seems plausible that a large and deep lake could have formed within a century. Wolfe (2001) concluded that a large lake formed within 200 years of caldera formation, based on dated deposits reflective of sublacustrine intracaldera eruptions. For comparison, Nathenson and others (2007) reported a likely filling time of 420 years for 600-m-deep Crater Lake in Oregon, using far better data to constrain precipitation, leakage, and other hydrologic parameters.

The elevation above sea level of the highstand of a postcaldera lake was estimated to be 475 m by Byers (1959) based on the highest wave-cut terrace on the bench surrounding Cone D. Almberg (2003) and others remeasured this feature at an elevation of 510 m using a high-precision GPS. This elevation is approximately equivalent to a knickpoint on the north wall of the caldera gates, and we suggest the knickpoint represents the equilibrium elevation of the deep lake as it may have begun to overtop the post-Okmok II caldera wall. As explained below, the 510-m contour factors into interpretations of other volcanic features within the caldera.

The crater lake drained rapidly in a catastrophic flood along what is now the Crater Creek drainage within about 500 to 1,000 years of caldera formation, based on radiocarbon dating of tephra deposits atop flood deposits (Wolfe, 2001). The flood carved distinctive topography into bedrock and into the indurated Okmok II ash-flow sheet northeast of the volcano (fig. 16) and formed a conspicuous, boulder-rich depositional fan that extended offshore into the Bering Sea. Based on field evidence of pyroclastic surge deposits contemporaneous with flood deposits, Wolfe (2001) proposed an eruption trigger for overtopping and catastrophic failure of the caldera rim.

Following the lake drainage event, at least one subsequent significant lake is suggested by three wave-cut terraces on the northwest slope of Cone D, interpreted by Byers (1959) as evidence of a second lake following the catastrophic flood. Wolfe (2001) presented evidence for a second, smaller flooding event associated with the 1817 eruption of Cone B based on stratigraphy, radiocarbon dating, and historical accounts. The 2008 eruption also produced flooding down Crater Creek, suggesting that lake development and flooding events related to eruptions have likely occurred multiple times since caldera formation.

The modern (pre-2008) caldera lake shown in this map was formed primarily by damming of the north caldera drainage system by the 1958 lava flow. More than a decade prior to the 1958 eruption, however, Byers (1959) noted a small, shallow lake north of Cone D "at an altitude of 1,075 feet

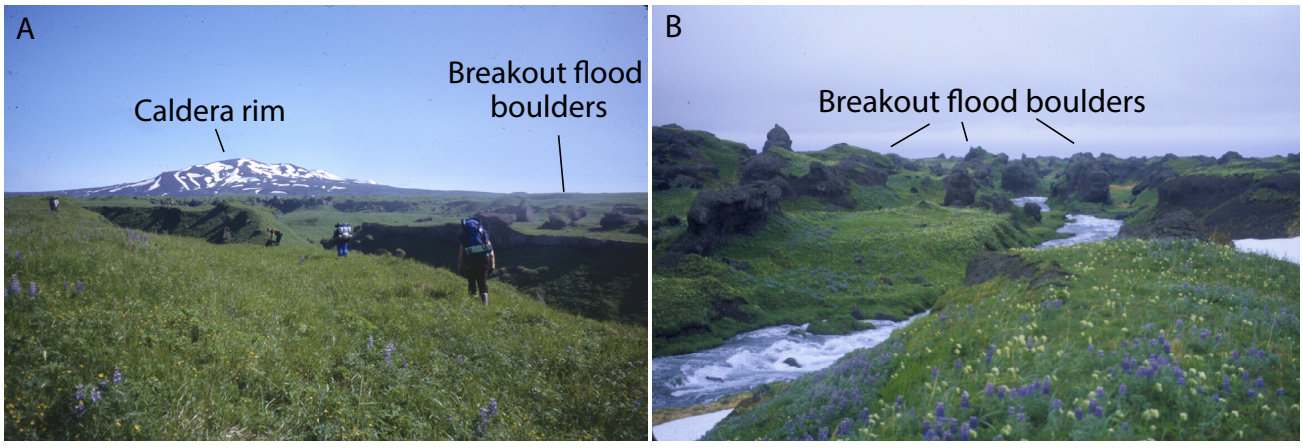

Figure 16. Photographs showing boulders along Crater Creek that were created by the breakout flood's excavation through the Okmok II pyroclastic flow deposits. The flood happened shortly after the 2,050 yBP Okmok II eruption (Wolfe, 2002). **A.** Crater Creek drainage, looking up toward the snow-covered caldera rim. In the background are large boulders created by the breakout flood; geologists in the foreground show the scale. AVO image database #166221. **B.** Crater Creek drainage, showing individual flood blocks approximately 2 to 3 m in height. AVO image database #179951. Photographs by Jessica Larsen (UAF/GI, AVO).

[320 m]." Similarly, the broad alluvial plain between Cones D and B was described by Byers (1947, p. 24) as an area of "small creeks flowing over saturated volcanic sand...[with] abundant patches of quicksand," reflecting the long-lived tendency for this portion of the caldera to accumulate and retain water.

During and after the 2008 eruption, surface hydrology within the caldera was drastically modified by the creation of new cones and explosion craters and the accumulation of pyroclastic debris, which together formed several new lakes. Some remained quite shallow and were ultimately ephemeral, but others appear to be long lived, changing size and depth seasonally, and changing shoreline shape with progressive slumping of 2008 pyroclastic deposits. Post-eruption landform changes are described in Larsen and others (2015) and are not shown here.

Postcaldera Eruptions

Intracaldera geologic history as interpreted by Byers (1959) suggests a general age progression of postcaldera vents (eruptions) based on geomorphologic criteria in relation to a rising lake, degree of modification, stratigraphic relationships where discernable, and the written historical record. The work presented here revises some of Byers' interpretations (1959) using modern understanding of volcanic processes, new field data, and radiocarbon dating of extra-caldera tephras. Careful tephrostratigraphic correlations based on component chemistry, however, have not been done, and some temporal relationships remain highly uncertain. Below are brief descriptions of intracaldera eruptive vents and deposits, as well as discussion of how they are placed stratigraphically in the postcaldera eruptive chronology. Some vents are polygenetic, whereas others suggest a single episode of activity.

Cones C and D [<2,050–1,000 yBP?]

Byers (1947, 1959) first deduced that prominent cinder Cones C and D (fig. 17) were among the oldest exposed post-Okmok II vents, citing textural evidence of subaqueous lava flows near

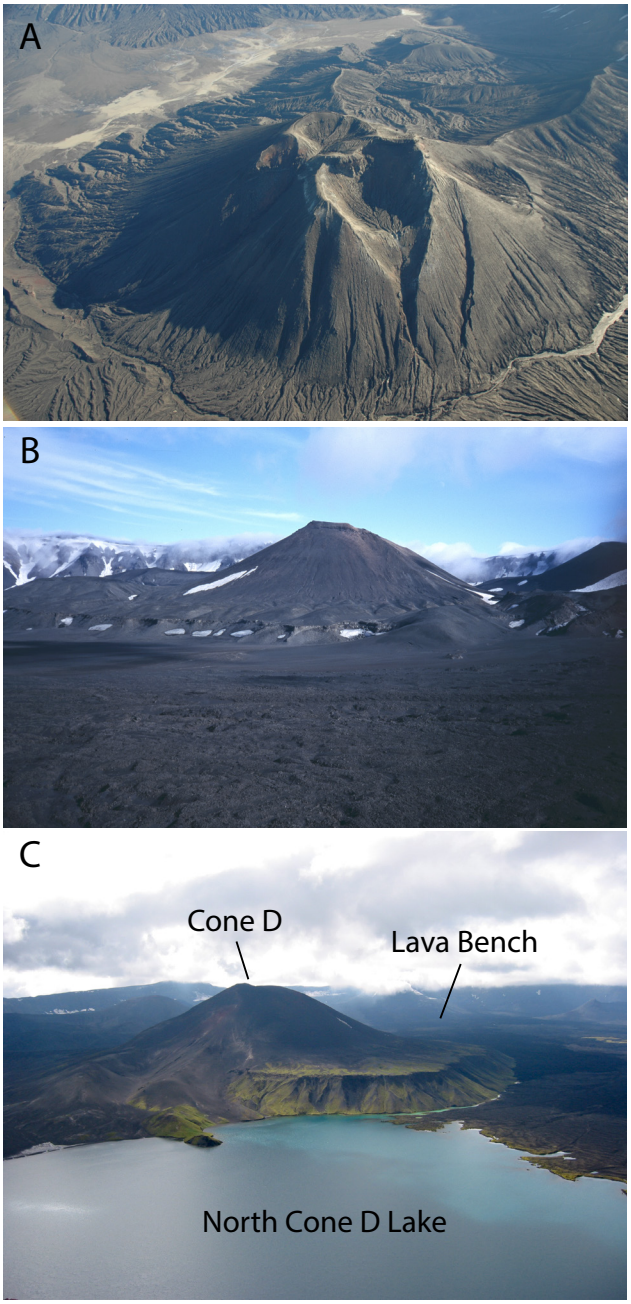

Figure 17. A. Cone C covered in ash deposits from the 2008 eruption of Ahmanilix cone. Photograph by Jessica Larsen (UAF/GI, AVO); AVO image database #33582. **B.** Cone C viewed from the caldera floor; photograph taken from north of the cone looking toward the south. Photograph by Christina Neal (USGS, AVO); AVO image database #35983. **C.** Photograph of Cone D prior to the 2008 eruption, showing the toe of the 1958 lava flow forming the lake shore (lower right), north Cone D lake (foreground), and the prominent lava bench surrounding the base of Cone D. Photograph by Christina Neal (USGS, AVO); AVO image database #14728.

their bases, which reflects the presence of a large, deep postcaldera lake. With increasing elevation, lava textures become consistent with subaerial emplacement. Almberg (2003) reinterpreted details of Cone D development, describing several stages of early sublacustrine eruptions and accumulations of bedded hyalotuff (units Duh and Dlh) now exposed on the east side of Cone D. Almberg (2003) concluded that the lava flow sequence (units Dsf and Df) represents late-stage Cone D activity following emergence from the lake. Cone D was then draped by hydrovolcanic deposits (Ds) from other sources, which in turn became interbedded with lacustrine clays and reworked volcaniclastic sediments prior to drainage from the first lake that formed after the Okmok II caldera-forming eruption. There is no evidence that Cone D was active following drainage of the lake that formed the 510-m-highstand lakeshore.

As Byers (1959) noted, Cone C is also a cinder and spatter cone with a surrounding lava bench exhibiting lava texture and volcaniclastic facies changes very similar to Cone D. The relative ages of Cones C and D are unclear, but their similar subaqueous to subaerial lava flow transitions suggest that they were active, likely repeatedly, over similar time frames.

Tuff Cones [<2,050–1,000 yBP?]

Hydrovolcanic eruptions producing maar craters, tuff rings, and cones have been very common from all sectors of the caldera floor since the Okmok II eruption, including the 2008 activity (Larsen and others, 2015). Byers (1959) mapped multiple pyroclastic cones (unit Qep) he ascribed to eruptions through, or in, the presence of large volumes of water early in postcaldera time. Building on Byers' interpretation (1959), we identify at least eight discrete centers of hydrovolcanic activity marked by tuff rings and tuff cones with relief of a few tens of meters to several hundred meters. These features are irregular topographic highs of pyroclastic debris that in cross section exhibit dramatic crossbedding, dune forms, planar and massive bedding, scoria falls, and variably palagonitized zones (fig. 18). Some tuff cones consist of curved, sometimes radiating, steep-sided, rilled ridges enclosing a closed or open basin. Others may be isolated remnants associated with the larger nearby cones. Most show evidence of modification by water, including subdued, rounded profiles, wave-cut benches, or overlying lacustrine clays and sandstone. Based on this, we infer that Cones H, I, J, K, and L predate the last highstand of the intracaldera Crater Lake. Cone G may postdate the highstand, as it has the least amount of well-defined paleo-shoreline at 510 m, the inferred elevation of the last highstand. Cone N is the only tuff cone clearly associated with an effusive phase; pods of massive lava interbedded with its unconsolidated and palagonitized deposits are visible in the inner walls of Cone E.

Extra-caldera tephra sections provide some constraints on ages of surge deposits related to this sequence of tuff cones. Wolfe (2001) reported maximum ages of post-Okmok II surge deposits from soil and charcoal as 1,890 ± 40 yBP (00-OK-104-14C) and 1,820 ± 40 yBP (00-OK-104-4). Another soil collected beneath surge deposits was dated at 1,280 ± 70 yBP (CNO04-33A; this study). The ages of these surge deposits allow correlations with hydrovolcanic eruptions that occurred within the first 1,000 years after caldera formation (app. B).

Cone F [~400–1,000 yBP?]

Cone F is a steep-sided cinder cone in the southern caldera. Unlike Cones C and D, Cone F produced a single prominent lava flow that extended northward between Cone C and the remnant of Cone L toward the central caldera. This lava flow plunged over an escarpment at the 510-m contour (interpreted as a former lake shoreline), leaving behind an evacuated channel with steep-sided levees (fig. 19). The distal portion of this lava flow is nearly completely buried by colluvium north of Cone C. Proximal portions are overlain by surge deposits from Cone E.

Cone E [~400 yBP]

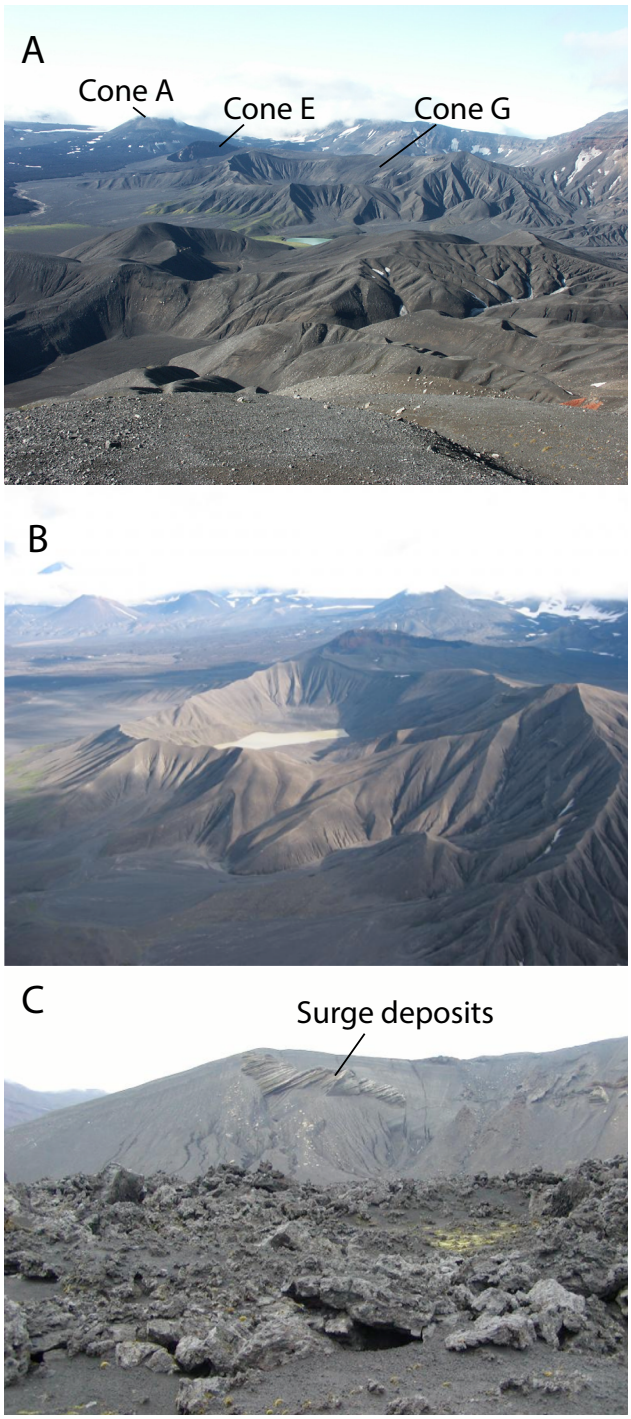

Figure 18. A. Overview photograph looking west showing tuff Cone G within the caldera; also labeled are cones A and E. Photograph by Chris Nye (DGGS, AVO); AVO image database #137671. **B.** Cone G with an eroded tuff cone morphology and lake in the bottom; photograph looking west. Photograph by Christina Neal (USGS, AVO); AVO image database #14123. **C.** Surge deposits within the walls of tuff Cone G, showing the prevalence of hydrovolcanism in the northern and eastern regions in the caldera. Photograph by Janet Schaefer (DGGS/AVO); AVO image database #12178.

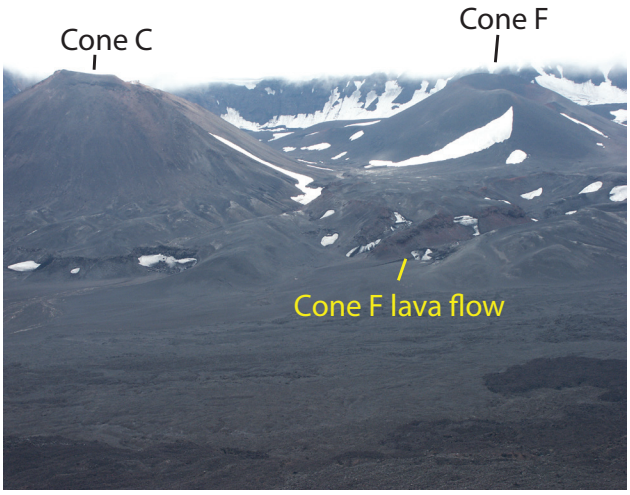

Figure 19. Photograph looking southwest showing Cones C and F, with the cone F lava flow shown in the foreground. Photograph by Janet Schaefer (DGGS, AVO); AVO image database #137501.

Cone E is a steep-sided cone truncated at the top by a deep crater that contains a turquoise lake approximately 450 m in diameter (fig. 20). It is uncertain if, in the postcaldera time, multiple eruptions occurred from this site, but the latest eruption broke through a pre-existing tuff cone complex. The eruption began with a Strombolian phase that produced spatter-fed lava flows and scoria fall deposits (unit Ec). Spatter-fed lavas (units Ec and Ef) traveled east into the central portion of the caldera and west into a circular basin formed by the central crater of Cone N. The eruption culminated in hydrovolcanic explosions that excavated a vertical-walled crater and showered a significant portion of the northeast and northwest Okmok Caldera flanks with distinctive pyroclastic surge and fall deposits. A radiocarbon date of 400 ± 80 ^{14}C yBP was obtained from a soil beneath distinctively pink, Cone E-correlated fall and surge deposits on the northeast flank of Okmok Volcano (CNO03-16; app. B). Young lahar deposits on the northwest flank of Okmok Volcano, also possibly correlative with the Cone E event, cap soils with radiocarbon dates of 380 ± 40, 430 ± 40, and 440 ± 40 ^{14}C yBP (01.OK.5.1, 01.OK.5.2, and 01.OK.5.3; app. B). Two samples identified as older than Cone E

based on stratigraphy produced radiocarbon ages of 560 ± 60 and 700 ± 30 yBP (CNO03-5D and CNO03-12N; app. B).

Cone B [C.E. 1817]

Cone B is a steep-sided scoria cone located just inside the Gates on the northeastern caldera floor (fig. 21). Byers (1959) describes Cone B as young; we support this conclusion and further interpret the feature using new field data and a review of historical accounts from Unalaska Island. The Cone B eruption sequence was complex and included both dominantly hydrovolcanic and magmatic phases from at least two vents along an arcuate vent system ~4 km long (Neal and others, 2003). Early activity produced at least one 50–70-m-deep maar crater at the base of the north inner caldera wall; explosive eruptions associated with this phase deposited more than 5 m of intercalated scoria fall and surge deposits on the north and northeast caldera rims. Historical accounts of ash fall in 1817 on Unalaska Island, 100 km downwind, attest to the size of this phase of eruption (Veniaminov, 1840; Grewingk, 1850; Litke, 1987). A sample from a poorly-developed soil beneath a near-surface coarse lapilli scoria fall unit produced a radiocarbon age of 180±30 yBP (CNO01-33; app. B), consistent with the record of historical accounts from 1817.

Following the explosive phase, Strombolian eruptions from multiple points along an arcuate fissure tracing the north caldera wall produced localized spatter deposits and short lava flows draping the inner caldera wall and extending south and east of Cone B. Activity localized at the site of Cone B produced a 120-m-high cone and an associated blocky ʻaʻā lava flow. Several meters of bedded coarse scoria fall on the north rim reflects protracted, high lava-fountaining; this fall deposit can be found in a section well outside the caldera to the northwest. Wolfe (2001) and Wolfe and Begét (2002) interpreted terraces within Crater Creek and young flood deposits as evidence of a flood associated with the 1817 event; historical accounts of flood inundation of a Unangan village near the coastline at the mouth of Crater Creek are consistent with this interpretation (Grewingk, 1850).

Figure 20. Oblique aerial photograph looking west showing Cone E, which hosts a blue-green lake approximately 450 m across formed by hydrovolcanic eruptions. Photograph by Chris Nye (DGGS, AVO); AVO image database #137461.

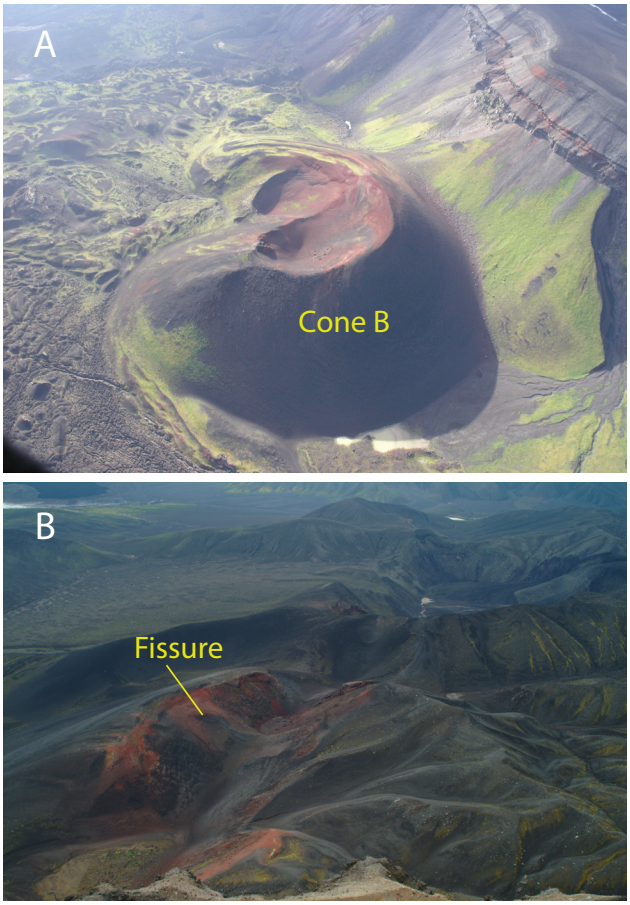

Figure 21. A. Oblique aerial photograph looking west showing Cone B, a cinder cone constructed during the 1817 eruption. AVO image database #136671. **B.** Photograph of the fissure associated with the 1817 eruption. AVO image database #136651. Photographs by Chris Nye (DGGS, AVO).

Cone A

Prior to the 2008 eruption, the recent eruptive activity within the caldera was centered at Cone A. Cone A typically produced Strombolian-style explosions, with tephra fallout distributed within the caldera as well as outside the caldera on the western and southern flanks. Lava flows produced during Cone A eruptions flowed across the caldera floor, traveling several kilometers toward the north and northeast, with notable high-volume flows in 1945, 1958, and 1997. In 2008, an eruption excavated several new vents through the terminus regions of the 1958 and 1997 lava flows (Larsen and others, 2015). The 2008 vents and deposits are not shown on this map.

Cone A eruptive activity likely started in 1899, when an explosive eruption that created a "black sand dump" was described by Robert Dunn (1908; Grey, 2003), who had hiked up to the caldera rim from Cape Aslik. Deposits from Cone M (unit Mc) and the wall fissure vent and flow (unit wff) could also be related to early Cone A activity.

Prior to the 1945 eruption, Cone A produced two other series of lava flows, included here as units afy and afo (Grey, 2003). Those two units were mapped as Qaf by Byers (1959). Based on differences in ash cover and lichen growth, Grey (2003) differentiated the Qaf unit into an older (afo) and younger (afy) series of lava flows from pre-1945 Cone A, although their exact ages are uncertain.

The 1945 eruption of Cone A had a similar eruption style as the later eruptions in 1958 and 1997, with Strombolian-style explosions and lava flows that traversed the caldera floor. The 1945 eruption was well documented and described by several observers (Byers, 1947; Robinson, 1948; Wilcox, 1959; Grey, 2003). A detailed summary of their accounts is available in Grey (2003). By the end of the eruption, the 1945 lava flow (unit 1945f) stretched approximately 6 km along the main lobe to the east of the cone, with a second lobe approximately 2.5 km in length to the west (Byers, 1959; Grey, 2003). Portions of the 1945f lava flow were later buried by the 1958f lava flow. The eastern lobe has an estimated thickness of about 12 m, with volume estimates of 1×10^7 to 2×10^7 m^3 (0.01 to 0.02 km^3; Byers, 1947; Reeder, 1984; Grey, 2003).

The 1958 eruption followed a similar general pattern of eruption style. This eruption was also well documented by pilots and sheep ranchers working and living in the area (Grey, 2003). The 1958 eruption was larger by volume than 1945 and produced a lava flow (unit 1958f) that extended 7.8 km across the caldera floor, ponding at the base of Cone D (Reeder, 1984; Grey, 2003). The flow has an estimated thickness of 12.8 m, an estimated area of 9.32 km^2, and therefore an approximate volume of 1.2×10^8 m^3 (0.12 km^3; Reeder, 1984; Grey, 2003).

In 1997, Cone A erupted again, with a similar sequence of activity as observed during 1945 and 1958. This eruption is described in detail by McGimsey and Wallace (1999) and summarized in Grey (2003). The 1997 eruption started on or before February 11, 1997, and lasted until March 26–31, 1997 (Moxey and others, 2001; Patrick and others, 2003). This eruption produced tephra deposits that accumulated between Cone A and the caldera wall in the southwestern sector (unit 1997t), with fallout deposits extending approximately 11 km outside of the caldera on the southern flanks. The 1997 lava flow (1997f) covered an area of approximately 7.5 to 9.8 km^2 (Moxey and others, 2001; Lu and others, 2003), with 8.8 km^2 estimated from the detailed map of Grey (2003). The flow was extruded during multiple episodes, and includes more than one flow lobe (Grey, 2003).

Several other eruptions from Okmok Volcano likely to have come from Cone A are described on the AVO website (Cameron and others, 2022), including those reported in 1931, 1938, 1943, 1960, 1981, 1983, and 1986. These events were described by eyewitness accounts but were not large enough to produce tephra deposits or lava flows discernable during fieldwork. Cone A (unit Ac) had grown to a height of approximately 200 m above the caldera floor after the 1997 eruption, with a volume estimate of approximately 7.53×10^7 m^3 (0.0753 km^3; Grey, 2003).

Glacial Ice, Moraine, Perennial Snowfield, Rock Glaciers

According to McAllister (1956), the glacier in the southwest corner of the caldera was active when observed in the summer of 1948. He describes it as stagnant at its eastern end and about 8 km long in an arcuate shape. During our field seasons, we were not able to observe direct evidence that this patch of ice was an active glacier. The aerial extent of glacial deposits mapped as Qg by Byers (1959) was much smaller when we observed the region in the early 2000's; the snow/ice field had shrunk considerably since the mid-20th century. Our observations indicate the presence of a perennial snowfield (unit g) covering the likely stagnant ice, mantled heavily in places by historical and prehistoric tephra deposits.

Glacial moraines are predominantly found on the flanks of Mount Vsevidof and Mount Recheshnoi volcanoes in the southwestern part of Umnak Island (Byers, 1959). Inside Okmok Caldera, debris-covered ice and ice-cored moraines are located at the base of the south caldera wall (sheet 2). Byers (1959) mapped regions with glacial till along the northwestern and eastern caldera walls adjacent to Cones G and H and to the southeast of Cone D. Byers (1959) describes those till deposits as "small, patchy end moraines" that consist of unweathered boulders and terminate poorly developed cirques in the caldera wall. The lack of weathering prompted Byers (1959) to assign an age correlating with the "Little Ice Age" (e.g., Matthes, 1941). We reinterpret those deposits to be from active rock glaciers, based on the appearance of curved ridges parallel to the terminus, indicating downslope movement of debris with interstitial ice. We did not confirm the existence of glacial till or moraines outside of the caldera; however, Jim Begét (written commun., 2001) described a small outcrop of glacial till near Cape Idak that warrants further investigation (station jeb_Pl_till; sheet 3).

FUMAROLIC ACTIVITY AND WARM SPRINGS

Within the caldera, there are three main areas with active fumaroles and warm springs: Cones A and C (fumaroles), and the base of Cone D and the north Cone D lake (warm springs). Fumarolic activity has been observed at Cone A, periodically coming from the more northern of the two craters at the summit. Byers and Brannock (1949) measured temperatures of 96–98°C from fumaroles emanating from the Cone A crater after the 1945 eruption. Steaming from Cone A was constant during the years of the AVO geologic mapping effort, although it appeared to increase and decrease in vigor. In 2004, we made several observations of incandescence in the vent in the northern Cone A crater, indicating that it was superheated at that time, though no temperature measurements were made. After the 2008 eruption, the fumarolic activity from Cone A ceased, and a small lake was observed in the northern Cone A crater during fieldwork in 2010.

Cone C has active fumaroles from one of its summit cones, from a region that extends in a gully slightly down the southern flanks of the cone and from the rim around one of the summit craters (Bergfeld and others, 2020). The fumaroles have remained active from Cone C during the geologic mapping work by AVO. Mineral encrustation and clay observed in the Cone C gully site are consistent with long-lived fumarolic activity (Bergfeld and others, 2020). Temperatures of the Cone C fumaroles have been measured as hot as 110°C by Begét and others (2005) and 95–96°C by Byers and Brannock (1949). Most recently, Bergfeld and others (2020) measured temperatures of approximately 97°C from those two sites.

Thermal springs at the base of Cone D have been recognized and mapped since the work of Byers and Brannock (1949) and Byers (1959). Byers and Brannock (1949) documented 16 thermal springs emanating from the base of Cone D and flowing into the adjacent lake. In 1946, they measured a range of temperatures from those springs of 5°C to 30°C, and in 2016, Bergfeld and others (2020) measured temperatures of 12.3 to 37.3°C. Water chemistry results and additional observations from those springs from September 2008 and August

2010 are described in Larsen and others (2015) and Evans and others (2015).

The most vigorous fumarolic and hot springs activity on Umnak Island occurs at Geyser Bight, which is not part of the area covered by this map. More information about the Geyser Bight area and other hot springs and fumaroles on Umnak Island can be found in several publications (Byers, 1959; Motyka and others, 1993; Bergfeld and others, 2020).

SURFICIAL DEPOSITS

Vigorous aeolian and fluvial reworking of abundant volcaniclastics has deposited significant amounts of unconsolidated material throughout the caldera. Alluvium is shown where it obscures underlying deposits. The very rapid pace of alluviation is evident by infilling of the 1817 maar crater and extremely active alluvial fans developing at the mouths of narrow, steep-walled gullies that drain the north interior caldera wall.

2008 ERUPTION VENTS AND FEATURES

Most geologic map fieldwork took place prior to the eruption in 2008; thus, the map, as presented in this report, shows the map units as exposed prior to the 2008 eruption. The 2008 vents, lake features, and footprint of the Ahmanilix cone are displayed as overlays on the geologic map (sheets 1, 2) and are derived from data presented in Larsen and others (2015).

COMPOSITION OF OKMOK VOLCANO MAGMAS

The petrology and geochemistry of many Okmok Volcano lavas have been described in detail in prior publications, including overviews by Byers (1959) and Miller and others (1992) and more focused studies of Cape Idak (Nye and Reid, 1986), Ashishik ridge (Bingham and Stone, 1972; Stone and Layer, 2006), Okmok I and II (Larsen and others, 2007; Finney and others, 2008), the Crater Creek Basalts (Finney and others, 2008; Larsen and others, 2013), the Middle Scoria (Wong and Larsen, 2010), the postcaldera cones (Larsen and others, 2013), and the 2008 eruption (Larsen and others, 2013). Here we provide a brief overview and present new data not previously published.

Okmok Volcano produces tholeiitic series magmas, according to the criteria of Miyashiro (1974; fig. 22), with FeO_T increasing relative to MgO as a function of increasing SiO_2. According to the total alkali versus silica classification diagram, Okmok Volcano has produced a spectrum of magmas, from basalt to rhyolite, over the course of its primarily Pleistocene to Holocene eruptive history (fig. 23).

Precaldera Pleistocene magmas that erupted from Okmok Volcano span a broad range, from high-MgO basalts of Cape Idak (Nye and Reid, 1986) to rhyolite lavas (figs. 24, 25). Prior to the Okmok I caldera-forming eruption, Okmok Volcano produced predominantly basaltic to basaltic andesite magma compositions. Andesite composition lavas are rare, as are rhyolites. There are two samples (04JSOK011A and B) of rhyodacite subglacial lavas outcropping in the Crater Creek–Gates region. A high-silica andesite (62.2 wt. % SiO_2; JS01OK5-1) is found near the top of one of the tuyas outcropping to the southwest of the caldera.

During the latest Pleistocene, the Okmok I eruption produced a spectrum of magmas ranging from basaltic andesite through andesite to rhyolite (75 wt. % SiO_2) compositions (figs. 26, 27). Although the basal stratigraphy is complex and rhyolite pumice can be found scattered throughout the pyroclastic flow deposits, it is likely that the eruption produced a relatively minor volume of rhyolite first, followed by andesite to basaltic andesite.

Similarly, the ~2,050 yBP Okmok II caldera-forming eruption produced three distinct magma compositions, from basaltic andesite to rhyodacite (68 wt. % SiO_2; high-SiO_2 dacite as classified by the TAS diagram but referred to as rhyodacite here and in prior publications; fig. 23). Stratigraphic and geochemical details of the Okmok II caldera-forming eruption are published by Burgisser (2005), Larsen and others (2007), and Finney and others (2008). The rhyodacite magma erupted first,

distributed primarily to the north and east of the caldera as thick pumice fall deposits. One pyroclastic density current deposit was identified to the northwest of the caldera. The andesite (~58 wt. % SiO_2) magma erupted second, interlayered with the rhyodacite, and is found primarily in deeply incised stream channels and high on the flanks of the volcano to the east of the caldera rim. Lastly, voluminous basaltic andesite to andesite (~53 to 57 wt. % SiO_2) pyroclastic flow deposits blanketed the flanks of the volcano in all directions but are thickest to the north, east, and south of the caldera.

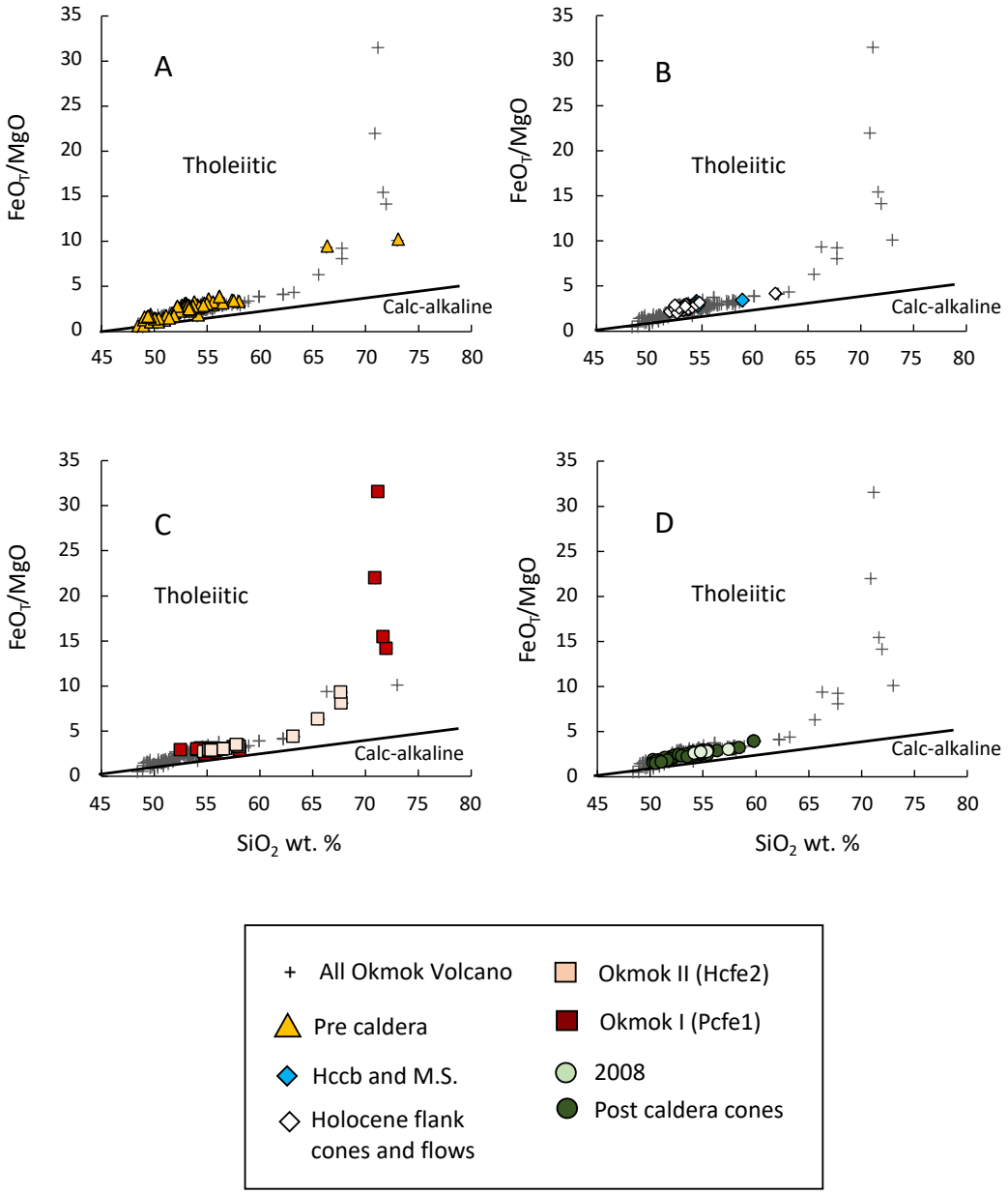

Figure 22. Geochemical discrimination diagrams showing FeOT/MgO versus SiO_2 (wt. %) with calc-alkaline and tholeiitic fields (after Miyashiro, 1974). **A.** Precaldera lavas and pyroclasts are indicated by yellow triangle symbols; all other data are shown by small plus symbols. **B.** Intracaldera lavas and pyroclasts are indicated by blue (Crater Creek Basalts and Middle Scoria pyroclasts) and white (Holocene flank lavas and cones) diamond symbols. **C.** Okmok I (Pcfe1) and II (Hcfe2) caldera-forming eruption samples are indicated by red (Okmok I) and light-orange (Okmok II) squares. **D.** Postcaldera lavas and pyroclasts are indicated by dark-green circles; the 2008 Ahmanilix cone samples are indicated by light-green circles.

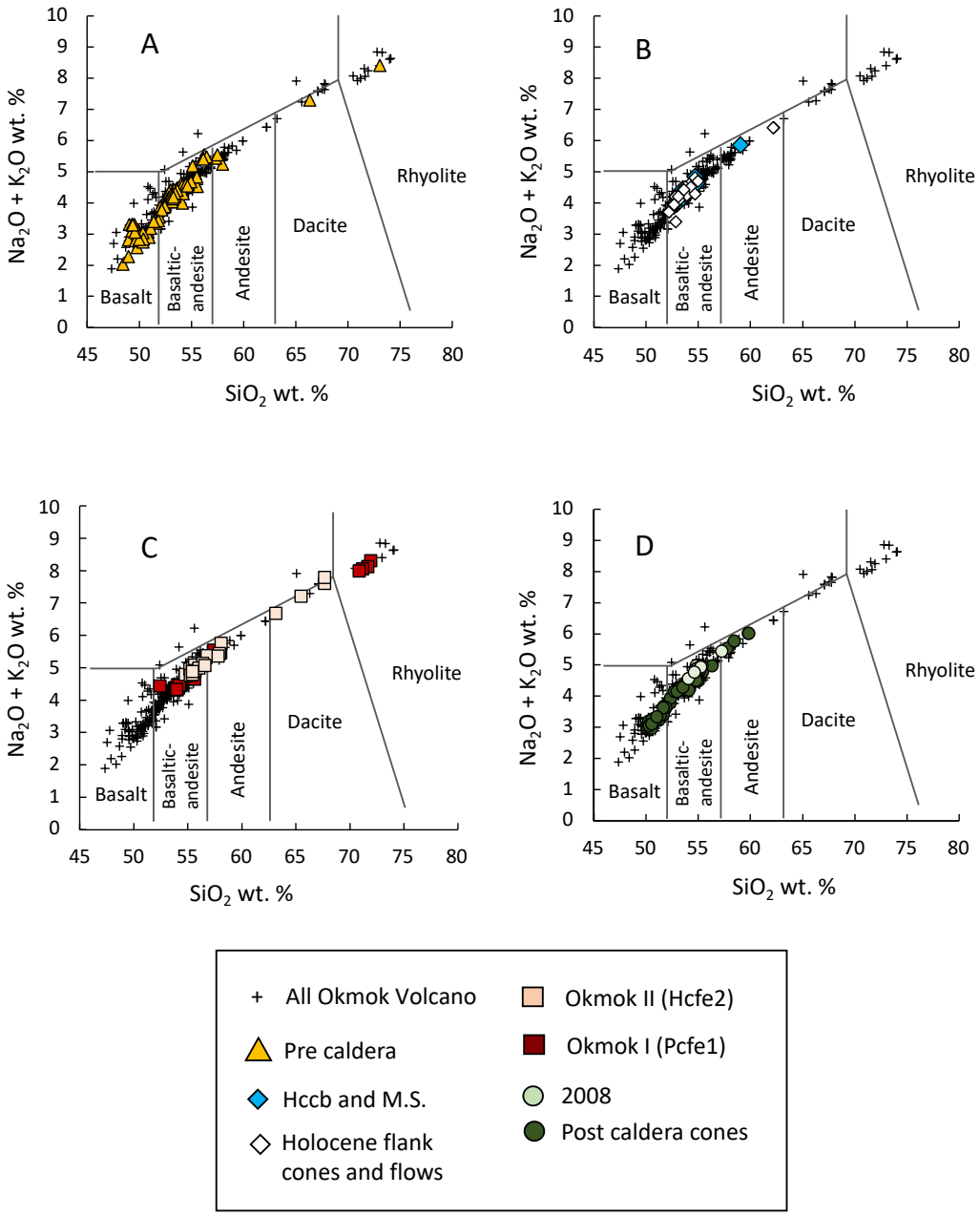

Figure 23. Total alkali versus silica ($Na_2O + K_2O$ vs. SiO_2 wt. %) for Okmok Volcano lavas and pyroclasts. Symbols are the same as in figure 22. **A.** Precaldera lavas and pyroclasts. **B.** Intracaldera lavas and pyroclasts from the Crater Creek Basalts (Hccb), Middle Scoria deposits, and Holocene flank lavas and cones. **C.** Okmok I (Pcfe1) and II (Hcfe2) caldera-forming eruption samples. **D.** Postcaldera cone lavas and pyroclasts, including the 2008 Ahmanilix eruption samples.

Between the two caldera-forming eruptions, Okmok Volcano produced predominantly basaltic andesite magmas. The Crater Creek Basalts (Hccb) increase from ~53 to 58 wt. % SiO_2 from the base of the section to the top along the west side of Crater Creek near the caldera rim (figs. 22, 23, 28, 29). The uppermost flow sampled in this region is andesitic in composition. Thick deposits of scoria along the flanks during the period between the two caldera-forming eruptions and during extrusion of the Crater Creek Basalts (Hccb) may represent explosive or phreatomagmatic phases of the eruptions that produced the thick Crater Creek Basalt lava flows. Those deposits include one particu-

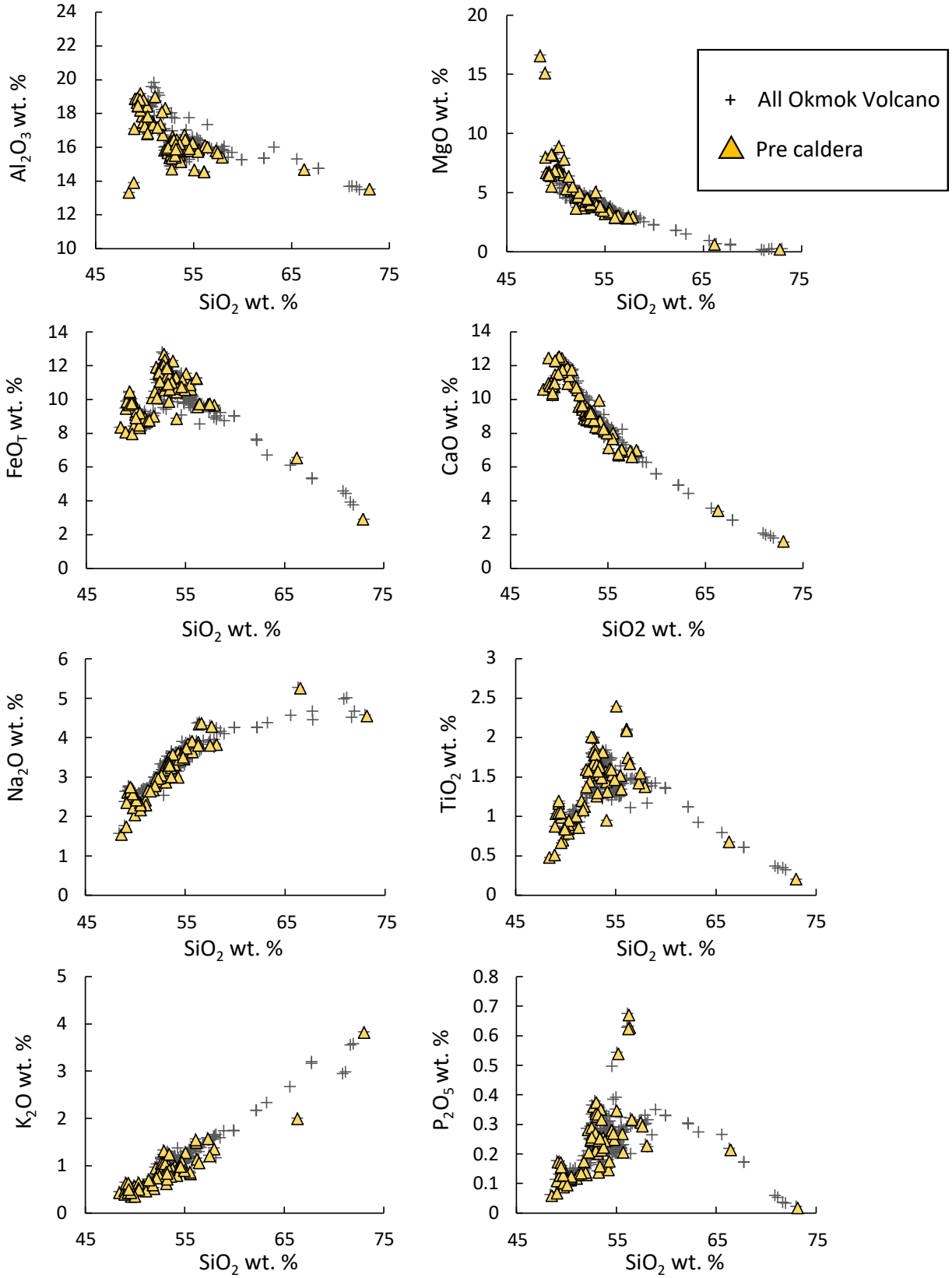

Figure 24. Harker variation diagrams showing precaldera lava and pyroclast data (yellow triangles) for select major oxides. All other Okmok Volcano data are shown as small plus symbols.

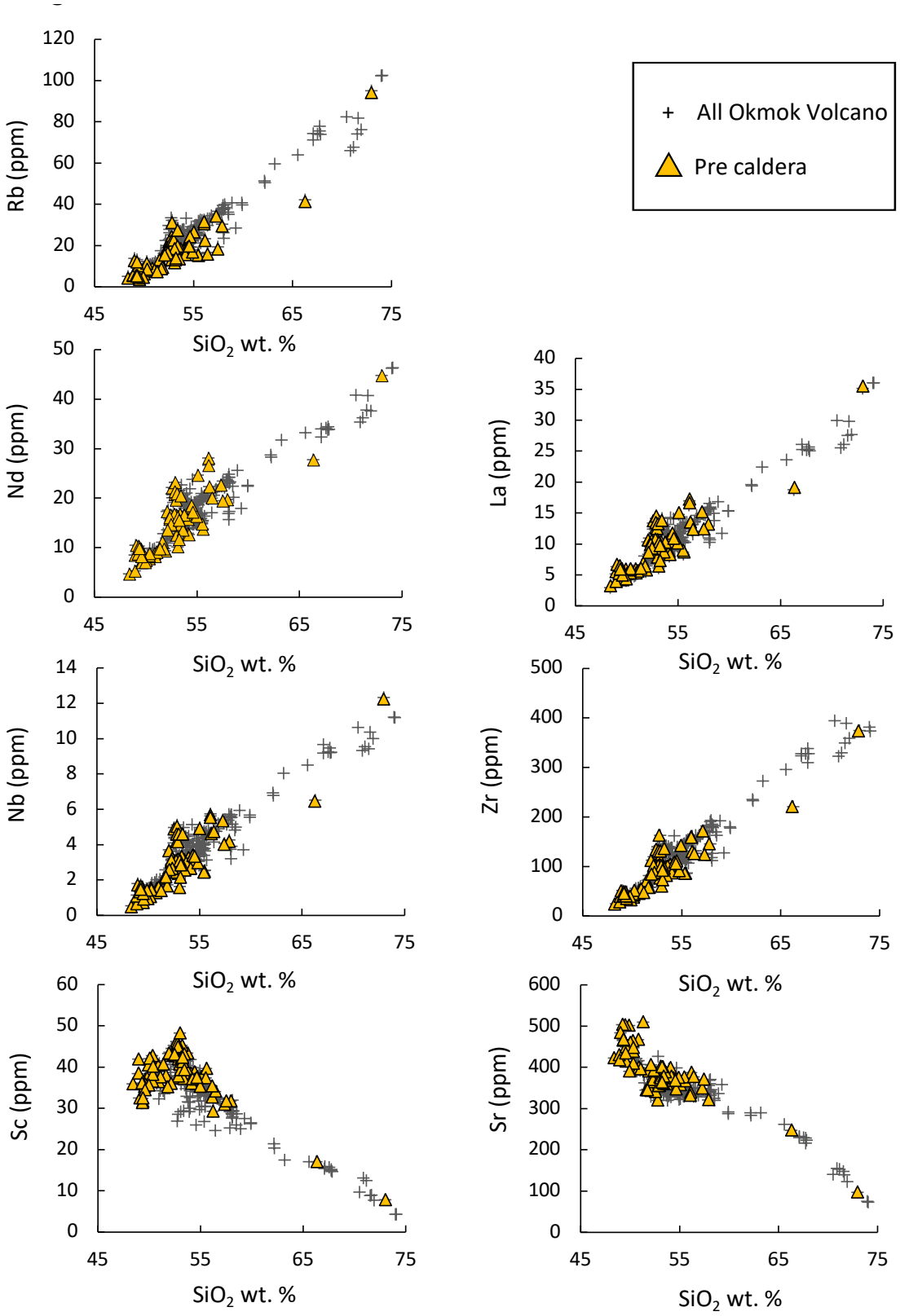

Figure 25. Harker variation diagrams showing precaldera lava and pyroclast data (yellow triangles) for select trace elements. All other Okmok Volcano data are shown as small plus symbols.

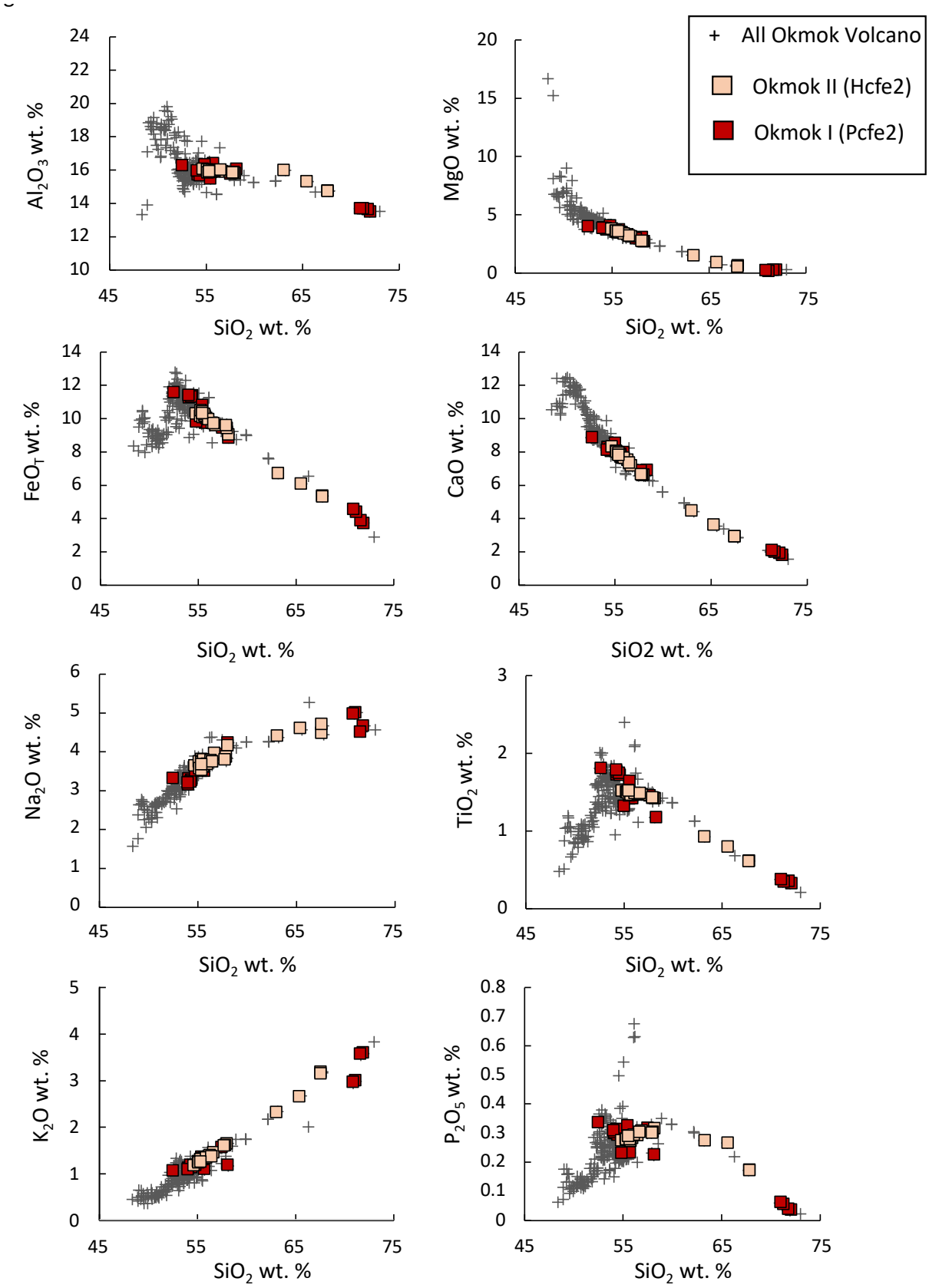

Figure 26. Harker variation diagrams showing Okmok I (Pcfe1; red squares) and II (Hcfe2; light-orange squares) caldera-forming eruption data for select major oxides. All other Okmok Volcano data are shown as small plus symbols.

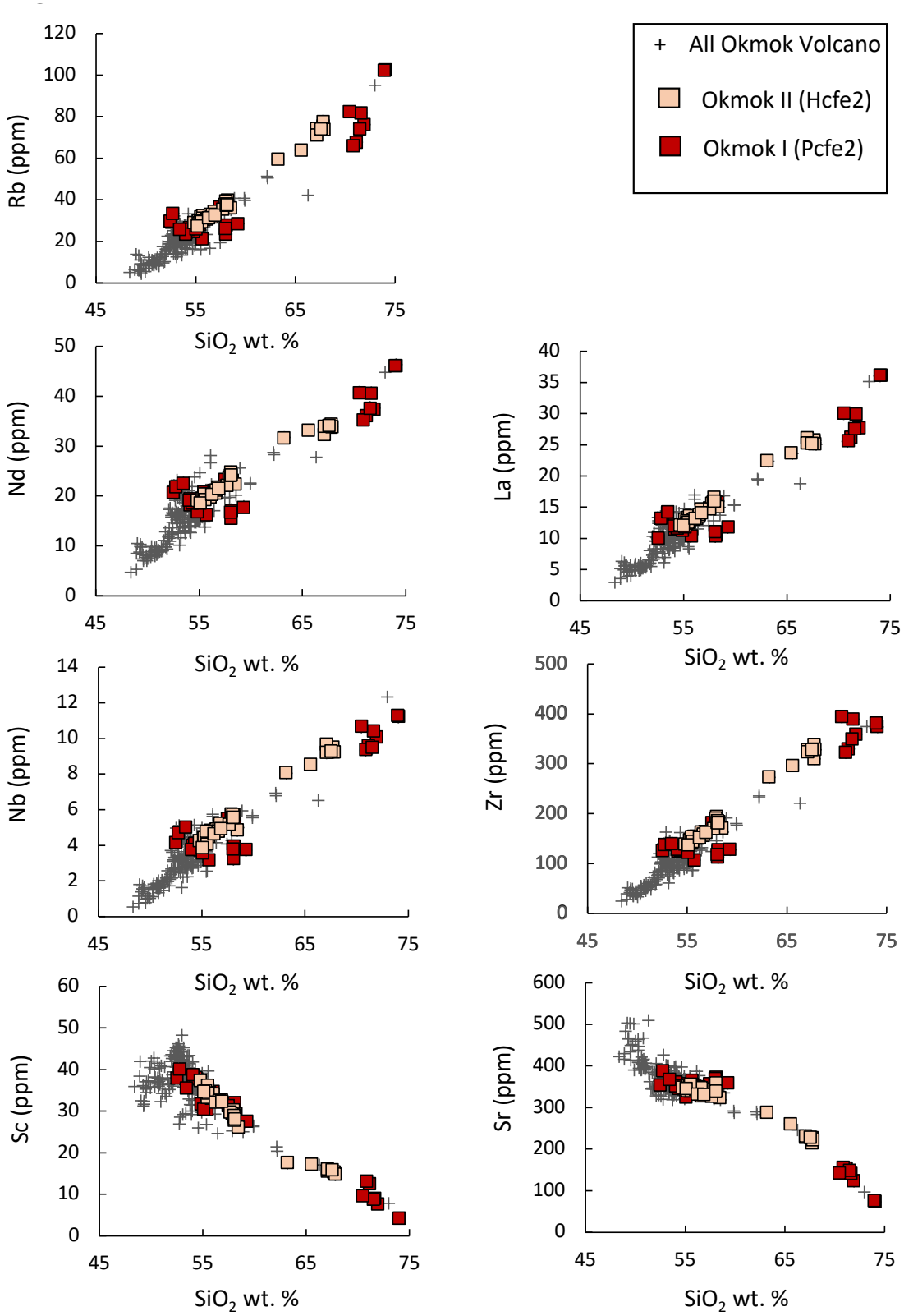

Figure 27. Harker variation diagrams showing Okmok I (Pcfe1; red squares) and II (Hcfe2; light-orange squares) caldera-forming eruption data for select trace elements. All other Okmok Volcano data are shown as small plus symbols.

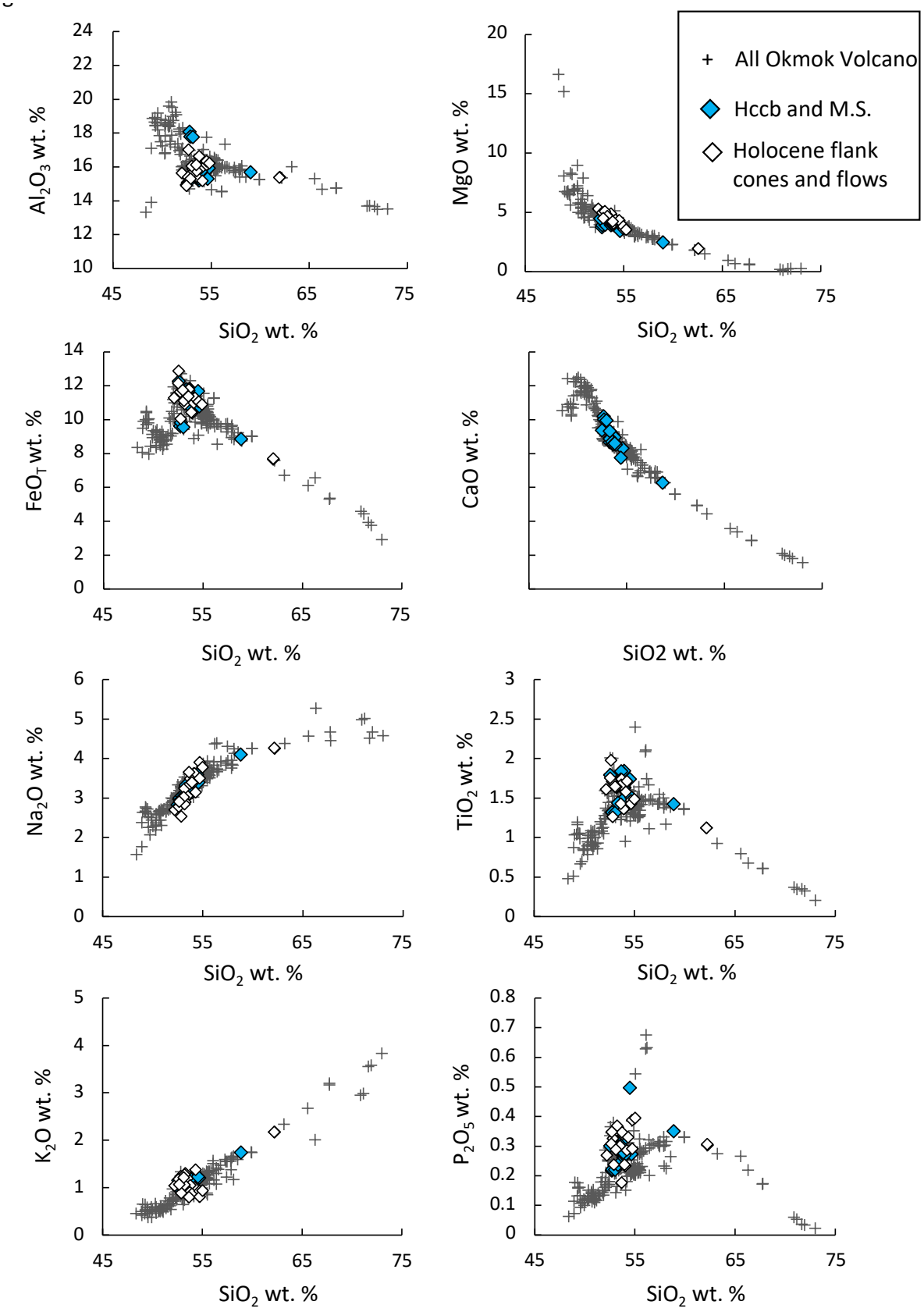

Figure 28. Harker variation diagrams showing intracaldera Holocene flank lavas and cones (white diamonds) and Middle Scoria pyroclast data (blue diamonds) for select major oxides. All other Okmok Volcano data are shown as small plus symbols.

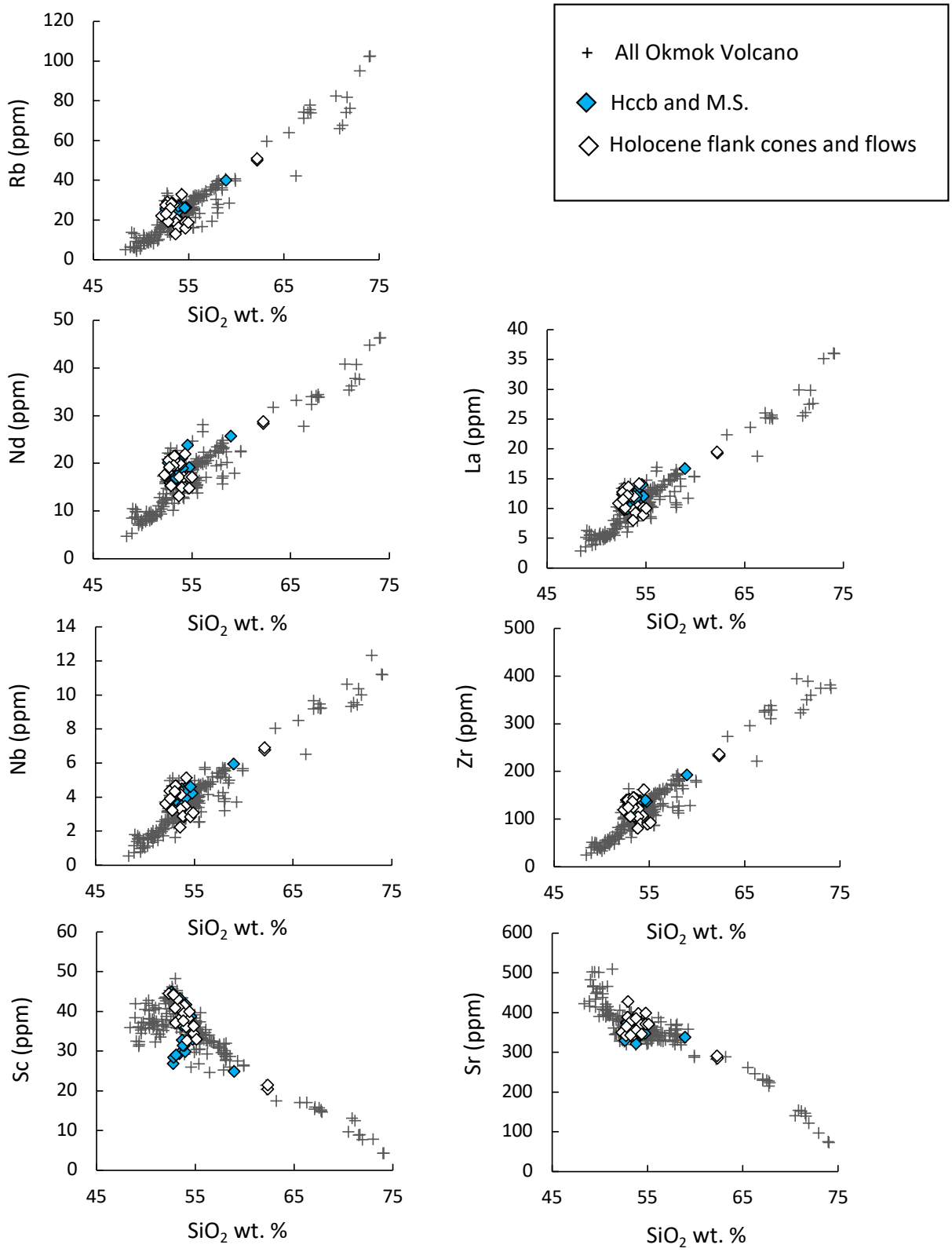

Figure 29. Harker variation diagrams showing intracaldera Holocene flank lavas and cones (white diamonds) and Middle Scoria pyroclast data (blue diamonds) for select trace elements. All other Okmok Volcano data are shown as small plus symbols.

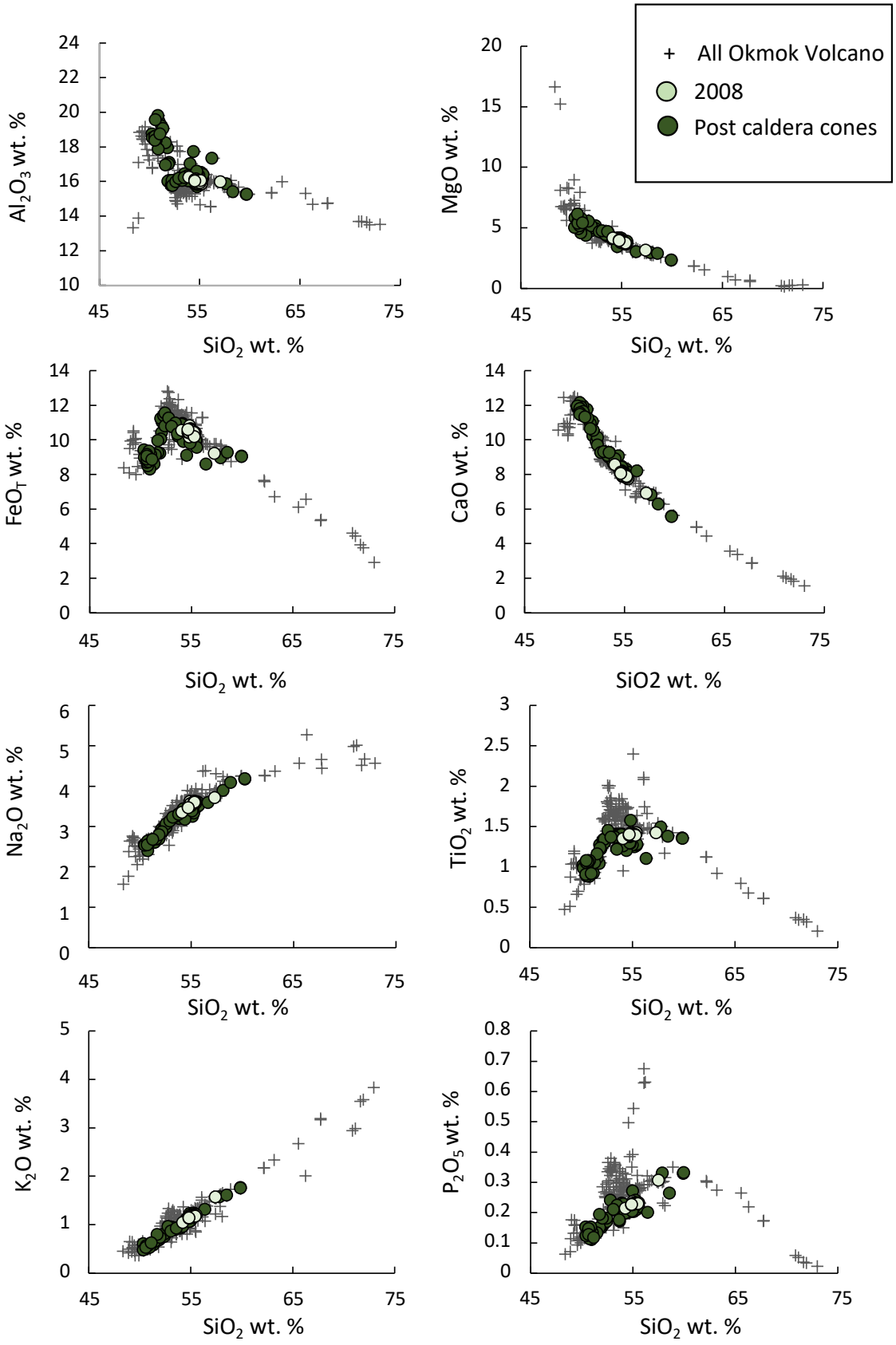

Figure 30. Harker variation diagrams showing postcaldera data (dark-green circles) for select major oxides. The 2008 Ahmanilix eruption data (not shown on map) are shown separately as light-green circles. All other Okmok Volcano data are shown as small plus symbols.

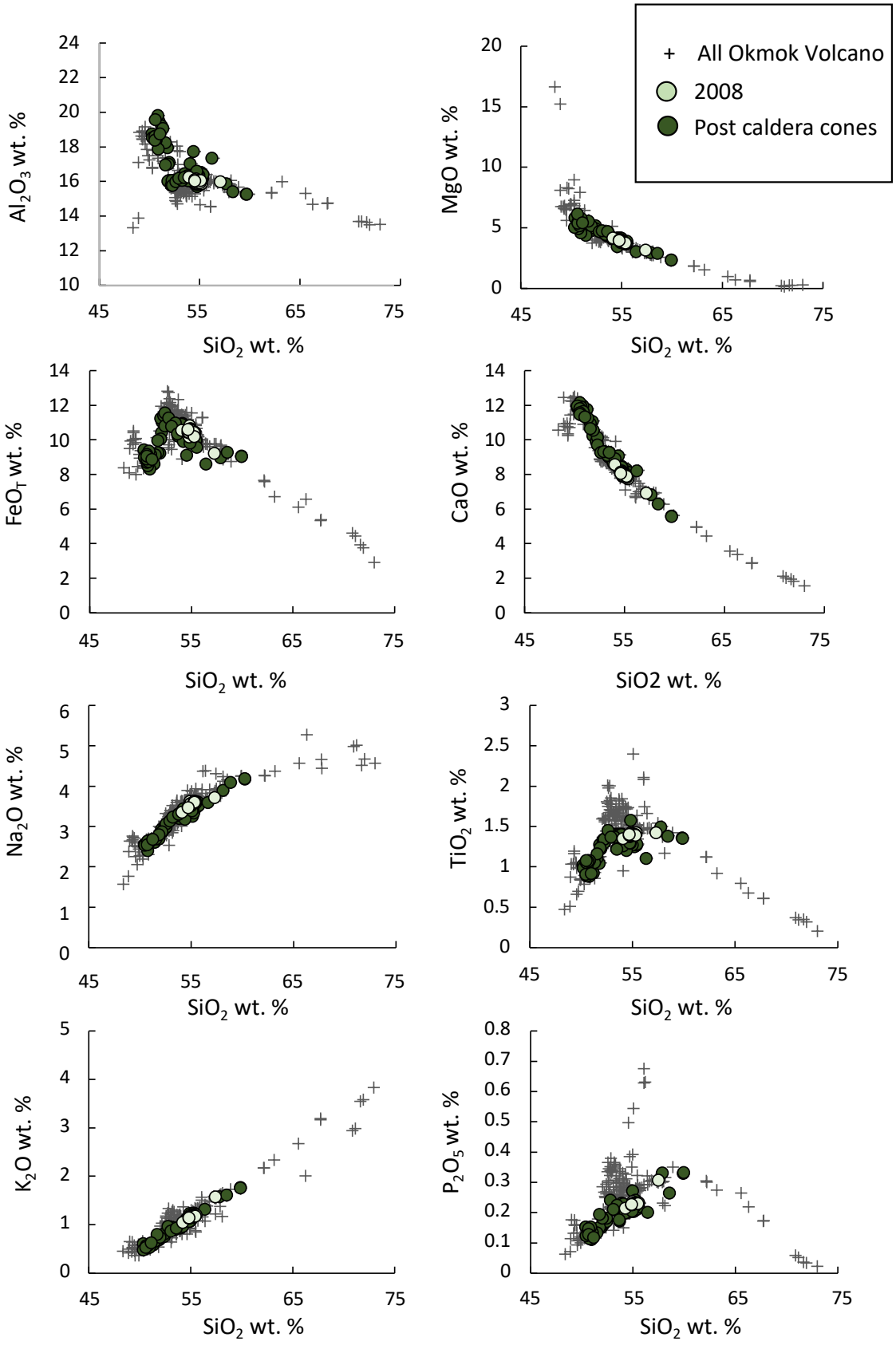

Figure 31. Harker variation diagrams showing postcaldera data (dark-green circles) for select trace elements. The 2008 Ahmanilix eruption data (not shown on map) are shown separately as light-green circles. All other Okmok Volcano data are shown as small plus symbols.

larly prominent scoria fall deposit that crops out in stream channels to the south and east of the caldera and has been studied in detail by Wong and Larsen (2010), who describe the eruption style of this "Middle Scoria" event as sub-Plinian to violent Strombolian. Compositionally, the Middle Scoria correlates with the basal to middle sections of the Crater Creek Basalts at 53 wt. % SiO_2.

After the Okmok II caldera-forming eruption, Okmok Volcano returned to a pattern of erupting primarily basalt, basaltic andesite, and minor andesite (figs. 22, 23, 30, 31). The compositions of samples from the post-Okmok II intracaldera cones are summarized by Finney and others (2008) and Larsen and others (2013). The postcaldera cones are compositionally segregated by region within the caldera, with a more SiO_2-rich group (~55–59 wt. % SiO_2) along the northern to western edge of the caldera (Cones B, E, G, H, I, and J) and a distinctly lower SiO_2 content group (~50–53 wt. % SiO_2) along the southern to eastern margins (Cones A, C, and D). Cone F is anomalous and plots between the northern and southern groups, with an SiO_2 content of ~54 wt. %.

The regional segregation in the postcaldera cone compositions does not correlate with cone age: Cones C and D are inferred to be the oldest postcaldera vents in the modern crater, and they have produced the least-SiO_2-rich lavas (Finney and others, 2008; Larsen and others, 2013), predominantly basalts with 50 wt. % SiO_2. The spatter and lava from Cones E and F and the hydrovolcanic products from Cones G–L are basaltic andesite to andesite, and all of those vents are intermediate in age, based on the mapped age relations. This indicates that the SiO_2 content of the cone lavas increased with time (Finney and others, 2008; Larsen and others, 2013), with Cones E and F producing basaltic andesite (54–55 wt. % SiO_2) and the hydrovolcanic tuff Cones G and H producing basaltic andesite to andesite compositions (54–58 wt. % SiO_2). However, hydrovolcanic tuff Cone L appears to have had a more basaltic composition magma (52 wt. % SiO_2).

The most recent activity prior to the 2008 eruption involved Cones A and B in the southwestern and northern sectors of the caldera. In 1817, Cone B produced primarily basaltic andesite lavas and scoria with 54–55 wt. % SiO_2 (Larsen and others, 2013). Cone I scoria is also basaltic andesite, with 54 wt. % SiO_2; however, a link between Cones B and I has not been established from field mapping. Geochemically, Cone B may be connected more with the magmas that fed prior Cones E and F and hydrovolcanic eruptions, than with the magmas feeding the most recent eruptions from Cone A over the past 60 years (Finney and others, 2008; Larsen and others, 2013). Beginning in the early 1900's, the historical eruptions from Cone A produced basalt to basaltic andesite with 51–53 wt. % SiO_2, showing a return to more mafic magma compositions in the southern sector of the caldera.

Although we do not show the 2008 eruption features on this map, it is important to include a brief overview of the geochemistry for comparison. The July–August 2008 hydrovolcanic eruption that produced the Ahmanilix tuff cone showed a shift in magma compositions toward higher SiO_2 content once again. This event produced approximately 0.26 km^3 (dense rock equivalent) of basaltic andesite and therefore is compositionally distinct from the 1997 eruption of Cone A, which produced primarily basaltic lavas (Larsen and others, 2015; Unema and others, 2016). The 2008 eruption magmas are tightly grouped around 55 wt. % SiO_2 yet show an abundance of basaltic glass in the finely fragmented ash deposits. Geophysics data (Freymueller and Kaufman, 2010; Larsen and others, 2013) suggest this indicates eruption triggering through an input of fresh basaltic magma likely from a central caldera reservoir.

DESCRIPTION OF MAP UNITS

For ease of map readability, all map units within the caldera that are younger than the second caldera-forming eruption (Okmok II, ~1,905–2,050 yBP) are represented without the leading epoch symbol (for example, Holocene alluvium within the caldera is labeled "al" instead of "Hal"). A capital letter preceding a unit name within the caldera refers to the intracaldera cone name, not the epoch (for example, "Pf" within the caldera refers to "lava flows from Cone P"; it does not indicate the deposits are Pleistocene). Cone names A, B, C, D, E, F, G, and H were preserved from Byers' original geologic map names (1959) and refer to the same volcanic features. Cones newly recognized during this study are Cones I, J, K, L, M, and N. Closer examination of both intracaldera volcanic deposits and the interpretations of their relative ages during this mapping project has altered Byers' original alphabetical age nomenclature pattern (1959; for example, newly mapped Cone M is interpreted to be younger than Cone B).

SURFICIAL DEPOSITS

al **Alluvium.** Active alluvial and fluvial channels. Includes bedded and stratified deposits of clays, silt, sand, gravel, and boulders redistributed by running water, locally mixed with aeolian sand and colluvium. On the flanks of the volcano, unit al consists chiefly of reworked pyroclastic deposits and locally includes older fluvial sediments in low river terraces and small areas of lahars, colluvium, and other sediments along the margins of active stream channels. Some active alluvial channels are not depicted in order to emphasize the coincident location of lahar or flood deposits (e.g., units Hfl, Hlh), or deposits associated with the first caldera-forming eruption that are exposed along the banks of modern creeks (unit Pcfe1).

ac **Colluvium.** Alluvial-colluvial fans, colluvium, and aeolian sand. Largely reworked postcaldera volcaniclastic deposits and lava flows. Includes some active alluvial and fluvial channels and fans, terrace deposits from older channels and ephemeral lakes, and poorly sorted alluvial and colluvial material deposited in short, steep fans at the bottoms of steep valleys. Material is moved primarily in wet debris flows that are subsequently reworked by intermittent streams.

t **Talus and colluvium.** Angular to subangular blocks of largely volcanic rock forming steep rubble aprons at the base of caldera walls, Cone C and Cone D bench lavas, the interior of Cone E, and other steep rock faces. Locally mixed with gravel, sand, and silt-sized material from wind- and water-reworked volcaniclastics.

lv **Lacustrine.** Deformed volcaniclastic and lacustrine sediments.

bs **Beach deposits.** Sand, pebble, gravel, and subordinate boulder accumulations on wave-washed beaches around the coastline of eastern Umnak Island.

d **Dune sand.** Active and partially stabilized, well-sorted, and stratified aeolian sand deposits forming dunes. These deposits are found mainly behind beaches with north and west exposures.

g **Glacial ice and perennial snowfield.** Crevassed glacial ice and perennial snowfield confined to the southern caldera wall. Aerial extent of icefield reduced from the portrayal of Byers (1959), who concluded that the ice was largely stagnant. Cone A eruptions of 1945 and earlier impinged upon a formerly more extensive lobe of ice that extended onto the caldera floor. Mantled heavily in places by historical and prehistoric tephra deposits.

m **Debris-covered ice, ice-cored moraine, till.** Largely stagnant, debris-covered ice, ice-cored moraine, and till confined to the southern caldera wall and floor. Heavily mantled with historical and prehistoric tephra deposits from Cone A and debris from the caldera wall. Differential insulation and melting have produced hummocky topography.

rg **Rock glacier.** Angular, poorly sorted boulders and cobbles in lobate deposits at the base of the western caldera wall behind Cones G and H and at the base of the eastern caldera wall, southeast of Cone D, where the terminus forms a steep snout. Curved ridges parallel to the terminus suggest downslope movement by deformation of interstitial ice.

Cones and Associated Volcanic Deposits Younger than ca. 2,050 14C yBP

Cone A

Ac **Cinder and spatter of Cone A.** Black to red oxidized scoriaceous lapilli, bombs, and spatter agglutinate forming Cone A, a ~240-m-high cinder and spatter cone in the southern portion of the caldera. Cone A marks the most recently active of the Okmok Caldera vents (prior to 2008) and is the general site of all well-documented eruptive activity in the 20th century (Byers, 1959; Grey, 2003). Its last eruption was February–April 1997 (McGimsey and Wallace, 1999; Patrick and others, 2003). The summit of Cone A is indented by two overlapping craters 200–250 m across and 60–80 m deep. Odors of H_2S and SO_2 noted in summers 2001–3. During fieldwork in 2002 and 2004, incandescence was observed inside a hole 2–3 m in diameter near the bottom of the more northern summit crater.

1997t **1997 tephra of Cone A.** Black, gray, and red-brown scoriaceous tephra consisting of ash, lapilli, and bombs from the 1997 eruption of Cone A. These deposits are locally several meters thick near the base of Cone A and difficult to distinguish from 1958 tephra deposits and other historical scoria falls. Coarse to fine ash and scoriaceous lapilli, some of which is likely 1997 in age, extend in patchy exposures across much of the caldera floor. The 1997t deposits are significantly reworked by wind and water and in places completely eroded away. A discontinuous blanket of ash and lapilli, likely from the 1997 eruption, extends up to 11 km south of the caldera. Despite an observation of light, fine ash fall 17 km east at Fort Glenn Ranch in 1997 (Tim Webb, oral commun., 2002), no deposit has been identified at that distance.

1997f **1997 lava flows of Cone A.** Black, glassy, blocky to scoriaceous ʻaʻā and minor "toothpaste" pāhoehoe erupted from Cone A between February and April 1997. These flows form two main lobes 10–50 m thick along the margins and extending as far as 5.5 km northeast of Cone A, covering an area of 8.9 km^2 with 1.65 × 108 m^3 of lava (Patrick and others, 2003). The 1997f flows display well-developed channel, levee, and surface ridge morphology; accretionary lava balls are common. Lava blocks in the 1997f flows are highly oxidized in places. Additional spatter-fed lava flows, channel overflows, and isolated small sections of rafted cone material extend up to 2 km from Cone A. Rootless fumaroles, some marked by primary sulfur deposits, continued to steam in the thicker portions of the lava flow until 2004. Lava from the 1997 eruption consists of <5 to 20 percent clean to "pitted" euhedral to subhedral plagioclase up to 2 mm, with lesser amounts of pyroxene than is typically found in crystal clots with plagioclase (Grey, 2003). Olivine is present and appears resorbed or skeletal (Grey, 2003).

1958f **1958 lava flows of Cone A.** Gray-brown to black, glassy, blocky to scoriaceous ʻaʻā and rare spiny and shelly pāhoehoe erupted from Cone A during a poorly documented eruption in August 1958. The 1958f flows form two main lobes that are 20–30 m thick and extend as far as 8 km northeast of Cone A to within ~1 km of the Gates. These flows cover a total area of 7.1 km^2 based on 1980 Landsat 7 image analysis (K.R. Papp, written commun., 2003). This value differs from the first published estimate of 9.36 km^2 (Volcanological Society of Japan, 1984). Estimated mean thickness of the flow is 12.8 m, with a total volume of 1.2 × 108 m^3 (Reeder, 1984). The northeast lobe impounded a lake (modified during the 2008 eruption) with a maximum depth of ~25 m, volume of 13.6 × 106 m^3, and surface area of 1.3 km^2 (Larsen and others, 2015). The 1958f lava flows display well-developed channels, levees, and surface ridges, with surfaces covered in places with a lichen mat up to 2 cm thick (K.R. Papp, written commun., 2003). Samples 01DGOK05 and 01DGOK06 contain 10–20 percent plagioclase phenocrysts that are 1–3 mm in size in gray, crystalline groundmass. Other samples contain sparse olivine and pyroxene about 1 mm in size.

1945f **1945 lava flows of Cone A.** Gray to black, glassy, blocky to scoriaceous ʻaʻā erupted from Cone A between June and December 1945. The 1945f flows are up-to-12-m-thick disrupted glacial ice in the southern part of the caldera and extend in two principal lobes ~2 km north and ~5 km northeast of Cone A (Byers, 1959). The volume of the 1945 flow is estimated to be 1×10^7 m^3 to 2×10^7 m^3 (Byers, 1959; Reeder, 1984). Tephra fall deposits from the 1945 eruption have been reported as thick as "several feet" on the caldera floor south of cone A and "several inches" on the caldera rim (Robinson, 1948; Wilcox, 1959). Tephra from the 1945 eruption is now reworked and largely buried by 1958 and 1997 deposits, and difficult to distinguish from other historical Cone A fall deposits. Samples 01DGOK14 and 01DGOK15 have at least 20 percent plagioclase phenocrysts that are up to 3 mm in size, with most 1 to 2 mm. Sparse 2-mm pyroxenes also occur with minor olivine (2 to 3 mm in size) in a glassy groundmass. The 1945 lavas are moderately vesicular.

afy **Lava flows of Cone A erupted prior to 1945.** Gray to black, glassy, blocky to scoriaceous, vesicular ʻaʻā erupted from Cone A prior to 1945, possibly historical in age. The afy lava flow is possibly associated with a perched lava pond seen in 1943 aerial photographs to be extending northwest from pre-1945 Cone A toward the southern base of Cone E. The afy flow impinged upon a formerly more extensive glacial lobe south of Cone A. Sample 01NYO-20 consists of a medium-gray lava with 30 percent or more plagioclase phenocrysts that are 1–3 mm in size. Sparse olivine phenocrysts are present, up to 1 mm in size. Pyroxene phenocrysts are either rare or absent. Hand sample descriptions indicate that this unit has a noticeably lower proportion of mafic phases than the afo unit (unit Qaf of Byers, 1959).

afo **Lava flows of Cone A erupted prior to 1945, older than unit afy flows.** Gray to black, glassy, blocky to scoriaceous, slabby pahoehoe and ʻaʻā erupted from Cone A prior to 1945, possibly historical in age. The afo unit is the same as unit Qaf of Byers (1959). The afo and afy flows are differentiated in age by the lack of ash cover on afy (Byers, 1959) and more significant lichen growth on afo (Dela Gray, written commun., 2002). A remnant of the afo lava flow is now exposed between the 1945 and 1997 flow lobes northeast of Cone A. Lava samples from the afo unit are vesicular and medium gray, with 20 to 30 percent plagioclase phenocrysts that are from 1–2 mm (01DGOK20) to 3–4 mm in size (01DGOK18). The lavas also contain sparse olivine and pyroxene phenocrysts that are 2–3 mm in size.

wff **Lava flows of southwest wall fissure.** Lava erupted from fissure vent(s) on the caldera wall northwest of Cone A, reported by Byers (1959). The wff lava flow consists of ʻaʻā with 3- to 5-m-high spires heavily mantled by 1997 tephra, other historical tephra, snow, and mass wasting deposits from the caldera wall. The wff unit presented in this map combines photo interpretation of 1943 aerial photography, Byers' map unit Qwf (1959), and outcrop examination. The west end of the fissure vent produced a lava flow that mantles the southwest caldera wall and Cone N hydrovolcanic deposits. The fissure vent eruption of wff lava was possibly related to early eruptive activity at Cone A. Sample 01NYO-11 is fine grained, finely vesicular, and medium gray, with approximately 5 percent plagioclase phenocrysts that are 3 to 4 mm in size, although one 1-cm plagioclase phenocryst is described. The plagioclase phenocrysts have pyroxene inclusions. Sparse green-brown olivine phenocrysts are also present. The wff lavas also contain enclaves, with sample 01NYO-12 exhibiting 30 to 40 percent plagioclase phenocrysts that are up to 5 mm in size. The enclaves also contain approximately 10 percent dark-green pyroxene phenocrysts that are 2 to 3 mm in size.

Cone M

Mc **Spatter of Cone M.** Red oxidized spatter and spatter agglutinate that forms Cone M, a 150-m-diameter scoria cone east of Cone A. Cone M is possibly historical in age and related to early eruptions at Cone A. The spatter deposit of Mc is surrounded by the 1945 ʻaʻā flow and is buried by tens of centimeters of primary and reworked post-1943 ash and lapilli scoria falls and juvenile lithic bombs from Cone A. A moraine visible in the 1943 air photos and now buried by younger deposits suggests the intracaldera glacier advanced around one limb of Cone M prior to its most recent retreat. Mc sample 01NYO-18 is

vesicular and scoriaceous, and pink to reddish gray. This sample contains 5–10 percent plagioclase phenocrysts that are typically 1 to 2 mm in size and lathe shaped. Mafic phases make up 3 to 5 percent in hand samples and are likely mostly pyroxene. Not shown in Byers (1959).

Cone B

Bc **Spatter of Cone B.** Red oxidized to black scoriaceous lapilli, bombs, and agglutinate forming Cone B, an approximately 120-m-high cinder and spatter cone at the base of the north caldera wall. The summit of Cone B is indented by two craters that are ~100–150 m across and up to 30 m deep. Related fissure and spatter vents and hydrovolcanic explosion craters extend 4 km along an arc parallel to the caldera wall west of Cone B. These features are correlated with Cone B based on geometry, youthful appearance, distribution, and character of ejecta. The 1817 age is based on written accounts of an eruption of appropriate magnitude that affected the sector northeast of the caldera (Grewingk, 1850) and modern radiocarbon ages for correlative tephra outside the caldera. Wolfe (2001) describes a flood deposit related to this eruption that destroyed an Aleut village at the coast. Bomb samples from Cone B consist of finely vesicular scoria that are variably red and oxidized to dark gray. Samples 01NYO-21 and CNO01-13 have sparse phenocrysts, with approximately 5 percent plagioclase up to 1 to 2 mm in size. Plagioclase that is fine grained and less than 1 mm in size is more abundant. Mafic phases visible in the hand samples consist of sparse pyroxene about 1 mm in size.

1817f **Lava flows of Cone B and related vents.** Red-brown oxidized to gray-black, blocky to scoriaceous ʻaʻā erupted from Cone B and related vents (unit Qbf of Byers, 1959). Byers (1959) distinguished between early and late phases of the effusive eruption from Cone B. Here, we include both within the same map unit. The main flow field from Cone B, ~5–10 m thick at the margins, extends approximately 2 km south of Cone B, and is mantled by coarse lapilli and ash scoria fall from Cone B, historical eruptions from Cone A, and reworked ash. Contains up-to-25-m-high fragments of Cone B agglutinate that rafted away from the vent. Dense, aphyric to sparsely plagioclase-phyric samples from the interior of large blocks contain trace plagioclase phenocrysts up to 1–2 mm across. Scoriaceous ejecta contains, rarely, inclusions of lithics and palagonitized volcaniclastics. Short, fissure-fed lava flows from a chain of vents along the base of the caldera wall west of Cone B are black, scoriaceous, vesicular, and aphyric (unit Qwf of Byers, 1959).

1817t **Upper tephra of Cone B and related vents.** Black to red, oxidized, glassy spatter, bomb, and coarse lapilli and ash-sized tephra draping the north caldera rim and wall and the northeast wall of a maar crater to the west of Cone B. Ribbon bombs are abundant in the 1817t unit. Remobilized spatter forms drapery on steep exposures of Crater Creek Basalts northwest of Cone B. Dense, glassy, black bombs from western vents overlie adjacent Cones H and J. Black lapilli and ash extend in a continuous blanket for several kilometers outside the modern caldera; bombs (up to 50 cm across) traveled as far as 1 km from the vent. Scoriaceous tephra forms prominent lapilli or ash horizon near the top of many stratigraphic sections outside the caldera to the northeast and east.

1817s **Mixed hydrovolcanic and Strombolian deposits of Cone B eruption.** Hydrovolcanic explosion debris and intercalated scoriaceous fall units from an approximately 100-m-deep maar crater against the north caldera wall west of the Cone B eruptive complex and possibly other vents within the Cone B region. Consists of gray to black, dense lithics and moderately vesicular scoria bombs, lapilli, and ash surge and fall deposits forming a sequence 2 to 6 m thick on top of the north rim of the maar crater, at least 3 m thick on the bench behind Cone B, and more than 4 m thick on the bench inboard of the east arcuate scarp. Steeply dipping remnants of fall and surge deposits, now deeply dissected, occur against the base of the caldera wall just north of Cone B. Overlain near Cone B by black, glassy spatter bombs up to 1.5 m across and scoriaceous lapilli from the final magmatic phase of the Cone B eruption (1817t). Hand sample 02NYOK109 is from an 85 × 20-cm spindle bomb, described as aphyric, glassy, finely vesicular basalt. This bomb sample is medium to dark gray. Phenocrysts are primarily sparse plagioclase up to 1 mm in size with a distinct chalky appearance relative to the other historical lava flows.

1817m **1817 maar vent and bomb field.** Concentration of juvenile, crystal-poor, highly fractured breadcrust bombs surrounding a circular maar structure. The vent region is filled with alluvium advancing from the south and southwest, originating from Cone G. Sample JS01OK03-1 is medium gray with a moderately vesicular texture of deformed vesicles. Phenocrysts consist of sparse plagioclase approximately 1 mm in size; smaller plagioclase crystals are abundant, giving the sample a "salted" appearance.

Cone E

Ec **Spatter, bombs, scoria, surge deposits, and spatter-fed lava flows of Cone E.** Cone E is a young spatter and agglutinate cone perched atop an older tuff cone complex. Cone E stratigraphy consists of black-gray spatter, scoriaceous lapilli, and lithic, glassy, scoriaceous juvenile bombs deposited on top of 2 m of orange-yellow, brown, maroon, and red silt-sand-lapilli surge deposits that make up the north rim and adjacent flanks of the cone. These deposits represent the most recent magmatic activity and explosions accompanying the collapse of Cone E, and form an approximately 200-m-deep, steep-walled crater. This crater now contains a 430-m-diameter (long axis) turquoise lake of unknown depth. Surge deposits associated with Cone E are interlayered with poorly sorted, muddy, lapilli-sized-scoria fall units containing abundant oxidized volcanic clasts. The surface bomb field consists of dense, gray, aphyric lavas and subordinate yellow palagonite clasts reamed from older pyroclastic deposits now exposed in the walls of Cone E. Glassy juvenile bombs are also found in the bomb field, containing 10–15 percent plagioclase phenocrysts with scattered olivine and clinopyroxene in a black, glassy groundmass.

Ef **Spatter agglutinate and spatter-fed, spiny pāhoehoe and ʻaʻā lava flows of Cone E.** Gray to red and oxidized in color, unit Ef forms the high south peak of Cone E and is correlative with lava flows extending west, east, and southeast from Cone E. Unit Ef is the same as unit Qef of Byers (1959). The Ef lava flows are 5–10 m thick and mantled by younger deposits of Ec. A sinuous feeder dike for this eruption is visible in the south wall of Cone E. Recent high-temperature fumarolic alteration is evident below the high point on the south rim. Hand samples 01DGOK04 and 01JLOK56E are medium to dark gray and variably vesicular with dense interiors, and contain 5–10 percent plagioclase phenocrysts that are 1–3 mm in size. Mafic phases consist of 3–5 percent olivines that are 1 mm in size, and sparse pyroxenes (2 mm) often attached to plagioclase.

Cone F

Fc **Spatter deposits of Cone F.** Gray-black to red oxidized scoria and spatter that forms steep-sided Cone F. Cone F has an elevation of approximately 220 m. Hand samples 01NYO-06 and CNO04-22 represent jigsaw-fractured bombs from Cone F that are finely vesicular and medium to dark gray. The bombs are phenocryst poor, with abundant plagioclase less than 1 mm in size, which gives them a "salted" texture.

Ff **Lava flow of Cone F.** This ʻaʻā lava flow is more than 15 m thick and extends approximately 600 m north of Cone F. The Ff lava flow is largely buried by Cone L deposits, lithic ejecta from multiple sources, and other younger tephras. The flow displays a distinctive leveed channel structure near its exposed terminus. The evacuated channel wall consists of brecciated, oxidized, clastic ʻaʻā rubble with a dense, smooth lava selvedge. This channel plunges steeply into a modern alluvial basin, suggesting a former lakeshore or extension of the Cone C lava bench in the southern caldera region. Scattered outcrops of the Cone F flow are visible through the alluvium. The Cone F lava flow overlies Cone C lavas. Hand sample 01NYO-08 contains isolated large vesicles and has abundant plagioclase phenocrysts less than 1 mm in size.

Cone L

Lh **Pyroclastic flow, surge, and fall sequence of Cone L.** Gray-tan to black, coarse-gravel- to sand-sized, poorly vesicular, blocky juvenile and lithic clasts are found in the Lh pyroclastic sequence. Individual beds in the Lh unit range in thickness from 1 cm to tens of centimeters. The surface of Cone L is littered with gravel- to boulder-sized (up-to-2-m) blocks of dense and vesicular lavas, palagonitized breccias, welded tuff, and

rounded, aphyric precaldera lavas. Cone L has an elevation of approximately 140 m and is deeply eroded and partially encroached upon by the south caldera glacier. Moraine pattern suggests that the glacier overrode portions of Cone L at some time prior to 1943. Portions of the northern extent of Cone L show possible fluvial reworking. Upper surge and fall units appear to overlie Cone F scoria and lava flow, suggesting a possible syneruptive relationship with Cone F. Sample CNO02-10 consists of medium-gray lapilli up to 2 cm in size and finely vesicular with dense outer rinds. Sparse plagioclase phenocrysts comprise ~5 percent of the sample and are up to 1 mm in size. Sample 01NYO-17 consists of medium-gray, ash-coated, vesicular lapilli with a quenched, dense outer rind. Difficult to observe mineral crystals in those ash-coated lapilli.

Cone C

Cc **Cinder, spatter, and surge deposits of Cone C.** Gray-black to oxidized red scoriaceous cinder, spatter, and agglutinate composing the steep upper flanks of Cone C. Unit Cc also includes ponded dense lavas exposed in summit craters, as well as the indurated, bedded pyroclastic surge sequence and coarse-gravel- to boulder-sized lithic debris discontinuously mantling the eastern summit crater and upper flanks of Cone C. Ten to fifteen meters of indurated volcaniclastics drape and plaster the inner wall of the eastern summit crater and consist of subcentimeter- to tens-of-centimeters-thick beds of surge and fall deposits containing lithic debris and glassy, black scoria. Bomb sags and crossbedding structures are abundant. Lithic debris consists principally of dense, aphyric, and conspicuous plagioclase-bearing lavas of Cone C. Fumarolic summit area with temperature of ~95°C was noted by Byers (1959) and is still active (Cr-Al thermocouple temperatures of 87–110°C were measured in 2001 by Ken Papp). Other warm areas high on the walls of several summit craters were still visibly steaming in 2004. Hand sample 01NYO-09 from this unit is medium gray and has relatively low vesicularity. Plagioclase phenocrysts 1 to 3 mm in size account for 10 to 20 percent of this hand sample. Most plagioclase phenocrysts are ~1 mm in size. Mafic phases are not obvious, with sparse olivine 1–2 mm in size.

Csf **Spatter-fed lava flow of Cone C.** This spatter-fed lava flow originates from the northernmost Cone C crater and extends 500 m down the west flank.

Cf **Cone-building lava flows of Cone C.** Gray-black, dense, massive, scoriaceous, and vesicular pāhoehoe and ʻaʻā lava flows that form the bench and bench-draping flows of Cone C. These lava flows can sometimes be described as thin, and include subaerial and sublacustrine flows. Sublacustrine textures are highly variable and include narrow streams of lava forming steep-sided ridges radiating from the terrace; "haystacks" of chaotically jointed, polyhedral fragments of dense lava; crudely and radially fractured pillow forms; contorted columns; and thin foreset sheet flows separated by hyaloclasite rubble. Lavas contain 10–20 percent conspicuous plagioclase phenocrysts up to 3 mm across and subordinate clinopyroxene and olivine in a glassy groundmass.

Cone D

Dc **Cinder and spatter deposits of Cone D.** Gray-black to oxidized red scoriaceous cinder, spatter, and agglutinate composing the steep upper flanks of Cone D.

Dsf **Spatter-fed lava flows of Cone D.** Gray-black to oxidized red, spatter-fed lava flows on the flanks of Cone D. Sample 01JLOK48B is dark gray, with moderate vesicularity. Conspicuous plagioclase phenocrysts comprise 30 percent of the sample, are equant shaped, and are 1 to 2 mm in size on average; some smaller crystals present. Sparse pyroxene phenocrysts are visible and average ~2 mm in size.

Df **Cone-building lava flows of Cone D.** Gray-black, dense, massive, scoriaceous, and vesicular pāhoehoe and minor ʻaʻā lava flows that form the lower flanks and lava bench of Cone D. Unit Df includes subaerial and sublacustrine flows. Cliff-draping flows are gray-black, dense pāhoehoe lava with curvilinear columnar joints and rare prismatically jointed pillow forms up to 50 cm across. Dramatic tubular and spherical internal void spaces are common. Lava tubes exposed in cross section range from 3.5 to 18 m in width (Almberg, 2003). Elsewhere, flows consist of thin, vesicular sheet flows and rubble piles extending from

bench top to the base of the exposed terraced platform forming primary slopes of up to 40 degrees. Lava samples described by Almberg (2003) and Finney (2004) are variable in phenocryst content. Almberg (2003) describes Cone D lava sample as glassy, with 10–20 percent conspicuous plagioclase phenocrysts and subordinate clinopyroxene and olivine. Finney (2004) describes one Cone D lava sample that has approximately 32 percent conspicuous plagioclase phenocrysts with sizes up to 2 mm.

Duh **Upper indurated hydrovolcanic deposits of early Cone D.** The Duh unit is described in more detail as the upper hyalotuff by Almberg (2003). The unit is cliff forming and finely layered, consisting of fine-grained ash (yellowish) and lapilli, "alternating . . . with beds of sub rounded [sic] to sub angular [sic], coarse (~5 cm) dense to poorly vesicular juvenile clasts" (Almberg, 2003, p. 15). The lapilli clasts have conspicuous plagioclase phenocrysts, which is typical of Cone D products (Almberg, 2003). The Duh beds dip 18° to 37° and strike to the northeast. In some locations, the Duh unit contains bomb sags; in others, it contains accretionary lapilli (Almberg, 2003).

Dlh **Lower indurated hydrovolcanic deposits of early Cone D.** This unit is described in more detail as the lower hyalotuff by Almberg (2003), with a summary reproduced here. The Dlh unit is more than 15 m thick and composed of weakly consolidated deposits that consist of ash to bomb-sized, dense, black scoria clasts that are weakly vesiculated. The scoria clasts contain conspicuous, white, 1- to 2-mm plagioclase phenocrysts. The unit appears welded with "polygonal cooling joints and chilled surfaces with what appear to be drip features" (Almberg, 2003, p. 12). Bedding, consisting of alternating layers of blocks and lapilli, is variable in orientation but is described as generally dipping away from the vent (Almberg, 2003).

Duv **Unconsolidated volcaniclastics of early cone D.** This unit crops out on the northeast side of Cone D and is described by Almberg (2003, p. 19) as two parallel ridges with steep walls, consisting of "unconsolidated juvenile ash and scoria" that does not appear to be bedded, and containing occasional lithic fragments. The unit is interpreted to have formed synchronously with the Duh deposits, consistent with the formation of the other tuff cones in the caldera. Tephra jetting may also have been an important process in primary deposition, with subsequent erosion and redeposition obscuring the original deposit bedding (Almberg, 2003).

Eruptive vents and deposits associated with a higher stand of an intracaldera lake. Hydrovolcanic deposits and lava flows of Cones G, H, I, J, K, N, and P, all of which are inferred to have erupted prior to lake draining (more than 1,560–1,010 ^{14}C yBP [Wolfe, 2001]). Relative ages are uncertain and based primarily on degree of modification.

Cone E Older Assemblage

Eof **Older lava flows of Cone E crater wall.** Inaccessible cliff exposures of gray, dense, ponded lava flows exposed in the inner Cone E walls. May be associated with the Ep sequence.

Ep **Hydrovolcanic deposits and lava flows of Cone E crater wall.** Inaccessible spatter and scoria deposits, bedded hydrovolcanic debris, lava flows, and tuff exposed in the near-vertical Cone E crater walls. The basal unit is yellow, massive to well-bedded, palagonitized volcanic breccia and sediments characterized by crude columnar jointing and chaotic, high-angle crossbedding. The Ep unit is overlain by oxidized scoria and agglutinate, bedded surge and fall deposits, and a ~50-m-thick, ponded lava lens with a brecciated base and margins, and convoluted columnar textures. Above this sequence is a section at least 100 m thick of gray, crossbedded, variably palagonitized hydrovolcanic deposits inferred to have come from Cone N.

Cone G

Gh **Pyroclastic deposits of Cone G.** Gray-tan, coarse-gravel- to sand-sized lithic fragments and poorly vesicular, blocky juvenile clasts forming the bedded pyroclastic sequence of Cone G, an approximately

260-m-high tuff cone enclosing a small lake in the western portion of the caldera. The Gh deposits are overlain on the south slope by scattered juvenile bombs and scoria from Cone E. Gh is the same unit as Qep, mapped by Byers (1959). Distal surge and fall facies from Cone G extend outside the caldera several kilometers and form the widespread rilled, unconsolidated deposit that covers much of the upper slopes outside the caldera. Samples from near the Cone G summit are basaltic andesite in composition and described as "vesicular and glassy feldspar-phyric" (BF00-G1; Finney, 2004, p. 55, table 2.1). They include a possible pillow lava sample with a glassy rind, vesicular interior, and visible plagioclase phenocrysts (Finney, 2004). Sample BF00-G2 collected from the summit region of Cone G is described as having ~15 percent plagioclase phenocrysts with ~1 to 2 percent pyroxene and olivine.

Gp **Palagonitized bedded deposits of Cone G.** Limited outcrops of yellow-buff to gray-brown palagonitized siltstone, sandstone, and gravel conglomerate present high in the tuff cone sequence Gh.

Cone H

Hh **Pyroclastic deposits of Cone H.** Gray-tan, coarse-gravel- to sand-sized lithic fragments and poorly vesicular, blocky juvenile clasts forming the massively bedded pyroclastic sequence of Cone H, an approximately 100-m-high tuff cone in the northwest sector of the caldera. The Hh deposits are best exposed in the summit crater and radiating limbs of the dissected tuff cone, and are overlain by lithic and juvenile bombs and scoria from a nearby maar (1817?) and related vents. Distal tephra from Cone H likely extends outside the caldera primarily to the west and northwest. More than 5 m of yellow-buff palagonitized volcanic breccia, conglomerate, sandstone, and siltstone are exposed in the inner wall of Cone H (Hp), indicating a perched lake once existed within the original tuff cone. This section is overlain by 4 m of gray to yellow-tan clay and silt, the base of which is gradational with palagonitized siltstone. The clay sequence is overlain by more than 6 m of a silt-and-sand-sized pyroclastic sequence, possibly of 1817 age. Sample BF00-H1 collected from near the summit of Cone H has 57.8 wt. % SiO_2 (low-silica andesite) and contains 15 percent plagioclase, ~5 percent pyroxene, ~1 percent olivine, and ~5 percent Fe oxides (Finney, 2004).

Hp **Palagonitized bedded deposits of Cone H.** A 10-m section of yellow-buff to gray-brown palagonitized siltstone, sandstone, and gravel conglomerate overlain by 1–3 m of thinly bedded, gray clays and 4–5 m of well-sorted, planar and crossbedded fine sands and clays perched near the summit of Cone H. Sits atop primary, unconsolidated pyroclastic deposits of Cone H.

Cone I

Ih **Pyroclastic, surge, and fall deposits of Cone I.** Gray-tan, coarse-gravel- to sand-sized, poorly vesicular, blocky juvenile clasts and lithic debris forming planar and crossbedded, moderately to poorly sorted surges and mixed surge and fall deposits of Cone I, a subdued remnant mound of a small tuff cone partially buried by 1997 lava flows. The beds range in thickness from subcentimeter to 10–20 cm. Surface is littered by blocks of dense, aphyric lava up to 1.5 m across.

Cone J

Jh **Pyroclastic, surge, and fall deposits of Cone J.** Gray-tan, coarse-gravel- to sand-sized lithic clasts and poorly vesicular, blocky juvenile clasts forming the pyroclastic sequence of Cone J, an approximately 120 m high, highly modified tuff cone in the northwest sector of the caldera. Gray-tan, silt-sized surge deposits cap the coarse tuff cone sequence and are in turn overlain by lithic and juvenile bombs and scoria from 1817 maar and related vents.

Cone K

Kh **Pyroclastic deposits of Cone K.** Gray-tan, coarse-gravel- to sand-sized lithic and poorly vesicular juvenile clasts forming the pyroclastic sequence of Cone K. This sequence overlies the east flank of Cone C and is interbedded with possible lacustrine and flood-related sediments on the Cone C bench. Total relief of Cone K is approximately 140 m.

Cone N

Nh **Pyroclastic deposits of Cone N.** Gray-tan, poorly consolidated, coarse-gravel- to sand-and-silt-sized, poorly vesicular, blocky juvenile clasts and lithic fragments forming the pyroclastic sequence of Cone N. These deposits are poorly exposed in several kīpuka against the southwest caldera wall. Deposits are moderately sorted and well bedded, with beds ranging in thickness from subcentimeter to tens of centimeters. Laminar and discordant crossbedding is well exposed, especially within buff-yellow palagonitized zones within the sequence (Np) on the outer southern flank of Cone E and inside Cone E. Outcrops define an approximately 1-km-diameter basin between Cones E and A that is interpreted as the source crater embayed by the highstand of the former intracaldera lake and now partially infilled by lava flows from Cones E and A. Sample 01NYO-19 consists of coarse lapilli fall deposits that have medium to high vesicularity. Some clasts have a distinctive quenched-rind texture, indicative of the phreatomagmatic eruption style. The dark-gray lapilli are fragile and fractured. Plagioclase phenocrysts are 1–3 mm in size and comprise 5–10 percent of the sample. Mafic phases are not clearly visible in the hand samples.

Np **Palagonitized deposits of Cone N.** Yellow-buff to gray-brown palagonitized coarse-gravel- to sand-and-silt-sized surge deposits within the unconsolidated Nh deposits in the southwest inner wall of the caldera. Np represents complexly bedded sequences with steep and variable dips that drape closely spaced crater forms.

Cone P

Pp **Palagonitized hydrovolcanic deposits of Cone P.** Yellow-buff to gray-brown palagonitized sands, silts, pebble conglomerates, and primary surge deposits exposed beneath the southwest edge of the Cone B lava flow. Complexly bedded sequences with steep and variable dips drape closely spaced crater forms. Graded bedding, rounded clasts, and soft-sediment deformation of finer grained beds suggest sublacustrine emplacement. Palagonitization is spatially variable, and indurated sequences grade abruptly into nonindurated zones. Dense lava fragments derived from underlying and possibly coeruptive lava flows are common. Sample CNO04-16A represents coarse-ash- to fine-lapilli-sized, angular juvenile fragments that are dark gray and microvesicular. No obvious phenocrysts observed in this sample.

Pf **Lava flow of Cone P.** Small outcrops of scoriaceous possibly sublacustrine ʻaʻā lava beneath palagonitized volcaniclastics adjacent to Cone B lava flow field. The Pf flow is draped by Ph and Cone B flows, and is inferred to have come from a vent now buried by the 1817 Cone B lava flow that fills a former small basin in this sector of the caldera. The Pf lava has trace plagioclase and pyroxene in a dark, glassy groundmass.

Undifferentiated Hydrovolcanic Deposits of Caldera Tuff Cones

hv **Undifferentiated hydrovolcanic deposits of caldera tuff cones.** Bedded, gray-tan to black, coarse-gravel- to sand-and-silt-sized pyroclastic surge and fall units on the western caldera rim and on the Cone D bench. Juvenile clasts are blocky and poorly vesicular. Deposits represent eruptions from multiple tuff cones within the caldera. This sequence can be traced to outside the caldera and thins progressively to the west. Individual beds range in thickness from a few centimeters to more than 3 m at the caldera rim. This unit is most likely derived from eruptions at the large tuff cones G and N in western Okmok Caldera but may include surge and fall deposits from eruptions at other vents. Discontinuous deposits of 1817 overlie these deposits on the upper flanks of Okmok Volcano. Erosion of this unit provides the source for Hwlh and Qlh mapped at the northwest coast. Byers (1959) recognized bedded deposits on the caldera rim and, although he inferred some were likely derived from postcaldera eruptions, included them within his Okmok Volcanics (Qvo) map unit. Wolfe's sample 00-OK-104-14C (2001) from this unit dates the maximum age of post-Okmok II surge deposits at 1,890 ± 40 yBP. On the Cone D bench, undifferentiated surge, fall, and intercalated lacustrine deposits vary in thickness; lava flows of Cone D are exposed where cover is thin. The lacustrine deposits are described as "yellow, orange and brown laminated silt and clay layers (5–20 cm) intercalated with coarse, angular, clast-supported, gravely [sic] layers

and coarse sands [that] mantle the upper bench surface. Foreset beds of coarsening upward scoria (5 cm), separated by local ash beds 3–6 cm thick, overlie clays, sands and gravels." (Almberg, 2003, p. 35). The surge deposits exposed on the Cone D bench are more than 2 m thick and consist of unconsolidated dark-gray deposits with abundant accretionary lapilli (4 to 5 mm in diameter).

Volcanic Deposits Exposed in the Caldera Wall

sv **Subaerial volcanics and associated feeder dikes and sills.** Basalt to basaltic andesite lava flows and interbedded scoria, along with feeder dikes. Sample 01NYO-28 from the sv unit has 54.49 wt. % SiO^2. This unit includes packages of related deposits with variable proportions of dikes, flows, and scoria. In the southeast caldera wall, the interior of a cinder cone has been exposed by caldera collapse. Here, the scoria dips moderately to the northeast or southwest, away from a central zone with numerous small dikes. Flows are rare. Another package exposed in the southwest wall is composed of several thin flows with small amounts of interflow scoria that fill a pre-existing valley. This unit can be broadly subdivided based on the outcrop color of the scoria. In the northwest, northeast, and southeast quadrants, the scoria is red, suggesting that deposits are relatively near their source vents. In fact, the two higher elevations on the west and northwest rims may be remnants of pre-existing precaldera cones roughly the same size as the larger postcaldera cones. In the southwest quadrant interflow—where lava flows comprise more of the section than scoria, and where dikes are absent—scoria is black, reinforcing the implication that these flows are farther from their source vent. This unit sits, for the most part, unconformably on the palagonitic unit below (unit pal). Sample 01NYO-28 is dark gray, fine grained, and moderately vesicular. It contains ~15 percent submillimeter-sized plagioclase crystals and sparse plagioclase phenocrysts 1–2 mm in size. Mafic phases are not clearly visible in this hand sample.

ml **Dense, glassy lava.** Pods of dense, glassy, massive lava with plagioclase phenocrysts occurring in contorted radiating columns a few to several tens of centimeters in diameter. Four samples have compositions of 53.5 to 55.0 wt. % SiO_2. Columns break easily along relatively flat surfaces perpendicular to the length of the column. These lavas are exposed primarily in the caldera wall in the Gates region, with small outcrops on the caldera floor adjacent to Crater Creek where the creek exits the caldera (sample 01NYO-23, $^{40}Ar/^{39}Ar$ isochron age 22 ± 50 ka). Byers described a unit in this region as "Vitreous Andesite" (unit Qva of Byers, 1959). In the northeast portion of the caldera, this lava forms irregular podiform, dike-like bodies surrounded by palagonitic tuff and breccia (unit pal). The contacts are often wispy, with flame-like, undulatory tongues cutting into the tuff. These lava tongues can break up so that pieces of the lava at millimeter, centimeter, decimeter, or larger are freely floating in the tuff (peperite). Thus, it appears that the lava was syneruptive with the tuff, and the contorted, jointed nature of the lava masses is a result of quenching against the unconsolidated water-saturated tuff. Outcrops of this unit are very similar in appearance to ice-contact lavas, but the intercalation of fragments of these lavas in the surrounding tuff suggests that they did not quench against ice, but against the water-saturated tuff. A small plug of massive lava on the western wall behind Cone G is not surrounded by palagonite and is presumably younger, ice-quenched lava.

pal **Palagonitic tuff and breccia.** Massive to bedded, orange, tan, and brown tuffs. Angular lava fragments are monolithic and similar in appearance and composition to the massive lava (unit ml). In several places, bedded units are steeply dipping and drape over pre-existing, massive, truncated, palagonitic tuffs. The steep dips are likely delta features, indicating that these tuffs were erupted subaqueously into a lake or large englacial vault. In places, packages of steeply dipping tuffs are truncated by horizontal lava flows at "passage zones" (Smellie, 2000), which mark old water-surface levels, many of which are substantially higher than the last highstand of water in the current caldera (Wolfe, 2001). This unit is widespread in the caldera walls and likely correlates with unit Pg on the flanks of the volcano. This unit was similarly mapped by Byers (1959) as unit Qtap.

Lahar and Flood Deposits Outside the Caldera

Prior to the 2008 eruption, flood deposits and alluvium produced during the 1817 eruption were well exposed where they formed terraces overlying the caldera lake flood deposits near the mouth of Crater Creek. They were also exposed in the 1817 flood channel along Crater Creek just within and below the caldera gate. These deposits may partly consist of volcaniclastic material reworked from pre-1817 surges and tephra fall deposits. The 1817 flood deposits occur over an area too small to depict at map scale so are noted here as younger than other major lahar deposits outside the caldera. They may be exposed again as overlying volcaniclastics from the 2008 eruption are eroded.

Hwlh **Western flank lahar deposits, younger than the second caldera-forming eruption.** Volcanic debris flows and alluvium up to several meters thick consisting of silt and sand with numerous clasts of gravel and occasional boulders. The deposits typically are preserved as unvegetated terraces along streams that start on the upper flanks of Okmok Volcano. They consist of massive, unsorted to poorly sorted, and poorly stratified debris flows composed of reworked and subrounded to subangular black to red scoria and lithic fragments mixed with volcanic ash as well as volcanic alluvium. The thickest zones are depicted on the map and overlie deposits of the second caldera-forming eruption (unit Hcfe2).

Hllh **Older lahar deposits, younger than the second caldera-forming eruption.** Multiple lahars and alluvium younger than the second caldera-forming eruption are exposed in high bluffs adjacent to beaches on the west flank of Okmok Caldera. The lahars range in thickness from several decimeters to a few meters, and are composed mainly of silt and sand, but also contain occasional gravel and boulders. These deposits are typically vegetated and are buried by several younger, thin tephra layers. They are typically poorly exposed away from the beach cliffs and are usually buried by younger lahars and tephra deposits, as well as reworked ash and alluvium on the upper slopes of Okmok Caldera.

Hfl **Flood deposits related to draining of Okmok Caldera lake (ca.** 1,560–1,010 yBP; Wolfe, 2001). Coarse-grained boulder and gravel-rich alluvial sediments deposited by an unusually high discharge flood event during the draining of an ancient lake from the caldera. The deposits are preserved in terraces and fans of sand and coarse gravel as much as 6 m thick. These deposits also include numerous water-transported and rounded boulders and clusters of boulders, some as much as 5–10 m in diameter.

Hfl-b **Deltaic facies of the ca.** 1,560–1,010 yBP flood deposits. Gravel-rich sediments forming extensive sets of coarse-grained foreset and topset beds deposited into the Bering Sea by an unusually high discharge during the flood event.

Hfl-c **Flood-related coulee channels and landforms.** Eroded and scoured areas of dry waterfalls, pinnacles, potholes, whalebacks, and other streamlined landforms cut into Okmok II ignimbrite, which were eroded by the ca. 1,560–1,010 yBP flood and are thinly mantled with flood sediments today. This unit also includes abandoned and deeply scoured flat-bottomed, coulee-like channels that contain thick gravel deposits and gravel terraces as much as 4 m thick, as well as huge boulders as much as 12 m in diameter.

Holocene Volcanic Deposits Outside the Caldera

Hcy **Cinder Cone at Cape Aslik.** A 270-m-high sparsely plagioclase-phyric basalt cinder cone at Cape Aslik to the west of Okmok Volcano. Sample 01NYO-01 has 53.45 wt.% SiO_2 and is medium to dark gray brown, with moderate vesicularity. Phenocrysts consist primarily of sparse plagioclase of 1–2-mm size, and mafic phases are not clearly visible.

Hfy **Lava flows at Cape Aslik.** This sparsely phyric basalt lava flow extends west from the cinder cone (Hcy) to the sea, where it is approximately 30 m thick; the lava flow surface is largely devoid of ash cover and appears little modified by erosion. Aslik lava flow sample 01NYO-02 is poorly to moderately vesicular,

with conspicuous plagioclase up to 1–2 mm in size and sparse olivine crystals 1–2 mm in size within a moderately fine grained groundmass.

Hfo **Flank lava flows deposited between the first and second caldera-forming eruptions.** The Hfo lava flows are generally found along the northern coast and in stream channels in the northern to western flanks and at higher elevations along the eastern flanks. The source vents for those flows are not visible and may be buried by pyroclastic fall and flow units related to the second caldera-forming eruption. Older flows in this group occurred after the first caldera-forming eruption, as seen by a baked upper contact on top of the Pcfe1 deposit at station 04JLOK007 on the north coast. Younger flows in this group occurred shortly before the second caldera-forming eruption, separated from unit Hcfe2 by an approximately 0.5–1-m-thick soil horizon. Hfo lavas typically have a medium-gray, fine-grained, phenocryst-poor texture that can be described as "sugary." Plagioclase phenocrysts are typically 1–3-mm size with abundances of 15 percent or less. Sparse mafic minerals consist of 1–2-mm-size clinopyroxene and olivine, found in less abundance than plagioclase. The lavas are nonvesicular in samples collected from flow interiors, and variably vesicular in samples collected near the margins. Hfo lavas are associated with scoria deposits on the eastern flanks near Magazine Ridge. Hfo scoria is vesicular, with proportions and types of phenocrysts similar to the lavas.

Hf **Holocene lava flows on the flanks.** Age relative to caldera-forming eruptions is unknown. The Hf lava flows likely represent separate eruptions that occurred over an unknown range in time during the Holocene. Separately mapped Hf flows have different compositions. For example, hand sample 04NYOK006 from an outcrop to the southwest of Mount Tulik represents a vesicular sample from a subaerial basaltic lava flow (52.1 wt. % SiO_2) that is 2 m thick, with a deep brick-red flow base. This lava flow contains approximately 20 percent plagioclase phenocrysts that are up to 5 mm in length, in a medium-grained groundmass. Sparse olivine phenocrysts are visible, with most being approximately 1-mm size. The flow unit that this sample came from is described as having a greater proportion of plagioclase compared with other Hf lava flows in the region to the southwest of Tulik Volcano. In contrast, another Hf lava flow mapped along the eastern caldera rim is markedly different in composition and in hand sample texture: hand sample JS01OK05-2 from this higher-elevation eastern rim lava flow appears to be platy and glassy, with a quenched rind. This flow is high-silica andesite in composition (62 wt. % SiO_2), as observed in samples JS01OK05-1 and JS01OK05-2 from outcrops high on the eastern caldera rim. The JS01OK05-2 hand sample shows a banded texture with microvesicular regions that could represent flattened pumice or fiamme. This hand sample contains sparse olivine and plagioclase phenocrysts that are 1–2-mm size.

Hc **Holocene cinder cones on the flanks.** Age relative to caldera-forming eruptions is unknown. Sample 01JLOK50 from the "Kidney Bean" cone located on the east flank of the caldera, south of Cape Idak, is uniformly fine grained, and coated with fine, brown, ashy soil. It is difficult to determine the petrography of this sample. Sample JS01OK10-1 is a black spindle bomb from on top of an Hc cinder cone located on the eastern caldera flanks. This sample is basaltic andesite (54.67 wt. % SiO_2) and highly vesicular, with a finely layered structure to the vesicularity. The sample includes 5 percent or less plagioclase phenocrysts that are 1-mm size and mostly chalky white. Mafic phases are not visible in hand sample.

Products of the Second Caldera-Forming Eruption (Okmok II, ca. 2,050 yBP)

Hcfe2 **Pyroclastic flow and fall deposits of the second caldera-forming eruption (Okmok II, ca.** 2,050 yBP). The depositional sequence begins with tan to light red-orange rhyodacite and iridescent dark-gray andesite Plinian and phreatomagmatic tephra fall deposits, overlain by voluminous, dark-gray basaltic andesite pyroclastic flow deposits that extend from the modern caldera rim to the coastline in all quadrants. Formerly mapped as Okmok Volcanics (Qo of Byers, 1959), the average radiocarbon age for Hcfe2 is 2,050 ± 30 yBP (app. B). Thick (up-to-1-m) deposits of the rhyodacite tephra fall occur at Reindeer and Ashishik Points on the north flank of the volcano. In one outcrop on the northwest flank of the volca-

no (04JLOK047), the rhyodacite is poorly sorted, matrix supported, and containing pumices in a finer grained, ash-rich matrix. This deposit does not have the well-defined sorting and layering of the tephra fall deposits found elsewhere. It is possible that this deposit represents a small pyroclastic flow resulting from partial collapse of the plume. The rhyodacite pumice deposits represent 0.25 km^3 magma on a dense rock basis (DRE; Burgisser, 2005). The andesite fall deposits extend to the east and are estimated at 0.35 km^3 dense rock volume (Burgisser, 2005). The basaltic andesite pyroclastic flow deposits have an estimated volume of 29 km^3 DRE, thus making up the majority of the magma volume erupted. This unit contains individual juvenile scoria fragments along with evidence for phreatomagmatic activity, including armored lapilli and lithic fragments. This unit dominates the plateau-like morphology of the modern flanks of Okmok Volcano. At location 04JLOK040 near the caldera's Gates region, the pyroclastic flow unit contains a small outcrop that is densely welded and includes fiamme. Surface features of the Hcfe2 pyroclastic density current deposits are variable in different locations around the caldera. The typical morphology is a relatively smooth and flat surface forming a plateau-like feature incised by stream channels. Directly to the south of Mount Tulik, the surface of the flow sheet is noticeably more irregular, with terrain marked by numerous mound-like structures. The individual mounds are about 20–60 m wide and of unknown height (but likely no more than several meters tall). These features are likely a result of fumarolic activity while the thick pyroclastic flow deposits were cooling. These features are very similar in appearance and relative size to fumarolic mounds described in the Bishop Tuff by Sheridan (1970).

Hcfe2-a **Agglutinate facies of the Okmok II caldera-forming eruption deposits.** Black scoriaceous juvenile bombs that are basaltic andesite in composition and variably sintered and welded; deposits occur on the northwest and north flanks and northeast caldera rim, as well as in stream valleys on the east flank ("Agglomerate" and "Welded Agglomerate" of Byers, 1959). The agglutinate facies consists of thick, clast-supported, fines-poor accumulations of spatter, ribbon bombs, and abundant lithic fragments. Location 04JLOK047 on the north flank of the volcano offers a good example of this facies (Larsen and others, 2007). The agglutinate facies can be found adjacent to the massive, matrix-supported pyroclastic flow deposits, often separated by an intervening stream channel, as seen at location 04JLOK047. In medial distance outcrops, the agglutinate facies transitions into an ash-rich pyroclastic flow facies containing a higher percentage of cauliflower scoria, ribbon bombs, and lithic fragments. Prominent outcrops occur at stations 04JLOK042, -044, -045, and -047. Hcfe2-a is difficult to display in map view, as it occurs in stratigraphic sections below the pyroclastic flow and fall facies of the second caldera-forming eruption (unit Hcfe2). Where warranted, an exaggerated polygon of Hcfe2-a has been drawn to note its location. For stratigraphic sections describing the Hcfe2 unit, see Larsen and others (2007).

Hccb **Lava flows and tephra deposits of Crater Creek Basalts.** Crater Creek Basalt (unit Qcb of Byers, 1959). Dominantly flat-lying basaltic flows that formed as intracaldera fill between the first and second caldera-forming eruptions. Along the northern wall of the second caldera that formed during the Hcfe2 eruption, 15 separate flows are stacked to an aggregate thickness of 150 m. Byers (1959, p. 313) describes "One to 10 feet of red ash or scoria" separating several of the flows. At the western end of this unit, the flows ramp up onto a pre-existing, eroded (glacially polished?) surface to an altitude of 900 m or more, suggesting that they were derived from a vent in the general vicinity of the intersection of North Arcuate Ridge and the caldera wall. In the Gates region, the Hccb map polygon encompasses an area that also includes small discontinuous exposures of Hcfe2, colluvium, and modern stream deposits. Despite the name, the Crater Creek Basalt unit encompasses a range of whole-rock compositions from basaltic andesite to andesite (Finney, 2004). The sequence is described as porphyritic to aphyric in crystal textures, with groundmass ranging from glassy to microcrystalline with microlites up to 50 μm in size (Finney, 2004). In all Crater Creek Basalt sequence samples described, phenocryst phases consist predominantly of plagioclase (10–30 percent; up to 2 mm in size), clinopyroxene (<5 percent; 0.5 mm) in clots with plagioclase or olivine, olivine (<1 percent), and Fe oxides (<5 percent; Finney, 2004).

Products of the First Caldera-Forming Eruption (Okmok I, ca. 12,000 yBP)

Pcfe1 **Pyroclastic flow and fall deposits of the first caldera-forming eruption (Okmok I, ca.** 12,000 yBP). This unit is exposed in deep stream cuts in the mid to low elevations along the flanks of Okmok Volcano. The thickest sections (up to 80 m) exist along the north flank, with excellent exposure visible in Colorado Creek. The depositional sequence begins at the base with debris avalanche deposits that grade upward into a thick sequence of juvenile-clast-rich wet surge and lahar deposits that contain mixed rhyodacite and andesite pyroclasts. The surge/lahar deposits are locally interlayered with rhyodacite to andesite juvenile and lithic-rich pyroclastic flows. Up section, the surges and lahars grade into massive ash-flow deposits that contain locally variable amounts of basaltic andesite and rhyodacite pumice and scoria. Accretionary lapilli as large as 5 cm occur in discrete layers through the middle and upper portions of this unit at Colorado Creek (station 01JLOK47). The top of the ash-flow deposits includes pyroclastic surge units, and pods of large lithic boulders along the eastern and southern flanks. The upper Pcfe1 ash-flow surface is undulatory at all locations studied, suggesting significant water interaction and a possibly sluggish, chilled pyroclastic flow deposit. The Pcfe1 unit was formerly mapped by Byers (1959) as unit Qo (Okmok Volcanics), lumped into the same map unit as the Hcfe2 caldera-forming deposits. The Okmok I (Pcfe1) caldera-forming eruption occurred about 12,000 years ago, with ^{14}C radiocarbon dates (11,540 ± 40 14C yBP; app. B) obtained from charcoal found directly beneath the pyroclastic flow deposits exposed on westernmost Unalaska Island, and dates associated with distal volcanic ash deposits from these eruptions found near the city of Unalaska 100 km to the east (Bean, 1999; Begét and others, 2005).

Pleistocene Volcanic Deposits Older than the First Caldera-Forming Eruption (Older than ca. 12,000 yBP)

Pv **Northwest flank near-vent spatter accumulation (Pleistocene).** Near-vent spatter accumulations that form a linear ridge on the northwest flank, upslope to the east of Aguliuk Point, together with lava flows (Pfnw). The lava and spatter surfaces are polished and locally striated, indicating that they were glaciated. In a saddle region along this ridge, two pyroclastic flow units drape the spatter and flow deposit. One is young, dark gray to black, and possibly from the second caldera-forming eruption (unit Hcfe2). The second outcrop is older, highly palagonitized, and interpreted to be tuff of the first caldera-forming eruption (unit Pcfe1). Sample CNO01-01 represents a bomb from the Pv unit. It is dark gray with fine-scale, moderate to high vesicularity. This sample contains sparse, conspicuous lathe-shaped plagioclase 2–3 mm long, in abundances of 3–5 percent. This bomb sample contains lithic inclusions of 1–1.5-cm size. Mafic phases are not visible.

Pfnw **Northwest flank lava flows (Pleistocene).** Lava flows on the northwest flank that form the bulk of the linear ridge, together with Pv near-vent spatter accumulations. Surfaces of the Pfnw flows are polished and locally striated. The flows are interpreted to be stratigraphically below deposits of the first and second caldera-forming eruptions. Samples from the Pfnw unit are too vesicular to date using $^{40}Ar/^{39}Ar$ methods. Sample CNO01-03 has a medium-gray, "sugary"-textured groundmass and is phenocryst poor. Plagioclase phenocrysts are sparse and up to 1 mm in size. Sparse olivine phenocrysts are up to 2–3 mm in size.

Psi **Basalt intrusive.** Aphyric and feldspathic basalt intrusive mapped by Byers (1959) as unit QTai. One occurrence mapped just north of North Arcuate Ridge within unit Ps. Not field checked.

Ps **Subaerial lavas (Pleistocene).** Thick sequences of mafic subaerial lavas around the flanks of Okmok, high along the caldera rim in the north, east, and southwest sectors, as well as along the coast and on Magazine Ridge; some with ice-contact features. These voluminous, edifice-building lavas range in composition from basalt to andesite, though are primarily basalt to basaltic andesite. Ps lavas have fine-grained groundmass often described as "sugary" textured. Typically, these lavas have sparse phenocrysts

of appreciable size, predominantly consisting of plagioclase, with smaller proportions of olivine and clinopyroxene. Plagioclase phenocrysts range from ~1 to 3 mm in size, and often have a distinctly elongate habit. Olivine is sparse and typically 2–3 mm. Clinopyroxene is found in a few samples, with phenocrysts 2–3 mm in size (sample 04JLOK009) and 3–4 mm in size (sample 04NYOK019). Some of these lavas correlate to outcrops mapped by Byers (1959) as QTab. Twenty samples were dated from this unit, with the oldest age obtained from an aphyric flow on North Arcuate Ridge (sample 04NYOK019; $^{40}Ar/^{39}Ar$ plateau age of 364 ± 19.7 ka; app. A).

Pg **Subglacial lavas and pyroclastic flows (Pleistocene).** Voluminous, interlayered lavas and pyroclastic flows that show distinct ice-contact features. These units are sometimes locally capped with glacial till (not shown). The lavas are aphyric, with a "sugary" texture. The pyroclastic flows are brownish red, variably palagonitized, and locally rich in lithics up to 0.5 m in size. The subglacial fragmental portions of these units are difficult to distinguish from the Okmok I pyroclastic flow deposits that outcrop along the south and east flanks. These units also include some units formerly mapped as QTap by Byers (1959). Those outcrops include yellow-buff to gray-brown sands, silts, pebble conglomerates, volcanic breccias, and pyroclastic flows exposed in caldera walls and in isolated outcrops on the flanks.

Pr **Flow-banded rhyolite (Pleistocene).** A biotite-phyric rhyolite (73 wt. % SiO_2) lava flow that outcrops high to the north of North Arcuate Ridge, extending in a ridge to the north of the higher-elevation caldera rim that resulted from the Okmok I eruption. The rhyolite is flow banded, with dense, black obsidian bands interlayered with light-pink, finely vesicular rhyolite. The outcrop has shed talus covering any contacts with older units below. Byers (1959) describes the unit as having bands of both dense, black obsidian bands and vesicular, light-gray felsite. In the obsidian, basaltic andesite inclusions or xenoliths are present, and xenocrystic labradorite, augite, and olivine likely originating from the inclusions are observed (Byers, 1959). Hand sample 04JLOK023A consists of black, dense, glassy obsidian with visible plagioclase phenocrysts 1–2 mm in size. The basaltic andesite inclusions described by Byers (1959) are also present in this sample.

Pif **Plagioclase-olivine basalt flow of Mount Idak (early Pleistocene).** This unit is common in the Mount Idak plateau area near the summit of Mount Idak and is described in detail by Byers (1959; unit Qbo). Pif lava includes euhedral plagioclase and magnesian olivine, with subordinate clinopyroxene microphenocrysts.

Pfo **Older edifice lavas (Pleistocene).** Lava flows that are probably older than the modern Okmok Volcano edifice. These include the thick sequence of basaltic lavas in the Ashishik ridge to the north and northwest of the caldera, which have ages of 1,869 ± 116 to 1,865 ± 83 ka (Stone and Layer, 2006). This unit includes the relatively primitive, high-MgO basalts of Cape Idak (48.9 wt. % SiO_2 and 15.2 wt. % MgO from sample id-01sc; Nye and Reid, 1986). These deposits have high relief compared with the younger, caldera-forming units and may be remnants of an older volcanic center. Lavas are medium to dark gray, typically with fine-grained groundmass. They are more plagioclase rich than the Pfm lavas, containing plagioclase phenocrysts up to 2–5 mm in size. Olivine is sparse and smaller, typically ~1 mm. In places, this unit is formerly unit QTab of Byers (1959).

Plp **Palagonitized pyroclastic rocks of Cape Idak (Pleistocene).** Palagonitized pyroclastic rocks exposed in steep cliffs at Cape Idak of unknown age and origin but likely related to an older volcanic center. Unit QTap of Byers (1959). No samples at this location.

Pfm **Mafic phenocryst basalt (Pleistocene).** Outcrops are found in the northeast sector of Okmok Volcano: Mount Idak region (sample id-07sc, $^{40}Ar/^{39}Ar$ isochron age of 1,942 ± 115 ka), west of New Jersey Creek near Ashishik Point, on the east flank at Magazine Ridge (sample 00JLOK34, $^{40}Ar/^{39}Ar$ isochron age of 341 ± 93 ka), and below unit Pal, low in the northeast caldera wall. Pfm basalts are characterized by light- to dark-gray groundmass with minerals in decreasing order of abundance: olivine, clinopyroxene,

and variable plagioclase. In the Idak area, Pfm basalts have abundant olivine, with crystals up to 4–5 mm and proportions up to 30–40 percent in some samples classified as picrites (e.g., samples id-01sc and id-05sc). Samples id-01sc and id-05sc have a fine-grained, dense groundmass and are plagioclase poor. The Pfm unit in the Idak area also includes variably altered lavas that are distinctly red to pink, with olivine and pyroxene crystals altered to deep red to brown. Sample id-13sc contains large clinopyroxene phenocrysts up to 3 mm in size, and in total has approximately 30–40 percent olivine and pyroxene phenocrysts. Ashishik region Pfm lavas are fine grained, with dense, "sugary" groundmass, and typically contain olivine and clinopyroxene mafic phenocrysts, with subordinate plagioclase. Phenocrysts are rarely larger than 2 mm; however, in sample as-09sc, plagioclase phenocrysts are up to 3–4 mm in size. Near Magazine Ridge, outcrops have a fine-grained groundmass with approximately 30 percent olivine and clinopyroxene phenocrysts up to 4–5 mm. These lavas also contain 15–20 percent plagioclase phenocrysts 2–3 mm in size, based on a hand sample description from sample 04JSOK019. Within the lower northeast caldera wall, adjacent to the pre-2008 toe of the 1958 lava flow, these basalts contain ~20 percent olivine and clinopyroxene, with clinopyroxene being ~50 percent more abundant than olivine. Plagioclase is subordinate and 15 percent or less in abundance. This lithology is exemplified by sample 04NYOK048 in the inner caldera wall to the north of Cone D. The unit is described by Byers (1959; unit QTam) as mafic phenocryst basalt.

Pbv **Bedded volcanic rocks (Pleistocene).** Basaltic lava flows mapped in small outcrops exposed along the east and southeast shoreline. Sample 02JLOK60 was collected at the outlet of Tulik River. This sample is very fine grained, aphyric with no visible phenocrysts, and light gray with a slightly pink tone. $^{40}Ar/^{39}Ar$ isochron age of this sample is 83 ± 76 ka.

Subglacial and Subaerial Lavas of Flank Tuyas

Ptf **Subglacial and subaerial lavas (early Pleistocene).** The Ptf unit comprises thinly bedded lavas that form six flank tuyas: Mount Tulik, Jag Peak, and tuyas 1–4 on the southwest flank (fig. 2). This unit was formerly mapped as Qbo by Byers (1959). Lavas are columnar jointed, with shattered, ice-contact surfaces. The Mount Tulik lavas are olivine- and plagioclase-phyric. Jag Peak lavas consist of a series of subaerial lava flows overlying a series of palagonitized pyroclastic deposits that form an apron around the vent. These flows are similar in appearance to those from Mount Tulik. Jag Peak lava flows are thin, with individual flow units 1–2 m thick, and exhibit wavy, low-angle cross-cutting unconformities. Plagioclase is abundant in these crystal-rich lavas, with ~30 percent plagioclase phenocrysts in sample 04NYOK042. Plagioclase phenocrysts are up to 3 mm in size. Subordinate olivine and clinopyroxene exist and are altered to a deep-reddish to brownish-red color. Clinopyroxene phenocrysts are large enough to display clear cleavage planes. Lava from tuya 3 has an $^{40}Ar/^{39}Ar$ isochron age of 1,095 ± 28 ka, and lava from tuya 4 (fig. 2) returned an age of 1,989 ± 237 ka.

Pth **Subglacial, bench-forming, fragmental deposits (early Pleistocene).** Palagonitized pillow fragment breccias, hyaloclastites, and subaqueous tuffs that form prominent benches around the base of the tuya satellite vents of unit Ptf.

Ptv **Near-vent lava plugs of flank tuyas and Kettle Cape (early Pleistocene).** Mapped by Byers (1959) as Qbv (plagioclase-olivine basalt of satellite vents) on the southwest flank tuyas and at Mount Idak, and as QTvp (vent and intrusive complex) at Kettle Cape. Sample 01NYO-27 is moderately vesicular and medium to light gray, with a "sugary"-textured groundmass. Olivine phenocrysts are 3–5 mm in size and compose ~5 percent of the sample. Some olivine phenocrysts are reddish brown with an oxidized outer rim. Conspicuous pyroxene phenocrysts are up to 7 mm in size and compose 10–15 percent of the sample. Submillimeter-sized plagioclase is visible in the groundmass at approximately 30 percent abundance. Plagioclase phenocrysts ~1 mm in size are visible and compose 5 percent of the sample.

Volcanic Deposits of Central Umnak Island

Qfsw **Plagioclase-rich lavas of Cinder Point and central Umnak Island (late Pleistocene to early Holocene).** The Qfsw lavas are plagioclase rich in a medium-gray groundmass and are distinctly different from the shield-building lavas from Okmok Volcano. The Qfsw lavas have 15–20 percent by volume plagioclase phenocrysts from lava flows east of Cinder Point and ~50 percent plagioclase in Cinder Point lavas, as seen in flow sample 01NYO-03. Individual plagioclase crystals are up to 1 cm in size, with equant habits. Lavas also contain sparse clinopyroxene and olivine grains that are 1 mm or smaller. Lava flow morphology is preserved, indicating late Pleistocene to early Holocene.

Qc **Vent and cinder deposits (late Pleistocene to early Holocene).** Vent and cinder deposits associated with Qfsw lavas of central Umnak Island.

Qvsw **Hydrothermally altered volcanic rocks (early Pleistocene).** Along the coast and near Cinder Point, these units are mapped directly from Byers' unit QTv (1959). Sample 47 ABy 44 is described as hydrothermally altered plagioclase basalt (Byers, 1959).

Qvp **Vent and intrusive complex; includes a few unaltered rocks (early Pleistocene).** These units were mapped directly from Byers' unit QTvp (1959). Byers (1959) briefly describes this unit as vent and intrusive complex rock associated with the bedded volcanics from unit Qvsw.

Qvq **Intensely altered, silicified, potassium-feldspathized rocks (early Pleistocene).** These units were mapped directly from Byers' unit QTvq (1959). Byers (1959, p. 293) describes this unit as consisting of "intensely silicified, potassium feldspathized rocks." The unit shows pervasive silicification and in places contains tourmaline as evidence of intense alteration.

ACKNOWLEDGMENTS

This work was partially supported by the U.S. Geological Survey under multiple years of cooperative agreement grants to the University of Alaska Fairbanks Geophysical Institute and the Alaska Division of Geological & Geophysical Surveys, currently Cooperative Agreement G19AC00171, and by USGS Volcano Hazards Program funding to the Alaska Volcano Observatory. We thank many geologists and geophysicists who provided their time, insights, and camaraderie at Fort Glenn in all kinds of weather, including Jim Begét, Deb Bergfeld, Alain Burgisser, Michelle Coombs, Cheryl Cameron, John Eichelberger, Jeff Freymueller, Rick Hazlett, Alexander Max Kaufman, David Lescinsky, Taryn Lopez, Doerte Mann, Steve McNutt, Michael Ort, and Guy Tytgat. Former undergraduate and graduate students who participated in the geology fieldwork at Okmok Volcano include a cohort from Pomona College and the University of Alaska Fairbanks: Leslie Almberg, Matt Patrick, Ben Finney, Delanora Grey, Ken Papp, Joel Unema, and Lily Wong. Reviews by Tim Orr, Julie Nolan, and Drew Downs provided helpful insight and are much appreciated. Bering Pacific Ranches Ltd. supported this work through lodging and logistics support. Access to Umnak Island was by charter flights or boat from the Port of Dutch Harbor. We thank Cliff Gill (Airborne Scientific), Don Graves (Miss Peppers), and Jimmer MacDonald (Miss Alyssa) for safe transport to Umnak Island in often challenging sea conditions. Maritime Helicopters and pilots Bill Springer, Rick Farrish, and Jon Combs made our work possible, providing efficient, safe, and professional transportation in the field area. Any use of trade, firm, or product names is for descriptive purposes only and does not imply endorsement by the U.S. Government.

REFERENCES

Allen, S.R., 2004, Complex spatter- and pumice-rich pyroclastic deposits from an andesitic caldera-forming eruption: the Siwi pyroclastic sequence, Tanna, Vanuatu: Bulletin of Volcanology, v. 67, p. 27–41.

Almberg, L.D., 2003, Hydrovolcanism in Okmok Caldera, Alaska: University of Alaska Fairbanks unpublished M.S. thesis, 57 p.

Bean, K.W., 1999, The Holocene eruptive history of Makushin Volcano, Alaska: University of Alaska Fairbanks unpublished M.S. thesis, Fairbanks, AK, 130 p.

Begét, J.E. and Larsen, J.F., 2001, Links between prehistoric high latitude volcanic eruptions, aerosol events, in the GISP2 ice core, Roman records, and Holocene climate change [abs.], in Challenges of a changing earth: Amsterdam, International Geosphere-Biosphere Program, p. 185.

Begét, J.E., Larsen, J.F., Neal, C.A., Nye, C.J., and Schaefer, J.R., 2005, Preliminary volcano-hazard assessment for Okmok Volcano, Umnak Island, Alaska: Alaska Division of Geological & Geophysical Surveys Report of Investigation 2004-3, 32 p., 1 sheet, scale 1:150,000.

Bergfeld, Deborah, Evans, W.C., Hunt, A.G., Lopez, Taryn, and Schaefer, J.R., 2020, A post-eruption study of gases and thermal waters at Okmok Volcano, Alaska: Journal of Volcanology and Geothermal Research, v. 396. doi.org/10.1016/j.jvolgeores.2020.106853

Bingham, D.K., and Stone, D.B., 1972, Paleosecular variation of the geomagnetic field in the Aleutian Islands, Alaska: Geophysical Journal of the Royal Astronomical Society, v. 28, p. 317–335.

Black, L.T., 1981, Volcanism as a factor in human ecology: The Aleutian case: Ethnohistory, v. 28, no. 4, p. 313–339.

Black, R.F., 1974a, Geology and ancient Aleuts, Amchitka and Umnak Islands, Aleutians: Arctic Anthropology, v. 11, no. 2, p. 126–140.

———1974b, Late-Quaternary sea level changes, Umnak Island, Aleutians: their effects on ancient Aleuts and their causes: Quaternary Research, v. 4, no. 3, p. 264–281.

———1975, Late-Quaternary geomorphic processes: effects on the ancient Aleuts of Umnak Island in the Aleutians: Arctic, v. 28, no. 3, p. 159–169.

———1976, Geology of Umnak Island, eastern Aleutian Islands, as related to the Aleuts: Arctic and Alpine Research, v. 8, no. 1, p. 7–35.

Boyd, T.M, and Jacob, Klaus, 1986, Seismicity of the Unalaska region, Alaska: Bulletin of Seismology Society of America, v. 76, no. 2, p. 463–481.

Brophy, J.G. and Marsh, B.D., 1986, On the origin of high-alumina arc basalt and the mechanics of melt extraction: Journal of Petrology, v. 27 no. 4, p. 763–789.

Burgisser, Alain, 2005, Physical volcanology of the 2,050 bp caldera-forming eruption of Okmok Volcano, Alaska: Bulletin of Volcanology, v. 67, no. 6, p. 497–525.

Buurman, Helena, Nye, C.J., West, M.E. and Cameron, C.E., 2014, Regional controls on volcano seismicity along the Aleutian arc: Geochemistry, Geophysics, Geosystems, v. 15 no. 4, p.1,147–1,163.

Byers, F.M., Jr., 1955, The petrology of Umnak and Bogoslof islands, Alaska: University of Chicago unpublished Ph.D. dissertation, 189 p.

———1959, Geology of Umnak and Bogoslof Islands, Aleutian Islands, Alaska: in Investigations of Alaskan volcanoes, U.S. Geological Survey Bulletin B 1028-L, p. 267–369, 5 sheets, scale 1 at 1:63,360, 1 at 1:96,000, and 1 at 1:300,000.

———1961, Petrology of three volcanic suites, Umnak and Bogoslof Islands, Aleutian Islands, Alaska: Geological Society of America Bulletin, v. 72, no. 1, p. 93–128.

Byers, F.M., and Brannock, W.W., 1949, Volcanic activity on Umnak and Great Sitkin Islands, 1946–1948: Eos, v. 30, no. 5, p. 719–734.

Byers, F.M., Fisher, B., and Hopkins, D.M., 1947, Volcano investigations on Umnak Island: U.S. Geological Survey Alaskan Volcano Investigations Report 0002, p. 19–53.

Cameron, C.E., Crass, S.W., and AVO Staff, eds, 2022, Geologic database of information on volcanoes in Alaska (GeoDIVA): Alaska Division of Geologic and Geophysical Surveys Digital Data Series 20. doi.org/10.14509/geodiva, doi.org/10.14509/30901

Cameron, C.E., Mulliken, K.M., Crass, S.W., Schaefer, J.R., and Wallace, K.L., 2019, Alaska Volcano Observatory geochemical database, version 2: Alaska Division of Geological & Geophysical Surveys Digital Data Series 8 v. 2, 22 p. www.avo.alaska.edu/geochem/. doi.org/10.14509/30058

Cameron, C.E., Schaefer, J.R., and Ekberg, P.G., 2020, Historically active volcanoes of Alaska: Alaska Division of Geological & Geophysical Surveys Miscellaneous Publication 133 v. 4, 2 sheets. doi.org/10.14509/30426

Cameron, C.E., and Snedigar, S.F., 2016, Alaska Volcano Observatory image database: Alaska Division of Geological & Geophysical Surveys Digital Data Series 13, www.avo.alaska.edu/images/. doi.org/10.14509/29689

Campita, N.R., Daag, A.S., Newhall, C.G., Rowe, G.L., Solidum, R.U., 1996, Evolution of a small crater lake at Mount Pinatubo, *in* Newhall, C.G., Punongbayan S., eds., Fire and Mud: University of Washington Press, p. 435–444.

Cohen, K.M., Finney, S.C., Gibbard, P.L., and Fan, J.X., 2013; updated, The ICS International Chronostratigraphic Chart: Episodes, no. 36, p. 199–204.

Cook, J.P., 1995, Characterization and Distribution of Obsidian in Alaska: Arctic Anthropology, v. 32, no. 1, p. 92–100.

Coombs, M.L., and Jicha, B.R., 2020, The eruptive history, magmatic evolution, and influence of glacial ice at long-lived Akutan volcano, eastern Aleutian Islands, Alaska: GSA Bulletin, 29 p. doi.org/10.1130/B35667.1

Cross, R.S., and Freymueller, J.T., 2008, Evidence for and implications of a Bering plate based on geodetic measurements from the Aleutians and western Alaska: Journal of Geophysical Research Solid Earth v. 113, no. B7.

Dalrymple, G.B., 1989, The GLM continuous laser system for $^{40}Ar/^{39}Ar$ dating; description and performance characteristics, *in* Shanks, W.C., III, and Criss, R.E., eds., New frontiers in stable isotopic research; laser probes, ion probes, and small-sample analysis: U.S. Geological Survey Bulletin 1890, p. 89–96.

Dalrymple, G.B., Alexander E.C., Jr., Lanphere, M.A., and Kraker, G.P., 1981, Irradiation of samples for $^{40}Ar/^{39}Ar$ dating using the Geological Survey TRIGA reactor: U.S, Geological Survey Professional Paper 1176.

Dalton, A.S., Margold, Martin, Stokes, C.R., Tarasov, Lev, Dyke, A.S., Adams, R.S., Allard, Serge, Arends, H.E., Atkinson, Nigel, Attig, J.W., Barnett, P.J., and others, 2020, An updated radiocarbon-based ice margin chronology for the last deglaciation of the North American Ice Sheet Complex: Quaternary Science Reviews, v. 234.

Davies, J.N., and House, L., 1979, Aleutian subduction zone seismicity, volcano-trench separation, and their relation to great thrust-type earthquakes: Journal of Geophysical Research, v. 84, n. B9, p. 4,583–4,591.

Dunn, Robert, 1908, On the chase for volcanoes: The Outing Magazine, v. 51, p. 540–550.

Finney, B.M., 2004, Magmatic differentiation at an island-arc caldera: A stratigraphically constrained multi-isotope study of Okmok Volcano, Aleutian islands, Alaska: University of Bristol, Ph.D. dissertation.

Finney, B.M., Turner, Simon, Hawkesworth, Chris, Larsen, Jessica, Nye, C.J., George, Rhiannon, Bindeman, Ilya, and Eichelberger, John, 2008, Magmatic differentiation at an island-arc caldera: Okmok Volcano, Aleutian Islands, Alaska: Journal of Petrology. doi.org/10.1093/petrology/egn008

Fleck, R.J., Calvert, A.T., Coble, M.A., Wooden, J.L., Hodges, K., Hayden, L.A., van Soest, M.C., du Bray, E.A., and John, D.A., 2019, Characterization of the rhyolite of Bodie Hills and $^{40}Ar/^{39}Ar$ intercalibration of Ar mineral standards, Chemical Geology, v. 525, p. 282–302.

Fliedner, M.M., and Klemperer, S.L., 2000, The transition from oceanic arc to continental arc in the crustal structure of the Aleutian Arc: Earth and Planetary Science Letters, v. 179, p. 567–579.

Fournelle, J.H., Marsh, B.D., and Myers, J.D., 1994, Age, character, and significance of Aleutian arc volcanism, *in* Plafker, George and Berg, H.C., eds., The Geology of Alaska: Geological Society of America The Geology of North America Series, v. G-1, p. 723–758.

Freymueller, J.T., and Kaufman, A.M., 2010, Changes in the magma system during the 2008 eruption of Okmok Volcano, Alaska, based on GPS measurements: Journal of Geophysical Research: Solid Earth, v. 115, no. B12.

George, Rhiannon, Turner, Simon, Hawkesworth, Chris, Morris, Julie, Nye, C.J., Ryan, Jeff, and Zheng, S-H., 2003, Melting processes and fluid and sediment transport rates along the Alaska-Aleutian arc from an integrated U-Th-Ra-Be isotope study: Journal of Geophysical Research, v. 108, no. 5, p. 6–25. doi.org/10.1029/2002JB001916

Gowan, E.J., Zhang, Xu, Khosravi, Sara, Rovere, Alessio, Stocchi, Paolo, Hughes, A.L.C., Gyllencreutz, Richard, Mangerud, Jan, Svendsen, J.-I. and Lohmann, Gerrit, 2021, A new global ice sheet reconstruction for the past 80,000 years: Nature communications, v. 12, no. 1, p. 1–9.

Grewingk, Constantine, 1850, Grewingk's geology of Alaska and the Northwest Coast of America [edited by Marvin W. Falk, translation by Fritz Jaensch published 2003]: Rasmuson Library Historical Translation Series 11, Fairbanks, AK, The University of Alaska Press, 242 p.

Grey, D.M., 2003, Post-caldera eruptions at Okmok Volcano, Umnak Island, Alaska, with emphasis on recent eruptions from Cone A: University of Alaska Fairbanks unpublished M.S. thesis, 135 p.

Hendricks, M.D., Ekberg, P.G., Athey, J.E., Wyatt, W.C., Willingham, A.L., and Naibert, T.J., 2021, AK GeMS data dictionary: A description of the Alaska geologic mapping schema: Alaska Division of Geological & Geophysical Surveys Miscellaneous Publication 170, 10 p. doi.org/10.14509/30669

Ingebritsen, S.E., Flinders, A.F., Kauahikaua, J.P. and Hsieh, P.A., 2020, Modeling Groundwater Inflow to the New Crater Lake at Kīlauea Volcano, Hawai'i. Groundwater. doi.org/10.1111/gwat.13023

Johnson, D.M., Hooper, P.R., Conrey, R.M., 1999, XRF analysis of rocks and minerals for major and trace elements on a single low dilution Li-tetraborate fused bead: Advances in X-ray analysis, v. 41, p. 843–867.

Kaufman, D.S., Young, N.E., Briner, J.P. and Manley, W.F., 2011, Alaska palaeo-glacier atlas (version 2): Quaternary Sciences, v. 15, p. 427–445.

Kay, S.M., and Kay, R.W., 1994, Aleutian magmas in space and time, in Plafker, George, and Berg, H.C., eds., The Geology of Alaska: Geological Society of America Geology of North America series, v. G-1, p. 687–722.

Knaack, C.M., Cornelius, S., and Hooper, P.R., 1994, Trace element analyses of rocks and minerals by ICP-MS: Washington State Geoanalytical Laboratory, Washing State University.

Lanphere, M.A., and Dalrymple, G.B., 2000, First-principles calibration of 38Ar tracers: implications for the ages of $^{40}Ar/^{39}Ar$ fluence monitors: U.S. Geological Survey Professional Paper 1621, 10 p.

Larsen, J.F., 2016, Unraveling the diversity in arc volcanic eruption styles: Examples from the Aleutian volcanic arc, Alaska: Journal of Volcanology and Geothermal Research, v. 327, p. 643–668.

Larsen, J.F., Neal, C.A., Schaefer, J.R., Begét, J.E., and Nye, C.J., 2007, Late Pleistocene and Holocene caldera-forming eruptions of Okmok Caldera, Aleutian Islands, Alaska, *in* Eichelberger, John, Gordeev, Evgenii, Izbekov, Pavel, Kasahara, Minoru, and Lees, Jonathan, eds., Volcanism and Subduction: The Kamchatka Region: Geophysical Monograph 172, American Geophysical Union, p. 343–364.

Larsen, J.F., Neal, C.A., Schaefer, J.R., Kaufman, A.M., and Lu, Zhong, 2015, The 2008 phreatomagmatic eruption of Okmok Volcano, Aleutian Islands, Alaska: Chronology, deposits, and landform changes: Alaska Division of Geological & Geophysical Surveys Report of Investigation 2015-2, 53 p. doi.org/10.14509/29405

Larsen, J.F., Neal, C.A., Webley, Peter, Freymueller, J.T., Haney, M.M., McNutt, Steve, Schneider, D.J., Prejean, S., Schaefer, J.R., and Wessels, R., 2009, Eruption of Alaska volcano breaks historic pattern: Eos, Transactions, American Geophysical Union, v. 90, n. 20, p. 173–174.

Larsen, J.F., Sliwinski, M.G., Nye, C.J., Cameron, C.E., and Schaefer, J.R., 2013, The 2008 eruption of Okmok Volcano, Alaska: Petrological and geochemical constraints on the subsurface magma plumbing system: Journal of Volcanology and Geothermal Research, v. 264, p. 85–106. doi.org/10.1016/j.jvolgeores.2013.07.003

Layer, P.W., 2000, Argon-40/argon-39 age of the El'gygytgyn impact event, Chukotka, Russia: Meteoritics & Planetary Science, v. 35, no. 3, 591–599. doi.org/10.1111/j.1945-5100.2000.tb01439.x

Layer, P.W., Hall, C.M., and York, Derek, 1987, The derivation of $^{40}Ar/^{39}Ar$ age spectra of single grains of hornblende and biotite by laser step-heating: Geophysical Research Letters, v. 14, no. 7, p. 757–760.

Lee, Jee-Yon, Marti, Kurt, Severinghaus, J.P., Kawamura, Kenji, Yoo, Hee-Soo, Lee, J.B., and Kim, J.S., 2006, A redetermination of the isotopic abundances of atmospheric Ar: Geochimica et Cosmochimica Acta, v. 70, no. 17, p. 4,507–4,512.

Litke, Frederic, 1987, A voyage around the world, 1826–1829, *in* Pierce, R.A., ed., Alaska History (29nd ed.): Kingston, Ontario, Limestone Press, 230 p.

Lu, Zhong, Fielding, E.J., Patrick, M.R., and Trautwein, C.M., 2003, Estimating lava volume by precision combination of multiple baseline spaceborne and airborne interferometric synthetic aperture radar: the 1997 eruption of Okmok Volcano, Alaska: IEEE Transactions on Geoscience and Remote Sensing, v. 41, no. 6, p. 1,428–1,436.

Lu, Zhong, Mann, Dörte, Freymueller, J.T., and Meyer, D.J., 2000, Synthetic aperture radar interferometry of Okmok Volcano, Alaska: radar observations: Journal of Geophysical Research, v. 105, no. B5, p. 10,791–10,806.

Lu, Zhong, Masterlark, Timothy, and Dzurisin, Daniel, 2005, Interferometric synthetic aperture radar study of Okmok Volcano, Alaska, 1992–2003: Magma supply dynamics and post emplacement lava flow deformation: Journal of Geophysical Research, v. 110, no. B2, 18 p. doi.org/10.1029/2004JB003148

Mann, D.H., and Hamilton, T.D., 1995, Late Pleistocene and Holocene paleoenvironments of the North Pacific coast: Quaternary Science Reviews, v. 14, no. 5, p. 449–471.

Mann, Dörte, 2002, Deformation of Alaskan volcanoes measured using SAR interferometry and GPS: University of Alaska Fairbanks unpublished Ph.D. dissertation, 122 p.

Mann, Dörte, Freymueller, J.T., and Lu, Zhong, 2002, Deformation associated with the 1997 eruption of Okmok Volcano, Alaska: Journal of Geophysical Research, v. 107, no. B4, p. 7–13.

Marsh, B.D., 1982, The Aleutians, in Thorpe, R.S., ed., Andesites: orogenic andesites and related rocks: Chichester, United Kingdom, John Wiley & Sons, p. 99–114.

Matthes, F.E., 1941, Rebirth of the glaciers of the Sierra Nevada during late post-Pleistocene time: Geological Society of America Bulletin, v. 52, p. 2,030.

McAllister, R.F., 1956, Unusual debris-covered ice cones from Umnak Island: Journal of Glaciology, v. 2, no. 19, p. 631–632.

McDougall, Ian, and Harrison, T.M., 1999, Geochronology and Thermochronology by the $^{40}Ar/^{39}Ar$ Method: Oxford University Press on Demand.

McDougall, Ian, and Wellman, Peter, 2011, Calibration of GA1550 biotite standard for K/Ar and $^{40}Ar/^{39}Ar$ dating: Chemical Geology, v. 280, no. 1, p. 19–25. doi.org/10.1016/j.chemgeo.2010.10.001

McGimsey, R.G., and Wallace, K.L., 1999, 1997 volcanic activity in Alaska and Kamchatka: Summary of events and response of the Alaska Volcano Observatory: U.S. Geological Survey Open-File Report OF 99-0448, 42 p.

Miller, D.M., Langmuir, C.H., Goldstein, S.L., and Franks, A.L., 1992, The importance of parental magma composition to calc-alkaline and tholeiitic evolution: evidence from Umnak Island in the Aleutians: Journal of Geophysical Research, v. 97, no. B1, p. 321–343.

Miller, T.P., and Smith, R.L., 1976, Two caldera-forming eruptions on Umnak Island, eastern Aleutian Islands [abs.], *in* Cobb, E. H., ed., The United States Geological Survey in Alaska: accomplishments during 1975, U.S. Geological Survey Circular C 0733, p. 45.

Miller, T.P., and Smith, R.L., 1987, Late Quaternary caldera-forming eruptions in the eastern Aleutian arc, Alaska: Geology, v. 15, no. 5, p. 434–438.

Miller, T.P., McGimsey, R.G., Richter, D.H., Riehle, J.R., Nye, C.J., Yount, M.E., and Dumoulin, J.A., 1998, Catalog of the historically active volcanoes of Alaska: U.S. Geological Survey Open-File Report OF 98-0582, 104 p.

Miyashiro, Akiho, 1974, Volcanic rock series in island arcs and active continental margins: American Journal of Science, v. 274, p. 321–355.

Motyka, R.J., 1977, Katmai Caldera: glacier growth, lake rise and geothermal activity, *in* Staff, A.G.S., ed., Short notes on Alaskan geology, 1977: Alaska Division of Geological & Geophysical Surveys Geologic Report GR 0055, p. 17–21.

Motyka, R.J., Liss, S.A., Nye, C.J., and Moorman, M.A., 1993, Geothermal resources of the Aleutian arc: Alaska Division of Geological & Geophysical Surveys Professional Report 114, 17 p., 4 sheets, scale 1:1,000,000. doi.org/10.14509/2314

Moxey, L., Dehn, J., Papp, K.R., Patrick, M.R., and Guritz, R., 2001, The 1997 eruption of Okmok Volcano, Alaska, a synthesis of remotely sensed data [abs.]: Eos, v. 82, no. 47, p. 1,375.

Myers, J.D., and Marsh, B.D., 1987, Aleutian lead isotopic data: additional evidence for the evolution of lithospheric plumbing systems: Geochimica et Cosmochimica Acta, v. 51, no. 7, p. 1,833–1,842.

Nathenson, Manuel, Bacon, C.R. and Ramsey, D.W., 2007, Subaqueous geology and a filling model for Crater Lake, Oregon: Hydrobiologia, v. 574, p. 13–27. doi.org/10.1007/s10750-006-0343-5

Neal, C.A., Begét, J., Grey, D., and Wolfe, B., 2003, The 1817 eruption of Okmok Caldera, Umnak Island, Alaska: new insights into a complex historical eruption in the eastern Aleutians [abs]: Eos Trans. AGU Fall Meeting, v. 84, no. 46.

Nye, C.J., 1983, Petrology and geochemistry of Okmok and Wrangell volcanoes, Alaska: University of California, Santa Cruz Ph.D. dissertation, 208 p.

Nye, C.J., Begét, J.E., Layer, P.W., Mangan, M.T., McConnell, V.S., McGimsey, R.G., Miller, T.P., Moore, R.B., and Stelling, P.L., 2018, Geochemistry of some quaternary lavas from the Aleutian Arc and Mt. Wrangell: Alaska Division of Geological & Geophysical Surveys Raw Data File 2018-1, 29 p. doi.org/10.14509/29843

Nye, C.J., Motyka, R.J., Turner, D.L., and Liss, S.A., 1992, Geology and geochemistry of the Geyser Bight Geothermal area, Umnak Island, Aleutian Islands, Alaska: Alaska Division of Geological & Geophysical Surveys Report of Investigation 92-1, 85 p., 2 sheets, scale 1:24,000. doi.org/10.14509/2480

Nye, C.J., and Reid, M. R., 1986, Geochemistry of primary and least fractionated lavas from Okmok Volcano, Central Aleutians: implications for arc magmagenesis: Journal of Geophysical Research, v. 91, no. B10, p. 10,271–10,287.

Patrick, M.R., Dehn, J., Papp, K.R., Lu, Z., Dean, K., Moxey, L., Izbekov, P., and Guritz, R., 2003, The 1997 eruption of Okmok Volcano, Alaska: a synthesis of remotely sensed imagery: Journal of Volcanology and Geothermal Research, v. 127, no. 1–2, p. 87–105. doi.org/10.1016/S0377-0273(03)00180-X

Reeder, J.W., 1984, Okmok: Bulletin of Volcanic Eruptions, v. 22, p. 92–94.

Reuther, J.D., Slobodina, N.S., Rasic, J.T., Cook, J.P., and Speakman, R.J., 2011, Gaining Momentum–Late Pleistocene and Early Holocene Archaeological Obsidian Source Studies in Interior and Northeastern Beringia, *in* Gobel, Ted, and Buvit, Ian, eds., From the Yenisei to the Yukon Interpreting Lithic Assemblage Variability in Late Pleistocene/Early Holocene Beringia: College Station, Texas A&M University Press, p. 270–286.

Robinson, G.D., 1947, The 1945 eruption in Tulik (Okmok) Caldera, Umnak Island, Alaska: Journal of the Washington Academy of Sciences, v. 37, no. 10, p. 368–369.

Robinson, G.D., 1948, Exploring Aleutian volcanoes: National Geographic Magazine, v. 94, no. 4, p. 509–528.

Schaefer, J.R., 2005, 30-meter shaded relief image of Okmok Volcano, Umnak Island, Alaska: Alaska Division of Geological & Geophysical Surveys Raw Data File 2005-1. doi.org/10.14509/7041

Schaefer, J.R., Larsen, J.F., and Unema, J.A., 2011, Digital elevation model (DEM) and shaded relief image of Okmok Caldera, 2010: Alaska Division of Geological & Geophysical Surveys Raw Data File 2011-6. doi.org/10.14509/23223

Sheridan, M.F., 1970, Fumarolic mounds and ridges of the Bishop Tuff, California: Geological Society of America Bulletin, v. 81, no. 3, p. 851–868.

Smellie, J.L., 2000, Subglacial eruptions, *in* Sigurdsson, Haraldur, Houghton, Bruce, Rymer, Hazel, Stix, John, McNutt, Steve, eds., Encyclopedia of Volcanoes, Elsevier, p. 403–418.

Steiger, R.H., and Jäger, E., 1977, Subcommission on geochronology: Convention on the use of decay constants in geo-and cosmochronology: Earth and planetary science letters, v. 36, no. 3, p. 359–362.

Stone, D.B., and Layer, P.W., 2006, Paleosecular variation and GAD studies of 0–2 Ma flow sequences from the Aleutian Islands, Alaska: Geochemistry, Geophysics, Geosystems, v. 7, no. 4. doi.org/10.1029/2005GC001007

Turner, D.L. and Nye, C.J., 1989. Geothermal resource assessment in the Aleutian Islands and Alaska Peninsula: University of Alaska Fairbanks Geophysical Institute Quarterly Progress Report, January 1–March 30, 1989, no. DOE/ID/12742-T1.

Unema, J.A., Ort, M.H., Larsen, J.F., Neal, C.A., and Schaefer, J.R., 2016, Water-magma interaction and plume processes in the 2008 Okmok eruption, Alaska: GSA Bulletin, 15 p. doi.org/10.1130/B31360.1

Veniaminov, Ivan, 1840, Notes on the islands of the Unalaska district [translated from Russian by Lydia T. Black and R.H. Geoghegan in 1984], *in* Pierce, R.A., ed., Kingston, Ontario, Limestone Press, 511 p.

Wilcox, R.E., 1959, Some effects of recent volcanic ash falls with special reference to Alaska: in Investigations of Alaskan volcanoes, U.S. Geological Survey Bulletin B 1028-N, p. 409–476, 5 sheets, scale unknown.

Wolfe, B.A., 2001, Paleohydrology of a catastrophic flood release from Okmok Caldera and post-flood eruption history at Okmok Volcano, Umnak Island, Alaska: University of Alaska Fairbanks unpublished M.S. thesis, 100 p.

Wolfe, B.A., and Begét, J.E., 2002, Destruction of an Aleut village by a catastrophic flood release from Okmok Caldera, Umnak Island, Alaska [abs.]: Abstracts with Programs, Geological Society of America, v. 34, n. 6.

Wong, L.J., and Larsen, J.F., 2010, The Middle Scoria sequence: A Holocene violent strombolian, subplinian, and phreatomagmatic eruption of Okmok Volcano, Alaska: Bulletin of Volcanology, v. 72, p. 17–31.

Wood, C.A., and Kienle, Juergen, eds., 1990, Volcanoes of North America: United States and Canada: New York, Cambridge University Press, 354 p.

York, Derek, Hall, C.M., Yanase, Yotaro, Hanes, J.A., and Kenyon, W.J., 1981, $^{40}Ar/^{39}Ar$ dating of terrestrial minerals with a continuous laser: Geophysical Research Letters, v. 8, no. 11, p. 1,136–1,138.

Zhao, Dapeng, Christensen, Douglas, and Pulpan, Hans, 1995, Tomographic imaging of the Alaska subduction zone: Journal of Geophysical Research, v. 100, no. B4, p. 6,487–6,504. doi.org/10.1029/95JB00046